FACULDADE DE ENGENHARIA DA UNIVERSIDADE DO PORTO

Effect of electromagnetic fields induced by mobile devices in the human brain

Vânia Filomena Madureira Vieira

Mestrado Integrado em Engenharia Eletrotécnica e de Computadores

Supervisor in FEUP: Maria Inês Carvalho

External Supervisor in INESC-TEC: Luís Pessoa

February 24, 2017

Abstract

The aim of this thesis is to understand if the mobile devices that produce electromagnetic fields could be a risk for the human body, specially for the brain. To achieve this purpose several scenarios were tested using an anatomical model of Virtual Family (ViP) that reproduces almost faithfully all the tissues of the human body. Four PIFA antennas were designed to operate at 900, 1800, 2100 and 2600 MHz. The main goal was to measure the Specific Absorption Rate (SAR) in the tissues of head, brain and hand regions depending on some variables that, according to previous studies, can influence the SAR value. The variables tested were the distance between the head and the antenna, the hand effect, the orientation of the antenna, tilt positions and frequency.

The simulations were performed in a recent simulation software named Sim4life, which is a innovative computational life sciences platform that integrates computable human phantoms to analyse biological real-world phenomena.

The results that were obtained are interesting and in accordance with literature. Regarding the distance between the head and the antenna, our results confirm that SAR decreases as the distance increases. This decrease is circa 25% for each 2 mm of distance. The presence of the hand is determinant to reduce SAR on head and brain. The decrease on SAR values is circa 17.5% in head tissues and circa 20.6% in brain tissues, just because the hand is present. The bottom orientations of PIFA reduce SAR on brain, but increase SAR in other tissues, mainly on hand. The decrease of local SAR in tissues is circa 85.7% in ear region, 28.9% in cheek region and 59.7% in brain. Tilt positions of PIFA are better than cheek positions in terms of SAR. The decrease is circa 44.6% in head tissues and 48% in brain tissues. The frequency effect is determined by the input power at which the antenna is working. At the considered power for each frequency of this project, brain tissues have lower SAR at 2100 MHz, despite the values at 1800 MHz are very close to the SAR values at 2100 MHz.

Agradecimentos

Findo mais um capítulo da minha vida. Provavelmente o mais árduo até agora. Posso assumir sem vergonha o enorme orgulho que sinto em mim, por todo o meu esforço conseguido mesmo quando a força me faltou.

Finalizo aqui mais uma etapa com a esperança que os meus sonhos e objectivos se concretizem.

Pensar nas pessoas que me ajudaram neste percurso não é difícil e agradecer-lhes com estas palavras nunca será suficiente.

Por isso agradeço,

Ao meu namorado Hugo, todo o amor e carinho com que me acompanha todos os dias, mesmo com a distância que nos separa. Obrigada por me teres apoiado incondicionalmente em todos os momentos!

Aos meus pais, Manuel e Helena, pela paciência para os meus desânimos e pelo alento e compreensão em relação ao futuro que eu anseio e tanto temi.

À minha irmã, Beatriz, que me faz rir e me diverte com toda a sua irreverência própria da idade e também pela sua companhia.

À minha orientadora Professora M.ª Inês Carvalho e ao meu sub-orientador Eng.º Luis Pessoa por todo o conhecimento que me dispensaram e que me fez evoluir neste projecto. Agradeço também ao colega Eng.º Hugo Santos pelo desenho das antenas que dele fizeram parte e também à empresa ZMT Zurich MedTech AG pelo fornecimento da licença do software Sim4life.

Saio com o sentimento de que o esforço foi grande mas a recompensa será maior.

Obrigada!

Vânia Vieira

"Recomeça...
Se puderes,
Sem angústia e sem pressa.
E os passos que deres,
Nesse caminho duro
Do futuro,
Dá-os em liberdade.
Enquanto não alcances
Não descanses.
De nenhum fruto queiras só metade.
E, nunca saciado,
Vai colhendo
Ilusões sucessivas no pomar.
Sempre a sonhar
E vendo.
Acordado,
O logro da aventura.
És homem, não te esqueças!
Só é tua a loucura
Onde, com lucidez, te reconheças."

Miguel Torga, Diário XIII

Contents

List of Figures

List of Tables

Abreviations and Symbols

3D	Three Dimensions
ABC	Absorbing Boundary Conditions
AC	Alternate Current
AM	Amplitude Modulation
B	Magnetic flux density
BMI	Body Mass Index
BMR	Basal Metabolic Rate
CAD	Computer Aided Design
CENELEC	European Committee for Electrotechnical Standardization
CNS	Central Nervous System
COST	European Cooperation in the field of Scientific and Technical Research
CT	Computed Tomography
D	Electric Displacement
DC	Direct Current
DNA	Deoxyribonucleic Acid
E	Electric Field
EEG	Electroencephalography
EHF	Extreme High Frequency
ELF	Extreme Low Frequency
EM	Electromagnetic
EMF	Electromagnetic Field
EMF-MED	Electromagnetic Fields in Biomedical Applications
FBW	Fractional Bandwidth
FCC	Federal Communications Commission
FDTD	Finite Difference Time Domain
FM	Frequency Modulation
G	Gain
GPS	Global Positioning System
GSM	Global System for Mobile Communications
H	Magnetic Field
HF	High Frequency
HPBW	Half Power Beamwidth
IARC	International Agency for Research on Cancer
ICNIRP	International Commission on Non-Ionizing Radiation Protection
IEC	International Electrotechnical Commission
IEEE	Institute of Electrical and Electronics Engineers

IF	Intermediate Frequency
J	Current Density
LF	Low Frequency
LTE	Long Term Evolution
M	Mass
MOM	Method of Moments
MRI	Magnetic Resonance Imaging
MSA	Microstrip Antenna
P	Power
PEC	Perfect Electric Conductor
PIFA	Planar Inverted F Antenna
PMA	Planar Monopole Antenna
RF	Radio Frequency
SAM	Specific Anthropomorphic Mannequin
SAR	Specific Absorption Rate
SLL	Side Lobe Levels
T	Period of Time
TV	Television
UHF	Ultra High Frequency
UMTS	Universal Mobile Telecommunication System
UPML	Uniaxial Perfectly Matched Layer
US	United States
ViP	Virtual Population
VHF	Very High Frequency
VSWR	Voltage Standing Wave Ratio
WHO	World Health Organization

Chapter 1

Introduction

1.1 Context and motivation

Nowadays electromagnetic fields (EMFs) exposition is patent in numerous everyday situations. User acceptance of the new technologies has been worldwide, therefore the number of users is large and is growing, particularly among young adults and children [1].

Mobile phones are the most evident source of EMFs, which most population carry around with themselves every single day. The mobile phones are held by the hand in close proximity to the head, and when hands-free kits are used, they remain close to the body. But, is this exposure harmful for health? Numerous studies have been conducted on this thematic but the conclusions are not cohesive and concrete.

Energy absorption is defined by SAR, the specific absorption rate, which is a measure of the energy absorbed in body tissues, in watts per kilogram (W/kg).

Nowadays the variety of mobile phones models is huge with smaller and more practical sizes. The antenna design for mobile phones had also a great progress, becoming embedded on the phone chassis as opposed to the mobile external antennas of fifteen years ago. When designing a mobile phone, one of the main objectives is to obtain the maximum performance, which implies a good output power, but this can translate into a increased SAR. Because of that fact, the tradeoff between a good device performance and a device that respect limits of SAR, making it as small as possible, is not always easy.

Wireless communication devices are the perfect example of a product made and developed by the technology and used daily for being essential and indispensable, although the eventual risks for health. One is not just talking about exposure to EMF on an individual level, but there is an increasing public and occupational exposure. Public discussion takes place nowadays because it is crucial to know if the risks taken make up for the benefits.

The ongoing problem in this controversy about the risks of exposure to EMF is the limited knowledge about the fact that very specific fields interacting with the human body can have harmful effects on health. These effects vary from person to person, with some people much more affected than others, due to their physical and biochemical natural differences. In fact, World

Health Organization (WHO) and International Agency for Research on Cancer (IARC) issued in 2011 a press release classifying radiofrequency electromagnetic fields as possibly carcinogenic to humans, based on an increased risk for glioma, a malignant type of brain cancer, associated with wireless phone use [1].

The World Health Organization (WHO) recommended that biological, biomedical and epidemiological studies should be conducted to verify that no health effects are caused below the exposure levels inducing thermal effects [2].

At present, public opinion has expressed its concerns regarding the effects of radiation, especially with regard to cellular systems - mobile phones and transmitting antennas - hence it is essential the developing and deepening of scientific studies that may in fact prove or disprove the existence of clear harm.

1.2 Goals

The aim of this work consists in the investigation of the effects on the body, specifically on the brain, due the EMF exposure using a recent simulator of EMF - Sim4life. In particular, to know how the radiofrequency (RF) radiation reaches the head, brain and hand regions, according to some variables that can influence this absorption. These variables are the distance between the antenna and the body, the presence of the hand, the antenna's feeder position, tilt positions and the communication band.

Sim4Life is a computational life sciences platform that integrates computable human phantoms, which makes it unique. These phantoms represent the most advanced tissue models for directly analyzing biological realworld phenomena. The absorption of radiation by the human body depends on many factors, and because of this fact diverse scenarios of everyday use of a cellular phone will be tested. The position of the phone relative to the body, the position of the antenna relative to the phone, frequencies and feeding powers to achieve conclusions about safe ways of use.

Although this work concerns the potential hazardous effects of EMF generated by mobile telecommunication devices, it is part of a larger research objective associated with COST Action BM 1309. This COST (Cooperation in the field of Scientific and Technical Research) action is an European network that investigates innovative uses of EMFs in biomedical applications (EMF-MED).

1.3 Dissertation structure

This document is organized in five chapters, including the present one. Chapter two addresses some background material on EMF, including the potential harmful effects to human health. In the same chapter, the antenna radiation is explored with the aim of understanding the technical concepts and the theory that supports the cellular phone radiation and antenna design.

In chapter three the problem addressed in this work is characterized and the methods and the models used to solve the problem are defined. Chapter four is dedicated to the simulation and the results obtained according to the different scenarios previous established. In the last chapter, chapter five, it will be made a confrontation between the results obtained in this work and the results of the literature and the final conclusions will be draw and the future work will be referred.

Chapter 2

Electromagnetic fields and waves

The concept of EMF was first proposed by scientist James Clerk Maxwell and represents the interaction of two vectors that quantify both electric and magnetic fields, which are invisible areas of energy or radiation produced under some circumstances. These vectors symbolize an exerted strength: the electric field (E) describes the force exerted on a unit electric charge and is expressed in volt per meter (V/m). Correspondingly, the magnetic field (H) is defined in terms of the force exerted on a moving unit charge, which expresses its dependence on the speed at which this unit charge travels and it is expressed in ampere per meter (A/m) [3].

Through E and H it is possible to determine other electromagnetic field quantities. The electric flux density, also known as electric displacement (D), is useful in the study of electric field in material media and it is obtained from E and electric permittivity (ε):

$$D = \varepsilon \cdot E \tag{2.1}$$

D measures the quantity of E that flows through a unit area and is expressed in coulombs per square meter (C/m^2). Likewise, E is also used to obtain the current density (J) together with electric conductivity (σ) and it is expressed in ampere per square meter (A/m^2):

$$J = \sigma \cdot E \tag{2.2}$$

Similarly to D is the magnetic flux density (B) which is expressed in Tesla (T) and is the product between H and magnetic permeability (μ):

$$B = \mu \cdot H \tag{2.3}$$

If the materials are linear, isotropic and non-dispersive, the previous material parameters are constants.

Electric and magnetics fields interaction is described by Maxwell equations which allow the study of every single phenomena on electromagnetic (EM) space. Considering time-harmonic

fields and using phasor notation, these four equations allow to relate the electric and magnetic fields with electric charge and electric current [4]:

$$\nabla \cdot \vec{D} = \rho \tag{2.4}$$

$$\nabla \cdot \vec{B} = 0 \tag{2.5}$$

$$\nabla \times \vec{E} = -j\omega\vec{B} \tag{2.6}$$

$$\nabla \times \vec{H} = \vec{J} + j\omega\vec{D} \tag{2.7}$$

where the quantity ∇ (pronounced "del") is a vector operation, ρ is the charge density, ω is the electrical angular frequency of the field. In the case of existing external sources is added on last equation the term $\vec{J_s}$ which is, in this case, the added source current density on the antenna:

$$\nabla \times \vec{H} = \vec{J} + \vec{J_s} + j\omega\vec{D} \tag{2.8}$$

EM waves contain an electric field E and a magnetic field H, which are perpendicular to the direction of wave propagation and that propagate with a propagation constant γ that depends on the medium parameters through

$$\gamma = \sqrt{j\omega\mu\sigma - w^2\mu\varepsilon} \tag{2.9}$$

For example, for a wave propagating along $+z$, the complex amplitude of E should vary as

$$E = E_0 e^{-\gamma z} \tag{2.10}$$

The propagation constant is in general a complex number, $\gamma = \alpha + j\beta$, with its real part α representing the wave attenuation in Np/m and its imaginary part β representing the phase constant. From this phase constant the spatial wave period λ (wavelenght) can be computed since $\beta = \frac{2\pi}{\lambda}$ and, moreover, the propagation velocity is given by $v = \frac{\omega}{\beta}$, which can also be written in the familiar form $v = \lambda f$.

If the medium electric conductivity is zero (i.e. lossless material), $\gamma = j\omega\sqrt{\mu\varepsilon}$. This implies that a EM wave propagating in a lossless medium suffers no atenuation ($\alpha = 0$) and, furthermore, that it propagates with a velocity given by

$$v = \frac{1}{\sqrt{\mu\varepsilon}} \tag{2.11}$$

If the propagation medium is vacuum, then $\mu = \mu_0 = 4\pi \times 10^{-7}$ F/m and $\varepsilon = \varepsilon_0 = 8.854 \times 10^{-12}$ F/m ($\simeq \frac{1}{36\pi} \times 10^{-9}$ F/m), and the previous expression gives the speed of light, $c \cong 3 \times 10^8$ m/s. In other materials such biological tissues the velocity is lower.

EMFs are often divided according to their frequency: Higher-frequency and Low to mid frequency (See Fig. 2.1). The first ones are part of ionizing radiation of the EM spectrum and through this the DNA or the cells can be damaged. Ionization is the process by which electrons are stripped from atoms and molecules by high-energy photons. Thus, this type of radiation has enough energy to remove electrons from their atomic orbitals, turning the atoms into ions [5]. Examples of this radiation includes X-rays and gamma rays.

Likewise, the second ones includes static fields (i.e. not vary with time), magnetic fields from electric power lines and appliances, radio waves, microwaves, infrared radiation, and visible light and are part of the non-ionizing radiation of the EM spectrum. This type of radiation does not have sufficient energy to cause ionization on living systems, which means they are probably harmless the DNA or the cells.

Low to mid frequency EMFs include extremely low frequency (ELF) which have frequencies up to 300 hertz (Hz), intermediate frequency (IF) which have frequencies between 300 Hz and 10 megahertz (10×10^6Hz) and radiofrequency (RF) which have range from 10 megahertz to 300 gigahertz (300×10^9Hz).

Nowadays the sources of electromagnetic fields are numerous due the electronic and electrical devices that are used everyday by a large part of the world population. Most of those devices use radio technology, that currently leads one of the biggest businesses in the global market as well as the use of wireless devices, such as cellular phones that is increasing dramatically [6]. In the following section, the biological effects of EMF will be addressed.

2.1 Biological effects of electromagnetic fields

Everyday the population is exposed to both electric and magnetic fields. Such fact makes one immediately think that EM energy, artificially created by numerous devices, can interact on biological systems in a harmful way. Biological effects are not necessary health effects, since not all the biological effects of EMF cause necessarily a health problem. According to ICNIRP (1998 cit. by [7]) a biological effect may or may not result in an adverse health effect, revealing the uncertainty about the hazard of EMF for health. A health effect is defined by a detectable impairment of the health of the exposed individual. Thus, it becomes necessary to study the side-effects resulting of the human EMF exposure, whether be high intensity such power lines or low intensity such mobile phone.

2.1.1 Interaction with cells and tissues

For a better understanding of the aim of this work, it is important to briefly characterize the cells and the tissues that compose the human body.

Biological cells are very complex structures that have electrical charges of high energy on their composition. These charges can change their orientation and their movement when subjected to the action of external electric fields.

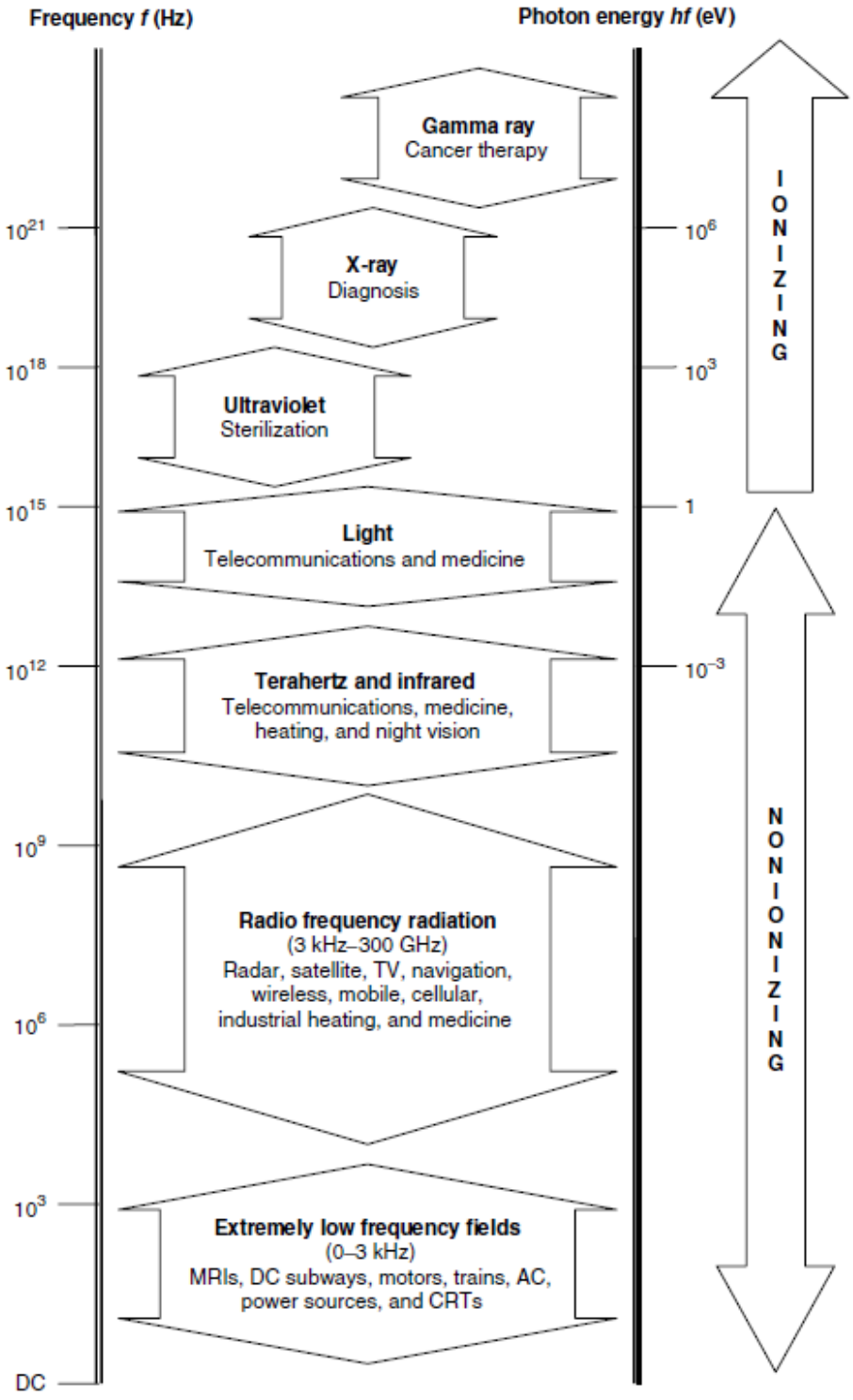

Figure 2.1: EM frequency spectrum.[6]

When an electric field is applied, the electrical charges change the distribution, concentrating strongly in the area of the cell closest to the action of this field. Therefore, interaction between EMFs and biological systems are analyzed at cell level, specifically through interaction with the cellular membrane to the cytoplasm and the nucleus. The nucleus contains the majority of the hereditary information, commonly known as DNA (deoxyribonucleic acid).

The tissues are biological materials that represent clusters of cells and they can be divided in four types: epithelial, connective, muscular and nervous. Epithelial tissues have the functions of protection and regulation of secretion and absorption materials. Connective tissues consist in fibers and gelatinous substances that support and connect the cellular tissue to the skeleton. They include many of the substances that ensure the important task of transporting materials between cells as bones and cartilage. Muscle tissues are part of muscles, hollow organs and cardiac muscles and have functions of contraction. For last, nervous tissues are used for sensory activities, and control of the human body. They send all information from sensory receptors to the central nervous system, but also from the central nervous system to the muscles, organs, and glands.

Electric fields of low frequency do not reach the body significantly, they only create electric charges on the surface of the body, inducing a flow of electric current on the body. Magnetic fields of low frequency that cross a body induce an electric current that circulates inside the body. This current has variable intensity which depends on the intensity of the magnetic field and on the length of the course whereby the electric current flows [7, 8] (See fig. 2.2).

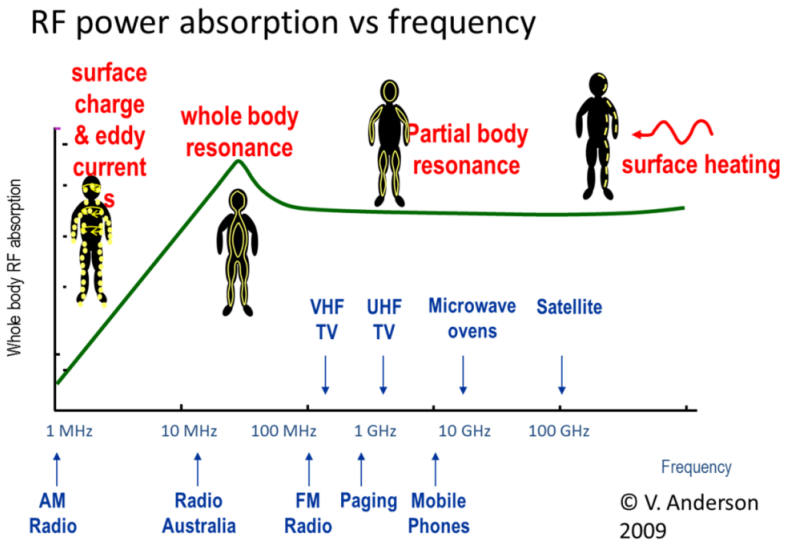

Figure 2.2: Diagram showing approximate frequencies for peak power absorption [7]

Radio-frequencies reach only a small distance into the body. The energy of these fields is absorbed and it is transformed on molecule movement. The friction between the molecules in rapid movement results in an increase of the temperature.

Table 2.1: Electrical properties of various human tissues at frequency 902.5 MHz (GSM) (cit. by [9]

Tissue type	**Conductivity** σ **[S/m]**	**Relative permittivity** ε_r **[-]**	**Density** ρ $[kg/m^3]$	**Specific heat** c_s **[J/kg.K]**
Bone	0.3406	20.7823	1810	1256
Brain	0.9434	52.7133	1030	3710
Skin	0.8674	41.3923	1010	3662
Muscle	0.9438	55.0261	1040	3639
Blood	1.5390	61.3524	1060	3894

The propagation of a EM wave in a body tissue is affected by the medium parameters already metioned: permittivity, conductivity and permeability. Body tissues are not magnetic and, therefore, their magnetic permeability is that of free-space, i.e., $\mu = \mu_0$ or $\mu_r = \frac{\mu}{\mu_0} = 1$. On the other hand, the values of σ and $\varepsilon_r = \frac{\varepsilon}{\varepsilon_0}$ vary with tissue type and are also dependent on frequency.

Actually, the tissue conductivity is dominant at low frequencies, whereas at high frequencies it is the relative permittivity that tends to become dominant.

Examples of electrical properties of various human tissues are in table 2.1 for a operational frequency of 902.5 MHz.

Human tissues can absorb EMF and induce conduction and displacement currents. However, this interaction between human tissues and EMF is influenced by many factors besides field frequency like configuration of exposure source, dielectric, age, exposure environment, field strength, time intensity factor, geometry and size of the tissue, orientation and field polarization [10].

Moreover, every region in the human body is extremely complex. For instance the human head, which is a complex structure of many different tissues and each of these tissues, like skin, bone or fat absorbs RF energy in its own way. Furthermore, even having the same structural components, different heads vary in volume and shape. Also, considering the children in a special way, due their body and brain being still in development, any exposure to RF is more detrimental for they than for adults [11].

It should also be mentioned that the brain and moreover the middle and inner ear are the most critical organs for cellular phone exposures[12].

2.1.2 Human health effects according to frequency

There are different descriptions of human health effects depending of the value ranges of frequencies under consideration. Indeed, extreme low frequency human health effects are different of Radiofrequency or Microwave human health effects.

Related to ELF and IF there have been concerns about the association between the exposure to this type of EM fields and human health. In fact, devices used everyday in home or in work, such as household induction heating cooker or electronic article surveillance tags for theft prevention, use the magnetic fields of the ELF and IF regions. However, no basic research data on the biological effects of IF magnetic fields are available (Shigemitsu et al. 2007 cit. by [13]) and the need of

further studies on health risk assessments of IF magnetic field, ranging from tens of kilohertz to about 100 kHz, is crucial .

Biological effects of Radio frequencies can be classified in three different ways. First, the high level effects or thermal effects, medium level effects or athermal effects and last, reduced level effects or non-thermal effects [14].

The thermal effects are expressed by the heating of the tissues due the absorption of the radiation that increases the human body temperature [5]. Such phenomena can be dangerous because the normal functions of the body can change as a direct consequence of temperature variation as a compensatory mechanism. For instance, there are descriptions of adverse reactions that increase the body temperature in 1ºC resulting of radio frequency radiation with frequencies between 1MHz and 10 GHz. These increase of temperature can develop eye injuries, high blood pressure, nausea, weakness and disorientation.

Thermal effects can be defined as an excess of energy generated on the human body and can not be dissipated by the normal thermoregulation mechanism, such as the blood flow and sweating [10]. Usually the body generates heat when feeding, a normal phenomena named basal metabolic rate (BMR). In that case, exposure levels compared to Basal metabolic rate (BMR) will produce thermal effects equivalent to thermoregulation, i.e. apparently harmless.

Athermal effects occurs when are present biological effects without the calorific energy involved, being the body temperature maintained in normal levels, through the thermoregulation mechanism. Athermal effects are the subject of ongoing research, since they are not well understood [5].

Non-thermal effects occurs when the radiation exposure does not originate temperature changes on the body [14].

The relative permittivity decreases with increasing frequency at the lower frequencies (See Fig. 2.3a). This fact is explained by the capacitance inherent in the cellular membranes. From about 100 MHz to about 10 GHz those membranes are short-circuited. The decline above 10 GHz is due to the water content and its frequency characteristics [5].

Figure 2.3b shows the resistivity of high water content human tissues, which is the inverse of the conductivity. The resistivity tends to decrease slowly with the increasing of the frequency at lower frequencies, but at high frequencies it decreases rapidly. This fact occurs due to the conductivity of water, which changes strongly on that point.

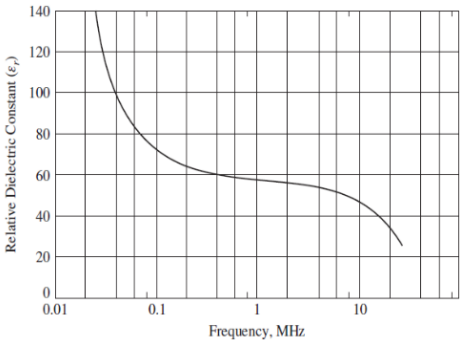

(a) Relative dielectric constant of representative human tissue.

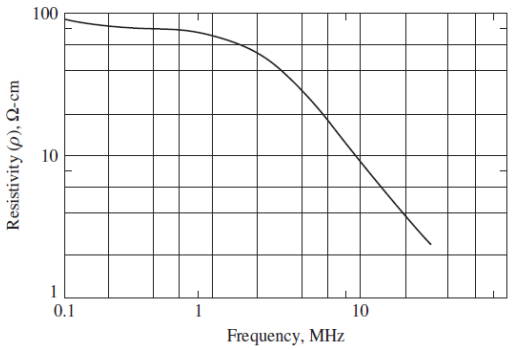

(b) Resistivity of representative human tissue.

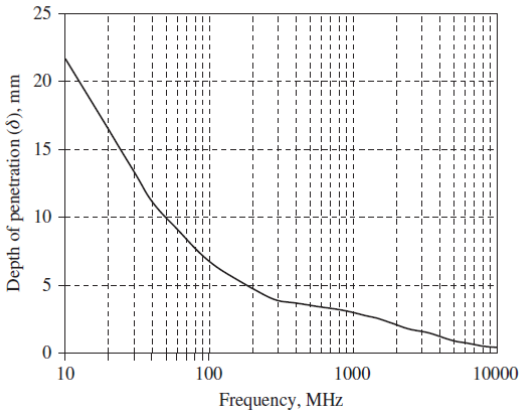

(c) Depth of penetration of RF energy in tissues with high water content.

Figure 2.3: (From [5])

The depth of penetration of RF energy in the human body tissues is figured in 2.3c. Depth of penetration or skin depth characterizes how well an electromagnetic wave can penetrate into a given medium and is defined as the distance associated with an attenuation of 1 Np. Representing the skin depth by δ and recalling that attenuation is associated with the real part α of the propagation constant, we have

$$e^{-\alpha\delta} = e^{-1} \Leftrightarrow \delta = \frac{1}{\alpha} \tag{2.12}$$

Moreover, from the expression of the propagation constant γ, we can obtain the attenuation constant as

$$\alpha = \omega\sqrt{\frac{\mu\varepsilon}{2}\left[\sqrt{1+\left(\frac{\sigma}{\omega\varepsilon}\right)^2}-1\right]} \tag{2.13}$$

and the skin depth in the form

$$\delta = \frac{1}{\omega\sqrt{\frac{\mu\varepsilon}{2}\left[\sqrt{1+\left(\frac{\sigma}{\omega\varepsilon}\right)^2}-1\right]}} \tag{2.14}$$

where ω is the angular frequency, μ is the magnetic permeability, ε is the electric permittivity and σ is electric conductivity [15].

The dependence of the skin depth on frequency is defined by the value of $\frac{\sigma}{\omega\varepsilon}$. For example, when the medium is a good conductor at a given frequency, that is, when $\frac{\sigma}{\omega\varepsilon} \gg 1$, the skin depth is approximately given by

$$\delta \cong \sqrt{\frac{2}{\omega\mu\sigma}} \tag{2.15}$$

implying that δ depends inversely on the square root of ω. On the other hand, when $\frac{\sigma}{\omega\varepsilon} \ll 1$, we have

$$\delta \simeq \frac{2}{\sigma\sqrt{\frac{\mu}{\varepsilon}}} \tag{2.16}$$

which does not depend explicitly the frequency. Taking into account that conductivity of body tissues increases with frequency (see fig. 2.3b), and assuming and assuming that the value of $\frac{\sigma}{\omega\varepsilon}$ is in the middle of these two extreme cases, it can be concluded that the value of skin depth of a medium decreases as the operational frequency increases [5, 7].

In fact, conductivity varies for different tissues and different field frequencies. For example at a frequency of 1 GHz, conductivity in Bone marrow is 0.04 S/m, while in cerebro-spinal fluid is about 2.45 S/m. Furthermore for a given tissue type, their conductivity increases considerably and non-linearly with frequency. For instance, for a frequency range between 10^5 and 10^{10} Hz the conductivity is hundred folded [16].

The water content of each tissue is important when analysing RF absorption. In the context of this work, it is expected that the maximum energy absorption will take place in the more absorptive high water content tissues near the surface of the head [6].

The biological effects of microwaves and radiofrequency fields are dependent of the electric field inside the body. The interaction between RF fields and biological tissues can be evaluated through dosimetry studies [10]. Dosimetry is a relatively new domain in electromagnetism [2] and describes the measurement of the absorbed dose delivered by ionizing radiation, i.e. it is the calculation and assessment of the radiation dose received by the human body. Numerical and experimental dosimetries require information pertaining to the electrical properties of the objects [17].

An extensive number of experimental studies In-Vivo [1] and In-Vitro [2] below the exposure limits (cit. by [18]) indicate that radiation from cell phones induces an array of biological impacts ranging from blood-brain barrier leakage to brain, liver, and eye damage in prenatally exposed offspring of rabbits and rats, to genotoxic effects [3] on human cells.

A study of 2008 cited on [7] reveals that due the position of the antenna in hinged phones is generally parallel and adjacent to the hinge, increase the risk of tumours of the parotid gland [4].

Also, a long-term study in Israel that studied the incidence of parotid gland tumors in that country, found an increase of 65% of cases between 2002 and 2006. According to the author [19], Israelis are heavy users of cellular phones, with a 6-fold increase in usage (by minutes) from 1997 to 2006. However, data on individual exposures to cell phones are not available to those authors, and because of that no causal association with parotid malignant tumors can be ascertained, which suggest the need of further research.

A study of 2016 [20] suggests that there is a correlation between EMRFR (Electromagnetic Radio Frequency Radiation) and Tinnitus, which is a the perception of noise or ringing in the ears. This study collected evidence for the association between exposure to EMRFR and tinnitus in some patients, particularly those suffering from electromagnetic hypersensitivity.

According to [21] (2016) there is risk of mutation and sexual trauma and consequently a risk of infertility due to the effect on male sexual cells, if the mobile phone is near to the waist. Other observational human study [22] found a significant 59% decline in sperm count in men who used cell phones for four or more hours per day as compared with those who did not use cell phones at all, which turn the decrease in sperm parameters dependent on the duration of daily exposure to cell phones.

A large study developed in adolescents reveals also that their exposure to cell phones can bring concerns for the future, like fertility or even the appearance of tumours in the proximal femur or pelvis, due the use in pockets near to the body [23]. There are far fewer studies of any type involving children than adults, although there is broad agreement that children are likely to be more susceptible to biological or health effects from cell-phone use [7]. According US Environmental Protection Agency (2013, cit. by [7]), the children are more sensitive to radiation due its rapid growth, and consequently the fact that there are more cells dividing and this constitutes a great opportunity for radiation to disrupt the process.

The fact that children are more vulnerable to EMFs are described and occurs for two main reasons. The first reason is the fact of children weight is smaller, which leads to an increase of the absorption of RF comparatively to adults under the same exposure conditions. The second reason is the position of areas of the brain that changed to some extent during growth with respect to the location of the ear and also the angle at which the phone sits between the ear and the mouth that is

[1] In vivo (Latin for "within the living") refers to experimentation using a whole, living organism as opposed to a partial or dead organism. Animal studies and clinical trials are two forms of in vivo research.

[2] In vitro (Latin for within the glass) refers to the technique of performing a given procedure in a controlled environment outside of a living organism.

[3] Genotoxic effects are effects that damage the genetic information within a cell causing mutations, which may lead to cancer.

[4] Parotid Gland is the major salivary gland presents on either side of the mouth and in front of both ears

more horizontal in a child, which brings differences in the location of the maximum energy from the phone in relation to an adult.

A study of 2010 [24] also concluded that it is the cerebellum the region most exposed in children while the temporal lobes were most exposed in adults. Tissues or regions that have a similar distance to the phone for adults and children, such as the pineal glands, do not experience age-dependent exposure.

The eyes are other organ that have a greater absorption in children than adults. This fact is due closer proximity the eyes to the phone, however, this does not represent a problem as the exposure of the eyes by mobile phones is very low [24]. Also in children the absorption of EMF in bone marrow is 10-fold higher than in adults as a result of its significantly conductivity.

Accordingly to WHO [8], radio-frequencies of low intensity do not cause adverse effects on human health, but some minor effects are described such as changes on cerebral activity, changes on reaction times and on sleep patterns. Same article also refers the increase of cerebral cancer, but since technology is recent, long term effects cannot be neglected.

2.1.2.1 Brain effects

Numerous sources of EMF are nowadays very close to the human body. An example is the cell phones that touch the head regularly, making it possible an interference with brain activity. The literature its controversial because it suggests that some aspects of cognitive functions and measures of brain physiology may be affected, but it does not offer a uniform view. These include changes in memory tasks, response patterns, normal sleeping EEG patterns, and other brain functional changes. Subjective symptoms such as dizziness, disorientation, nausea, headache, and other unpleasing feelings such as a burning sentient or a faint pain might be a direct result of RF radiation although such symptoms are very general and may have many causes. [25].

The actual outcomes from the majority of studies have no serious implications for human health, but some studies went further and reveal correlations between EMF produced by cellular phones and increasing risk on brain. In particular, in long-term studies, taken place for over a decade, it has been found significantly increased risks of brain cancer [18].

A large amount of studies that refer brain effects are performed in-vivo, mostly in rats. Evidence has been found of alterations of cognitive functions, gene expression alterations in cerebellum, cortex and hippocampus and changes of neurotransmitter levels such as decrease of cholinergic activity [26].

Other studies have been conducted in humans. A study of 2011 [27] concludes that there were suggestions of an increased risk of glioma, a type of tumor that starts in the brain or spine, in long-term mobile phone users with high RF exposure and of similar. Previous studies mentioned in this paper analysed risk in relation to amount and duration of use of mobile phones, but this paper suggest that their impact can be substantially modified by communication system, frequency band and tumour location. Thus, it is important to take these into account in future studies.

An extensive review of 18 epidemiological studies [7] has shown the risk of acoustic neuroma[5] and glioma[6] increases with prolonged exposure (more than 10 years) to cellphone radiation with the risk highest for ipsilateral [7] exposure, which means the tumour is on the same side of the head as that to which the phone is usually held [28]. Another meta-study[8] (Khurana et al., 2009 cit. by [18]) found a nearly 2-fold increase risk of brain cancer in 10 years of ipsilateral use.

A study of 2016 showed the people who spend more than 50 minutes a day using a cell phone could have early dementia or other thermal damage due to the burning of glucose in the brain [21].

According to Hardell (2008, cit. by [7]), one can correlate age of first use of a mobile phone and incidence of glioma, with a 5-fold increase after 10 years in those who start using them before reaching the age of 20. But this results were produced in a very small sample, which demand a further research with this age group as time passes.

It has been shown that RFR leads to increase in the permeability of the blood–brain barrier (BBB)[26], which is hydrophobic barrier[9], formed by vascular endothelial cells[10] of the capillaries in the brain, with tight junctions between these endothelial cells. The function of this barrier is to protect the mammalian brain[11] from potentially harmful compounds in the blood. When this barrier is damaged or the permeability is increased, the normally excluded molecules can pass through, possibly bringing toxic molecules out into the brain tissue.

In children the biological effects of EMF can be grossly different than adults. This was the conclusion reached by a study of 2010 (Christ et al. cit. by [7]), who demonstrates that exposure to RF in the brain from cellphone calls is higher in toddlers and children than adults.

All of these findings and more studies of last ten years resulted in the International Agency for Research on Cancer (IARC) declare that RF radiation (range of 30 kHz to 300 GHz) is a Class 2B carcinogen, i.e. a possible human carcinogen [1]. They defined carcinogenicity of category 2B substances to have limited (or inadequate) evidence in humans but less than sufficient evidence in experimental animals.

2.1.3 Radiation measurement on biological tissues

The absorption of energy is defined by SAR, the specific absorption rate. The Institute of Electrical and Electronics Engineers (IEEE 2005 cit. by [29]) defines "specific absorption rate (SAR) as the time derivative of the incremental energy absorbed by (dissipated in) an incremental mass contained in a volume element of given density.". The International Commission on Non-Ionizing Radiation Protection (ICNIRP) (1998 cit. by [29]) defines "specific energy absorption rate (SAR) as the rate at which energy is absorbed in body tissues, in watt per kilogram (W/kg). SAR is the dosimetric measure that has been widely adopted at frequencies above about 100 kHz".

[5] Neuroma is a tumor of nerve tissue.

[6] Glioma is a type of tumor that starts in the brain or spine in glial cells.

[7] Situated on or affecting the same side.

[8] Meta-study or Meta-analysis is a statistical analysis that combines the results of multiple scientific studies.

[9] Barrier that exclude water molecules.

[10] Endothelial cells are part of endothelium, which is a type of epithelium that lines the interior surface of blood vessels and lymphatic vessels.

[11] Mammalian brain is the middle layer of the brain (See appendix B

For an EMF, in the case of a harmonic excitation and after steady state has been reached, SAR is given by the following expression:

$$SAR = \frac{\sigma_E}{2\rho}|E^2| \tag{2.17}$$

σ_E is the tissue electric conductivity (S/m), ρ is mass density of the tissue (kg/m^3) and E is the amplitude of generated internal electric field (V/m).

Part of the energy carried by a time-harmonic EM field is deposited in lossy objects by inducing conduction currents. The power loss (L) produced by the conduction current σE results in Joule heating of the region. In paricular, L can be computed by integrating the power density within the lossy volume R:

$$L(R) = \frac{1}{2}\int_R \sigma E \cdot E^* dv \tag{2.18}$$

where $E \equiv E(r,\omega)$ is the time-harmonic electric field phasor (V/m), $E \cdot E^*$ is E^2 which denotes the squared magnitude of the induced electric field and $\sigma \equiv \sigma(\vec{r})$ is the electric conductivity $(1/\Omega m)$ at every location $r = (x,y,z) \in R$.

The total SAR of a body is obtained by an arithmetic mean of the SAR values for each point of the body. The accuracy of SAR value depends on the accuracy of the parameters. So it is important to use in 2.17 the most realistic electrical conductivity and mass density of the tissue, as well as induced electric field.

The expression 2.17 is the one used in Sim4life simulator to obtain local SAR. However, the local SAR is not always useful, because it is too sensitive to approximation in the computational methods. Moreover, due the heat conduction, the energy deposited at a point is invariably smeared out, which makes a value of a single point not significant thermally.

For this motive, the averaged form of SAR is the one mostly presented in literature. This form has multiple definitions based on different types of approaches: over the region mass (M) or over the region volume (V):

$$\langle SAR \rangle_M = \frac{1}{M}\int_{R(M)} SAR(r) dm \tag{2.19}$$

$$\langle SAR \rangle_V = \frac{1}{V}\int_{R(V)} SAR(r) dv \tag{2.20}$$

where M is the mass of the integration region R,

$$M = \int_R \rho dv \tag{2.21}$$

and V is the volume of the integration region R,

$$V = \int_R dv \tag{2.22}$$

These two equations are both commonly used, but on different contexts. The equation 2.19 (in W/kg) is mainly used to perform dosimetry studies by the telecommunications community, while the equation 2.20 (in W/m^3) is currently used to study the exposure of Magnetic Resonance Imaging (MRI) machines [30].

The mass-averaged SAR can be rewritten in terms of power loss (L) by substituting equation 2.17 in equation 2.19 and considering $dm = \rho dv$. This leads to a combining expression to compute and compare values of SAR, that is,

$$\langle SAR \rangle_M = \frac{1}{2M} \int_{R(M)} \sigma E^2 dv = \frac{L(R)}{M} \tag{2.23}$$

Since the exposure to EM fields could be a problem, several organizations and governments have developed exposure standards, to regularize the emission of electromagnetic waves. These standards recommend safe levels of exposure for uncontrolled environment to which the general public is subject, and also for controlled environment, of which work environments where persons are exposed as a consequence of their employment are examples. These limits are different because those persons are fully aware of the potential for exposure and can exercise control over their exposure [5].

The recommended safe levels are not completely consensual across organizations, but the various implemented safe levels are all similar [5].

With reference to SAR values for uncontrolled environments, both the local tissue SAR and whole body average are important. The whole body mass averaged SAR should not exceed 0,08 W/kg, while the IEEE limit is 1.6 W/kg over 1 g of tissue (reference for United States) and the CENELEC (European Committee for Electrotechnical Standardization) limit is 2 W/kg over 10 g of tissue (reference for Europe) [31]. Due to the fact that these limits are calculated averaging different amount of tissue, the two limits are not directly comparable. This standard tissue averaging technique of the local SAR values over 1 or 10 g contribute to decrease the uncertainty in estimating SAR.

Those standards were developed considering a short-term exposure and were not developed to protect against possible long-term exposure to low-level RF radiation because such hazards, if any, are not well understood [5].

For estimating the values of SAR in 1g or 10g of tissue, it is used a quantity named Peak Spatial Average SAR that is defined in the latest standard by IEEE and International Electrotechnical Commission (IEC)[12][30].

This type of evaluator - Peak Spatial Average SAR - is implemented as an averaging operation on a quantity Q

[12]IEEE/IEC62704-1 Recommended Practice for Determining the Peak Spatial-Average Specific Absorption Rate (SAR) in the Human Body from Wireless Communications Devices, 30 MHz - 6 GHz: General Requirements for using the Finite Difference Time Domain (FDTD) Method for SAR Calculations

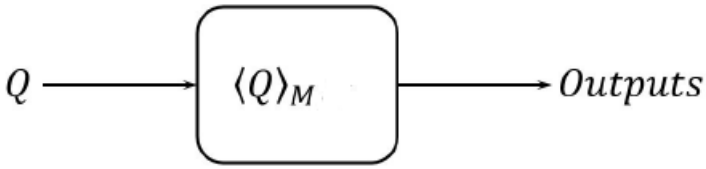

Figure 2.4: Peak Spatial Average SAR over a mass - Basic working principle [30].

over a predefined region mass (1g or 10g of tissue),

$$\langle Q \rangle_M = \frac{1}{M} \int_{R(M)} Q(r) dm \tag{2.24}$$

where M is defined on equation 2.21 and refers to the mass of the integration region R.

Peak Spatial Average SAR is obtained using equation 3.8 with $Q = SAR(localSAR)$. Further will be explained how the simulator uses this formula for the calculation.

Several factors can influence the local SAR. These factors include the antenna type, antenna radiation efficiency, antenna inclination with the head, distance of antenna from head, effect of the hand holding the handset, and the structural accuracy and resolution of the head model [6]. Therefore, each investigator can set various conditions to obtain the SAR values.

The way of determining SAR is either done via computer modeling or experimental measurements done with "dummy" models of the human anatomy comprised of materials which mimic the electrical characteristics of human tissues, since there is no practical way of measuring SAR in humans.

In biological tissues, the absorption of microwave energy may result into an increase of their temperature. Before any heat exchange mechanisms, in an initial period, it can be shown that the change of the temperature is linear and the SAR can be estimated by

$$SAR = c_h \frac{dT}{dt} \tag{2.25}$$

where c_h is the specific heat capacity of the tissue ($J/(kg \cdot °C)$) and dT/dt is the temperature rise in the tissue in the time interval of the irradiation [32]. SAR is sometimes confused with thermal effects of non-ionizing radiation, due its value deriving from transient temperature rise. However SAR is just a dosimetric quantity expressing the rate with which the energy of non-ionizing radiation is deposited inside the tissues.

By way of example, relating SAR with heating temperature, a SAR of 1 W/kg equates to a heating rate of less than 0.0003 °C per second in muscle tissue. In about one hour, this corresponds to a rise in temperature of 1 °C. A tissue disruption has been observed at a SAR of 4 W/kg, in a reversible mode. The permanent adverse effects have been found at a SAR above 5 W/kg [5].

In particular in head and brain tissues, according to [33], a temperature increase of 4.5 °C in the brain has been noted to be an allowable limit, which does not lead to any physiological damage

(for exposures of more than 30 minutes). Additionally in skin, the threshold temperature of the pricking pain is 45 °C, corresponding to the temperature increase of 10-15 °C.

Also, other aspect to take in consideration is the fact of the electrical properties of tissues – especially of the head – in all animals change with age. The main change is the relative permittivity, which is calculated to be around 40 in an adult human brain, while in a young child's brain is between 60 and 80 leading to duplicate the radiation absorption and SAR [16].

Not only the above mentioned parameters should be taken into consideration when calculating SAR with EMF from mobile phone. Others parameters are important and should be treated carefully in the analysis. These parameters are operational frequency and antenna power, mutual positions of the device and head, design of the device, size and the shape of human head, distribution of tissues within the head [9].

For a relation with temperature of the tissues, it can be said that the differences in temperature between different locations of a tissue or organ are extinguished short time after the beginning of a constant exposure and temperature gets evenly distributed within a whole organ or even body. Moreover, specific heat is independent from the external field and depends only on tissue properties [16].

SAR translates a good rate to measure the effects of the EM radiation in human tissues, however sometimes this measure is not enough. It can be thought that a high level of SAR in any tissue above the SAR limits means directly that the device or antenna is dangerous for human use. But to better conclude that, as mentioned before, it is necessary to know the time of exposure of tissues to EM fields and to obtain the increase of temperature of the tissues. Finally, it is necessary to obtain the increase of temperature of the tissues to conclude if the radiation effects are dangerous for human use or not.

An helpful equation for a practical analysis the heat transfer due the increase of the temperature of biological tissue on humans is Penne's bio heat equation that considers the thermoregulation and the blood flow of the tissue, [34]:

$$\rho c \frac{dT}{dt} = \nabla(k\nabla T) + Q_{met} + Q_{ext} - \rho_b c_b w(T - T_b) \tag{2.26}$$

where ρ is mass density of the tissue (Kg/m^3), k is thermal conductivity of the tissue ($W/m/°C$), ρ_b is blood mass density (Kg/m^3), c_b is blood heat capacity ($J/Kg/°C$), T_b is body core temperature, T is the final temperature considering the EM fields exposure, Q_{met} is metabolism heat source (W/m^3), Q_{ext} is external heat source (W/m^3) which is equal to the electromagnetic power absorbed and w is blood perfusion rate ($1/s$), which is the volume of blood flowing through unit mass of tissue per minute.

Relatively to frequency, studies [15] concluded that SAR is affected by operational frequency, increasing with the frequency.

2.2 Antenna radiation

An antenna is defined by the IEEE as the part of a transmitting or receiving system that is designed to radiate or to receive electromagnetic waves [5]. Mobile phones are equipped with several antennas that allow the transmission of electric signals through empty space.

2.2.1 Mobile phone antenna design

In the last decades, the technological advances on cell phones antennas are significant. Antenna designers have been challenged by the small mobile terminals and the importance to have more sophisticated elements to equip the antenna. The focal point of antenna design is shifted from its physical features, such as small size and light weight to sophisticated electromagnetic structure. Numerous aspects, like propagation features, local environments, system compositions and performance, Signal Noise Ratio (S/N) and bandwidth features, have to be taken into consideration when designing an antenna.

2.2.1.1 Parameters of Mobile Phone Antennas

Radiation pattern

The radiation pattern or antenna pattern is a graphical representation of the power radiated through the antenna as a function of direction. The antenna pattern is actually a three-dimensional plot, but it is common to describe this 3D pattern with two planar patterns, called the principal plane patterns. These principal plane patterns are obtained by making two slices through the 3D pattern through the maximum value of the pattern. Thus, the antenna's radiation properties are commonly characterized by these two principal plane patterns, working better for antennas that have well-behaved patterns, because, in that case, not much information is lost when only two planes are shown.

Directivity

Directivity is one of the antenna parameters that represent the measurement of the direction of the radiation pattern, helping to determine the efficiency of the antenna. An isotropic antenna, i.e. an antenna that radiates equally in all directions would have effectively zero directionality, and its directivity would be equal to 1 (or 0 dB).

The directivity can be calculated by determining the maximum value of the magnitude of the radiation pattern.

As the signal received by a mobile phone can be sent from different directions, the concept of directivity is not useful is this particular case, so the mobile phone antenna should have a low directivity (between circa 2 dB for a half-wave dipole antenna and 5-8 dB for a microstrip antenna).

Polarization

Antennas are also classified by their polarization, which is a fundamental antenna concept. This concept defines the type of plane wave polarization the antenna is most sensitive to. The polarizations of electromagnetic wave depend on the electrical field, which is perpendicular with the magnetic field and can be classified in three different types: Linear, circular or elliptical.

Linear polarization means that the electrical field vector direction is constant.

Other possibility is having the electric field vector direction rotating in time as it travels through space. In this case, wave (or antenna) is elliptically polarized. As a special case, if the wave spins out in a circular path, it means that the wave is circularly polarized. Elliptical and Circular polarization can be divided into two types regarding the direction in which the ellipse or circle, is right elliptical/circular polarization if it is rotating clockwise as seen from the source or, on the contrary, left elliptical/circular polarization if rotating is anti-clockwise.

Polarization of antennas is one of the fundamental characteristics of any antenna since it implies that certain antennas are sensitive to particular types of electromagnetic waves. In practice, it means that two antennas with the same polarization in a given path will provide the most efficient communication.

Input Impedance

Antenna input impedance relates the voltage to the current at the input to the antenna. The knowledge of the input impedance is advantageous because it allows the choice of more suitable transmission line.

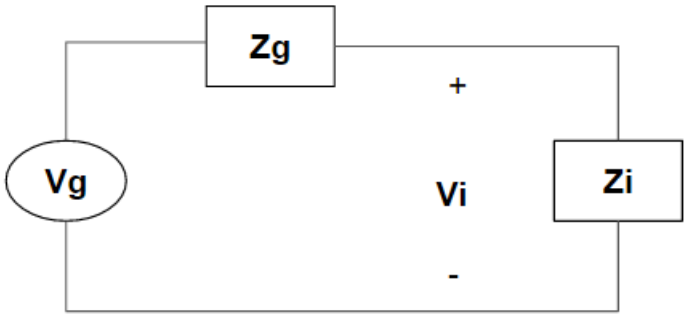

Figure 2.5: The equivalent circuit of an antenna and the transmission line.

Figure 2.5 represents a equivalent circuit of an antenna and the transmission line, which must have an impedance (Z_g) matched with antenna impedance (Z_i), otherwise the impedance mismatch will cause a reflection wave back to the signal source. More specifically, the maximum power at the antenna from source is achieved when Z_g is equal to Z_i conjugated.

VSWR

The Voltage Standing Wave Ratio (VSWR) is a real number (greater or equal to 1), which represents a measure of how well matched the antenna is to the transmission line or receiver. If VSWR is equal to 1, it indicates that the antenna is perfectly matched to the transmission line or receiver (no mismatch loss). If the antenna is not perfectly matched to the transmission line or receiver, it means that it exists a mismatch loss and VSWR value is greater than 1.

Antenna efficiency

The efficiency of an antenna is the most fundamental and important antenna parameter and can be understood as a measure of how much power is radiated by the antenna relative to the antenna input power. Antenna's efficiency is translated by the expression:

$$\xi = \frac{P_{radiated}}{P_{input}} \tag{2.27}$$

If the value of efficiency (ξ) is high, this means the antenna radiates most of the power present at it. On the contrary, if the value of efficiency is low, the antenna has most of the power absorbed as losses within the antenna, or reflected away due to impedance mismatch.

Efficiency can decrease due to conduction losses (relative to finite conductivity of the metal that forms the antenna), dielectric losses (relative to conductivity of a dielectric material near an antenna) and impedance mismatch loss. Typical mobile phone antennas have efficiencies in range of 20% to 70% (i.e. from -7 to -1.5 dB). The efficiency of an antenna is directly related with the antenna gain, as it can be seen above.

Antenna gain

Antenna Gain is a measure of power radiated in a particular direction (typically the peak direction of radiation). Antenna gain (G) can be related to directivity (D) and antenna efficiency (ξ) by the expression:

$$G = \xi \cdot D$$

The gain of an antenna is the result of the ratio of the power gain in a given direction to the power gain of a reference antenna (commonly an isotropic antenna, i.e. an antenna with a spherical radiation pattern) in the same direction. Being the gain of an isotropic antenna equals to 1 (or 0 dB), the antenna gain expressed in dBi is obtained by the following expression:

$$G_{dBi} = 10 \times \log\left(\frac{G_{Numeric}}{G_{Isotropic}}\right) = 10 \times \log(G_{Numeric})$$

Isotropic antenna is not always used as the reference, it also can be used a theoretical dipole as the reference in case of omnidirectional antennas of higher gain, being the power rating difference between dBd and dBi approximately 2.2, i.e. 0 dBd = 2.2 dBi.

An antenna with gain doesn't create radiated power, the gain is just a characterization of the way the power is radiated.

In particular the mobile cellular antennas should have a low gain, since the cellular antenna can be held in any orientation, and can be in any position relative to the network tower.

Antenna Beamwidth and Side lobe Levels

Antenna Beamwidth and Sidelobe Levels are a characterization of the antenna's pattern, which can be divided in a main lobe, a side lobe and a back lobe, depending on the portion of the pattern in which the lobe appears (See Fig. 2.6).

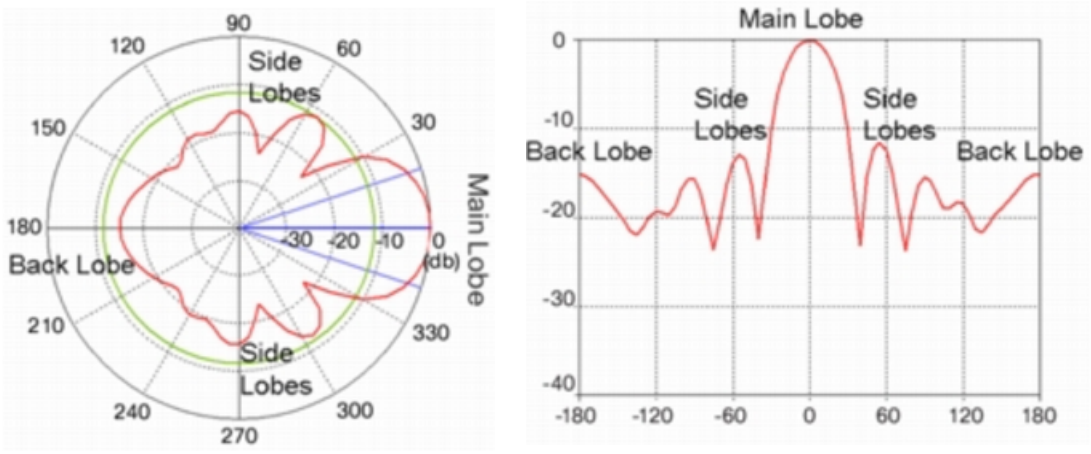

(a) Pattern in polar coordinates

(b) Pattern in cartesian coordinates

Figure 2.6: Radiation Patterns in Polar and Cartesian Coordinates Showing Various Types of Lobes

The main portion of the pattern is called the main beam (in the case of the figure 2.6a is centered at 0 degrees) and represent the region around the direction of maximum radiation (usually the region that is within 3 dB of the peak of the main beam).

The other portions besides the main beam are called side lobes and usually represent unwanted radiation in undesired directions, which can never be completely eliminated. The particular side lobe that is located in the opposite direction (in the case of the figure 2.6a at 180 degrees) is called the back lobe. The sidelobe level (SLL), the is maximum value of the sidelobes and represents an important parameter used to characterize radiation patterns.

Other important value to characterize radiation patterns is the Half Power Beamwidth (HPBW), which is the angular separation between the two points in which the magnitude of the radiation pattern decrease by 50% (or -3 dB) from the peak of the main beam. This is illustrated in Figure 2.6a, HPBW is shown as the angle between the two blue lines in the polar plot.

Related to gain, it can be said that antennas with wide beamwidths typically have low gain and antennas with narrow beamwidths tend to have higher gain.

Effective area

Effective area, also know by effective aperture is a measure of the power captured by an antenna from a plane wave. The power received by the antenna gets associated with collective area known as effective area. It can be expressed as a function of the antenna gain and the wavelength:

$$A_e = \frac{\lambda^2}{4\pi} G$$

Bandwidth

An antenna radiates in a frequency range, which is called Bandwidth. This parameter is absolutely important in an antenna design, since it is through it that an antenna can be suitable to perform certain operations, e.g. very narrow bandwidths cannot be used in wideband operations.

Bandwidth is typically quoted in terms of its Fractional Bandwidth (FBW). The FBW is calculated through the ratio of the frequency range to the center frequency (Examples of two typical antennas in table 2.2.

Table 2.2: The Bandwidth for Two Common Antennas

Antenna	Center Frequency (MHz)	Frequency Range (MHz)	FBW
Patch	1000	985-1015	0.03
Dipole	1000	960-1040	0.08

2.2.1.2 Antenna types

The choice of the type of antenna for a particular type of phone is normally determined by dimensional considerations and SAR regulations. There must be a compromise among volume, impedance bandwidth and radiation characteristics of an antenna while making the smallest possible antenna.

The firsts mobile handsets employed monopole antennas that had omnidirectional radiation patterns with horizontal polarization. Monopole antenna is an antenna which consists of a one straight rod conductor and it is installed over a ground plane (conductive surface). Monopole antennas are fed at lower end, close to ground plane which works as a reflector.

However, these type of antennas caused severe limitations due the linear polarization. Monopole antennas were replaced with the next generation of helical antennas that has a wide bandwidth and circular polarization [35].

External antennas, such as monopole and helical antennas, generally have excellent bandwidth and efficiency performance, but have a high SAR. Nowadays, the external antennas were shifted into the device becoming internal antennas. These internal antennas were gradually introduced into mobile phones to facilitate more flexibility in the industrial design and SAR reduction [36].

Some of the types of internal antennas inside mobile phones are the Planar inverted-F antennas/microstrip antenna (PIFA/MSA), the ungrounded monopole type [36] and fractal antenna[37]. Those kinds of antennas can cover a single band, dual band, wideband and multiband based on the design of the antenna.

A PIFA is generally considered to be a MSA on a finite ground plane with a ground connection. It can be considered a planar monopole antenna (PMA) if the antenna is an inverted-F antenna (IFA) with no ground plane parallel to the antenna.

PIFA are widely used in mobile phone design due its advantages [5, 38, 35]. The main advantage is having reduced backward radiation toward the user's head, due to the ground plane upon which the PIFA resides. This feature helps reduce the power absorption by the head, minimizing SAR in hand-held environment and enhance antenna performance [5, 35]. Other advantage is its capacity of hiding into the housing of the mobile when compared with other types of antennas (e.g. whip/rod/helix antennas). A third advantage is the moderate to high gain in both vertical and horizontal states of polarization, which is useful in certain wireless communications where the antenna orientation is not fixed and the reflections are present in the environment [5, 35]. Other advantages relate to PIFA economical benefits, multiband operation, low profile, lightweight, circular polarisation or diversity of polarisation.

The fact that PIFA can easily be implemented in a small space and embedded in a handset constitutes other advantage of this type of antenna [39]. PIFAs can have several configurations and variations of their form. Often one or both arms are folded around a supporting plastic mold or printed onto it. The variations of PIFAs include shorted patch, stacked shorted patch, shorted patch antenna with L probe feed, shorted U-slot patch, and folded shorted patch. To improve its impedance match, a shorting pin and wall are commonly added to such antennas (cit. by [35]). Sometimes the antenna is printed onto a flexible printed circuit board material and then positioned inside the handset [5, 35]. However, there are also a significant problem: the narrow bandwidth. This problem can be fixed by designing a wideband or multiband antenna, which can cover more frequency such as using one antenna that can cover the very important mobile phone bands which are in use in most countries GSM, UMTS, Wi-Fi and LTE.

In a real scenario, a cellular phone has several antennas inside it. There are basically four types of antenna present in a modern mobile. These are namely a primary cellular antenna, used to transmit or receive, a diversity cellular antenna (MIMO antenna), used to receive, a GPS antenna, used to receive and a Wi-Fi antenna, used to transmit or receive.

For these specific mobile phone functions, the manufacturers either use a single antenna with multi-band operations (GPS/ Wi-Fi/cellular works in different frequency bands) or some antennas with single or double band operations. PIFAs have other advantage here because this type of antenna can quite easily be made into multiband antennas by creating separate current paths on the antenna, through the use of slots and parasitics.

2.2.2 Human body effects on antenna performance

In the real situations the antenna is not isolated. The antenna is not only surrounded by elements that provide additional functions to the mobile terminal, but also this mobile terminal is operated by a person, which alone constitutes a material that can cause effects on the antenna performance.

The human body can influence the performance of the antenna, since its effect on the electric and magnetic fields around it can be substantial. Due to the conductivity of the biological tissue

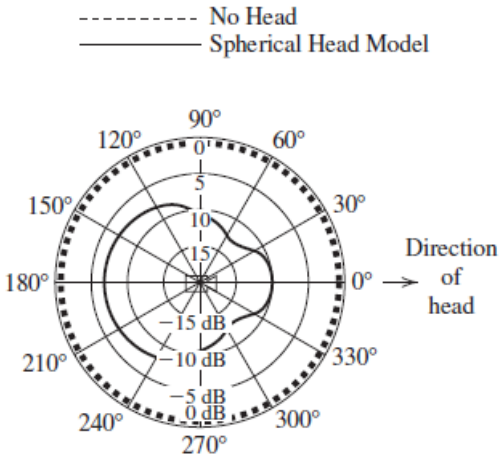

Figure 2.7: Computed radiation patterns in the azimuthal plane for a vertically oriented monopole at 900 MHz. (From [5])

in the human body, the electric field in close proximity to it is reduced significantly. On the other hand, the magnetic field is increased, in accordance with the boundary conditions on tangential E and tangential H [5].

The rising use of mobile phone handsets increase the attention to this body-field interaction and the current reduced size of these types of devices makes the influence more severe. The effect of the human body on mobile phone performance (mainly the radiation pattern and impedance) can be done via experimental measurements or via computer simulation using the FDTD method, as will be seen further on this document.

The main effects of the human body on the radiation from a handset is to decrease the overall radiated power, decrease the radiation in the direction of the head relative to the opposite direction, and in some cases detune the handset antenna [5]. According the same author, a simulated far-field pattern of a monopole antenna on a rectangular box model of a handset located 1.5 cm from the head has a different shape compared to omnidirectional pattern of the monopole without the head present as it can be observed in figure 2.7.

Therefore, it can be concluded that the head alters the pattern of the monopole alone, not only in terms of the shape of the pattern, but also in terms of radiated power level that has a marked decrease when the head is present, due to the absorption of power by the head. Moreover the radiation efficiency is reduced for the monopole antenna system according to

$$\xi_R = \frac{P}{P + P_0 + P_{loss}} \tag{2.28}$$

where P is the power radiated, P_0 is the power dissipated in ohmic losses [13] on the antenna P_{loss} is the power absorbed by the human body. P_{loss} decreases when the distance between the antenna

[13] Ohmic Loss is the process of loss by which the passage of an electric current through a conductor produces heat.

and the head increases, since the tissues of the human body are lossy dielectrics at RF frequencies [5].

The antenna input impedance is other parameter that changes in the presence of the head, and it is visible in the low level of the return loss. This change occurs due the high relative permittivity of biological tissues which leads to change of impedance in the near field zone of the antenna[40]. Some detuning can also exist, when the head is present.

In a planar inverted-F antenna (PIFA), the position of the hand also cause effects on the antenna performance. If the hand covers an appreciable portion of the PIFA, the input impedance of the PIFA is noticeable affected. As the hand is closer to the feed point of the antenna, the PIFA detunes. If the hand is not covering any part of the antenna, the performance is almost the same as if no hand were present.

Several publications have investigated the human body effect on antennas and trough them it can be concluded that the degradations are caused mostly by the operator's hand and head. For those reasons, the placement of the antenna in the handset is a very important question.

Furthermore, there are different factors (e.g. position, distance, band, type of antenna) that determine the intensity of the effects [41].

Chapter 3

Problem characterization

3.1 Defining the problem

The problem focuses in the analysis of the effects on brain of the radiation emitted by an antenna close to the head. The main goal is to measure Specific Absorption Rate (SAR) in the tissues of head, brain and hand regions depending on some variables that, according to studies conducted so far, can influence the SAR value. The variables tested will be the distance between the head and the antenna, the hand effect, the orientation of the antenna, tilt positions and frequency.

3.2 Proposed solution

To analyse the problem, various scenarios will be simulated to search for SAR in the different tissues of the human body. In particular, the tissues that will be the object of study will be the ones in the head, brain and hand.

It is known that the SAR value changes according to some variables. The variables chosen to test SAR in this project were the hand, the distance, the position of the antenna and the frequency. To study the effect of these variables on SAR value, the model will be in a "on call" mode, i.e. the mobile phone is held by the hand and leaning against the ear.

The methods and the models of human body and cell phone will be described in detail in the next subsection. The standard that will be used to calculate the EM effect on the tissues is IEC 62704-1, which is the recommended practice for determining the Peak Spatial-Average SAR in the Human Body from Wireless Communications Devices, in ranges of frequencies between 30 MHz and 6 GHz.

3.2.1 Methods and models

3.2.1.1 Human Head and Hand Model

The human head is a highly complicated structure in terms of material electric properties. In terms of magnetic properties of human tissues, they do not vary significantly, the relative magnetic

permeability is assumed to be $\mu_r = 1$ [32].

The first simulations were performed with a basic EM Phantom, which is a physical model of the human head (Fig. 3.1) that can reproduce the effect of the electromagnetic radiation on human head.

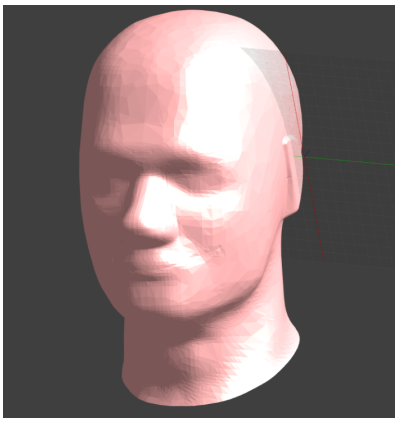

Figure 3.1: SAM head.

This particular CAD EM phantom, known in the literature as SAM head (The Specific Anthropomorphic Mannequin), is based on the 90th percentile dimensions of an adult male head based on an anthropomorphic study of US Army personnel. SAM is composed of a shell of 2 mm filled with homogeneous liquid to represent head tissues. The characteristics of these two materials in the simulations conducted here are shown in table 3.1.

Table 3.1: SAM model elements characteristics

	Type	Mass density ρ [kg/m^3]	Electric conductivity σ [S/m]	Relative permittivity ε_r
SAM shell	Dielectric	1000	0	3.7
SAM liquid	Dielectric	1000	0.97	41.5

Although the SAM head is a really good model of the real human head, it has limitations, since it only has two layers. The real human head contains many different kinds of tissue, and the fluid inside the SAM shell only represents the average electrical properties of the head, and cannot indicate the differential absorption of specific brain tissue [18].

Thus, a more differential anatomical model was considered in order to perform simulations with more faithfulness. That model is part of virtual population (ViP) [42], which consists of 15 detailed anatomical human models based on MRI data from healthy volunteers. The variety of tissues are characterized in an extensive literature-based tissue parameter database [43], specifying its dielectric and thermal properties, perfusion and density [44].

The ViP model chosen was Duke (Fig, 3.2), which consists in an anatomically realistic 3D model of human body with the characteristics specified in table 3.2.

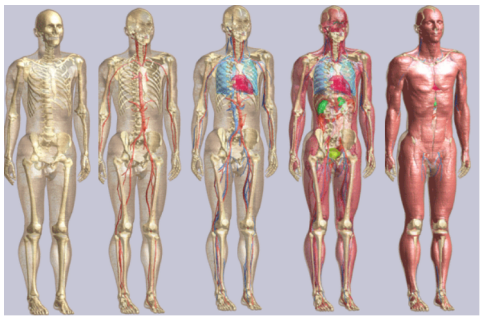

Figure 3.2: Realistic phantom Duke

Table 3.2: General Information of Duke [42]

Sex	male
Type	young adult
Age [Years]	34
Height [m]	1.77
Weight [kg]	70.2
BMI [kg/m²]	22.4

Just like in real biological tissues, the tissues of the realistic phantom have different electrical properties according to frequency (See table 2.1), which are available in a materials database inherent to the simulator itself.

To document the complexity of the human model, the image 3.3 shows two planes of the Duke torso, the mid-coronal plane (i.e. vertical plane that divides the body into ventral and dorsal sections) and the mid-sagittal plane (i.e. which divides the body into right and left sections).

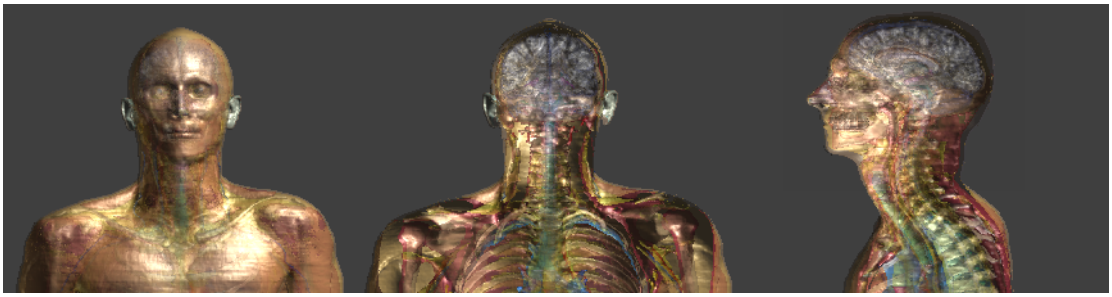

Figure 3.3: Duke torso complete with no section, dorsal section and left section

In terms of location, the antenna will be placed close to the ear, parallel to an imaginary line drawn between the beginning of the helix of the ear and the labial commissure of the corresponding side (See figure 4.7).

3.2.1.2 Antenna Model

The firsts tests that were performed, were used to test the simulator platform (Sim4life) and to gain confidence in the results. Therefore, the first mobile phone model tested was a simple monopole

antenna consisting of a block of $40 \times 16 \times 140$ mm, a cylinder with 2.5 mm of radius and 79 mm of length and a feed point with 1 mm between them (See fig. 3.4). Both the block and the cylinder are made of PEC (Perfect Electric Conductor) materials.

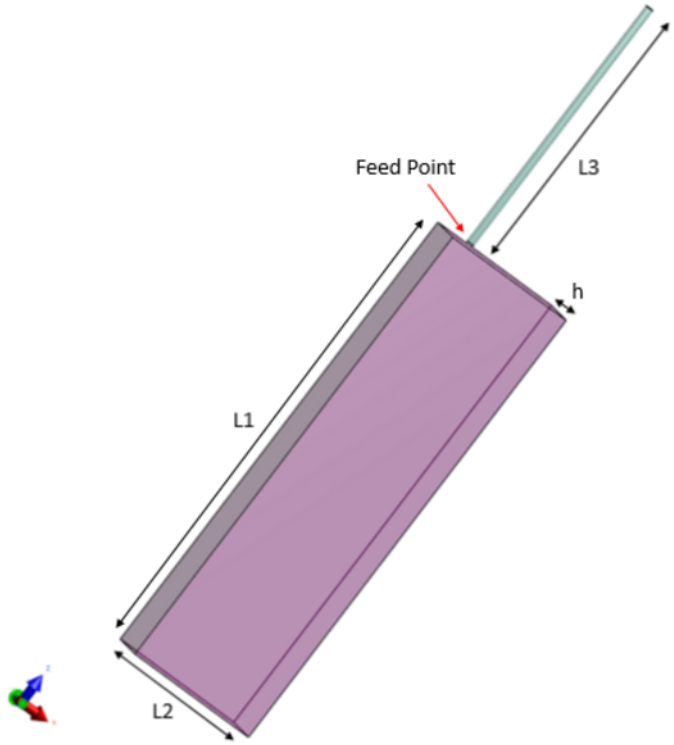

Figure 3.4: Monopole antenna mounted on top of the PEC box.

Table 3.3: Monopole antenna dimensions (in mm).

L_1	L_2	L_3	h
140	40	79	16

This antenna will operate at 900 MHz and to the feed point is connected a generator of a harmonic signal of 1V of amplitude with 50 Ohm internal impedance (Zg). Thus, when designed and simulated on vacuum, the monopole antenna has the characteristics shown in table 3.4.

The values in table 3.4 are related to each other by the following expressions:

$$I = \frac{U}{Z_i} \tag{3.1}$$

$$Pi = \frac{1}{2}\mathrm{Re}\{UI^*\} \tag{3.2}$$

$$\Gamma = \frac{Z_i - Z_g}{Z_i + Z_g} \tag{3.3}$$

Table 3.4: Monopole antenna characteristics at 900 MHz on free space.

Name	Value	Unit
Voltage (U)	$0.73e^{j1.29}$	[V]
Current (I)	$0.01e^{j2.15}$	[A]
Power (Pi)	1.70	[mW]
Reflection Coefficient (Γ)	$0.56e^{-j0.77}$	-
Return Loss	4.97	dB
VSWR	3.59	-
Input Impedance (Zi)	66.29 - 77.03i	[Ohm]

$$VSWR = \frac{1+|\Gamma|}{1-|\Gamma|} \tag{3.4}$$

The radiation diagram of this type of antenna is practically omnidirectional as can be seen in Figure 3.5b. The electric and magnetic field are represented in figure 3.6.

As it can be seen on figure 3.5b the far-field of this monopole antenna is almost omnidirectional, whereas the near field is greater on the bottom of the phone and through the antenna on the top of the phone (Fig. 3.6a). The magnetic field is represented on figure 3.6b.

Then, in order to take into account a more realistic mobile phone antenna, an antenna of type PIFA was designed to respect the dimensions of the more modern mobile phones (Fig. 3.7 and Table 3.6). The dimensions are different according to the corresponding operational frequency. The model of the antenna has a low cost FR4 substrate with dielectric constant of ε_r = 4.4 and electric conductivity of σ = 0.0022 S/m. This prototype was again fed through a 50 Ohm internal impedance.

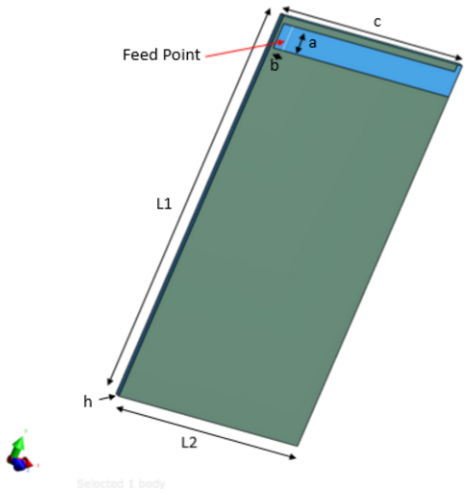

Figure 3.7: PIFA at 900MHz

The antennas have to work with a certain input power and they differ according to the generation that the mobile phone belongs to. The second generation (2G) GSM phones operate with a

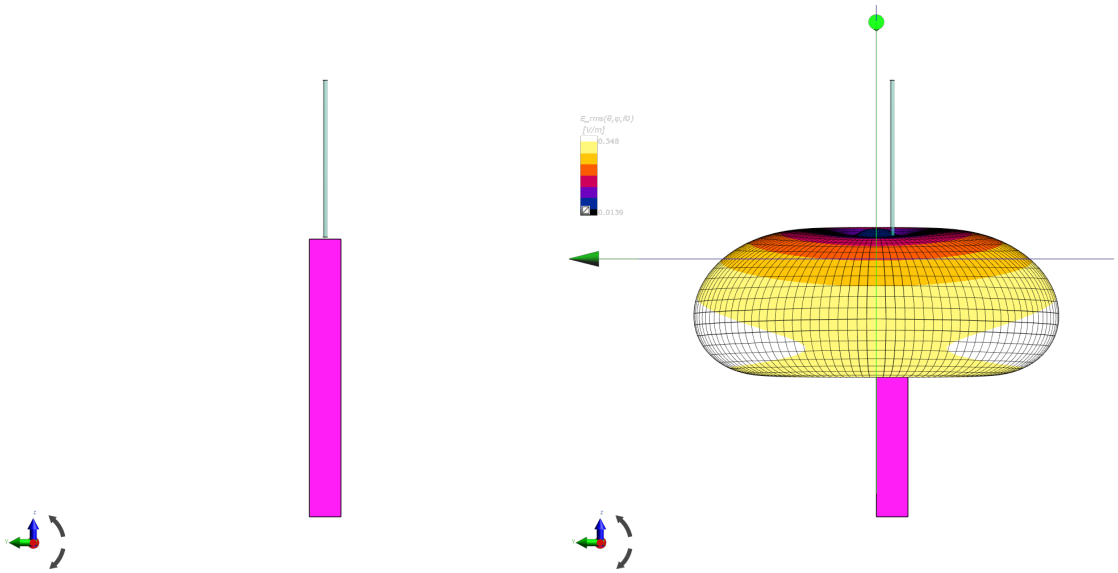

(a) (b)

Figure 3.5: Representation of Monopole Antenna on yz-plan (a) and its Far Field (b) of a monopole antenna at 900 MHz.

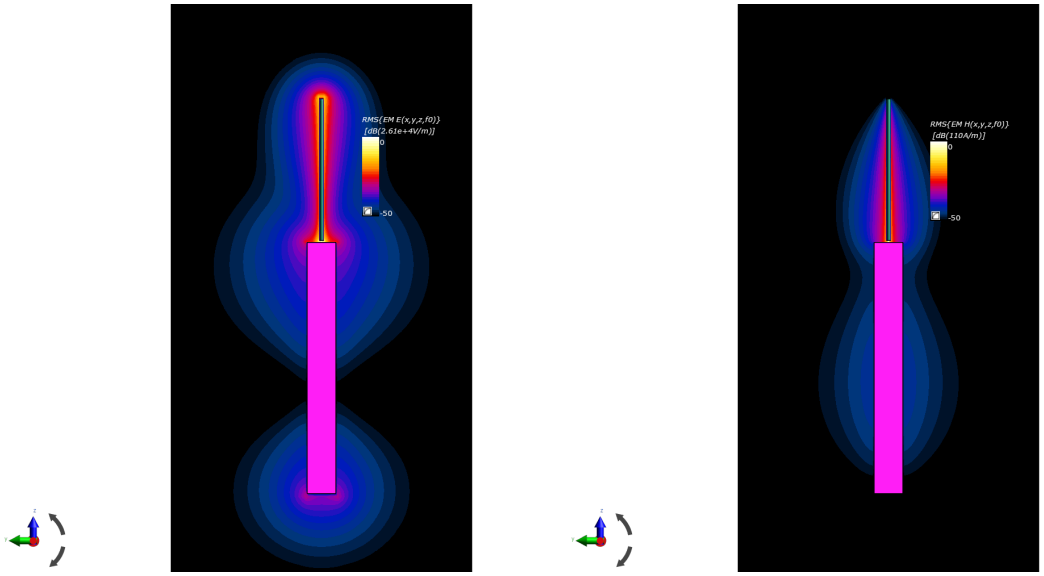

(a) (b)

Figure 3.6: Representation of Electric Field on yz-plan (a) and Magnetic Field on yz-plan (b) of a monopole antenna at 900 MHz.

peak power of 2W or 1W for the 900 and 1800 MHz band, respectively. Despite this, the average power is 133 mW for GSM 900 and 62 mW for GSM 1800, according to Lauer et al. (2013) [45]. The third generation (3G) devices have an average power below 1mW for voice calls.

The power is transmitted in different ways, according the telecommunication standard that is used. For instance, in GSM, the mobile begins the call by transmitting at full power and after several seconds the power control algorithm reduces the power to the minimum required to maintain the radio link, while the UMTS tarts the call by transmitting at the lowest possible power and gradually increases it until the base station receives its access request message and sends back an acknowledgement, which avoids the unnecessary increase of the uplink noise in the cell and guarantees that the initiating of a call is done directly at the minimum transmit power required by the radio link [46].

Furthermore, in GSM the procedure described is renewed after every hand over to another cell, which led to the general advice for limited usage of the mobile phone while travelling fast (and changing many cells). Also, it is a good practice to avoid initiating the call with the phone next to the head, due the call starting with full power [46].

Considered the different frequencies that are used nowadays, four PIFAs were designed for the frequencies 900, 1800, 2100 and 2600 MHz simulating the various generation mobile systems (2G, 3G and 4G) and will be used as the following table:

Table 3.5: Generic Input Powers used on SAR studies according to frequency (900MHz [47, 48, 49, 50, 51, 52], 1800MHz [50, 53, 54, 55], 2100MHz [46], 2600MHz [56, 57]).

	Input Power [mW]
GSM 900	600
GSM 1800	125
UMTS 2100	125
LTE 2600	199

In this work, despite reality, it will be assumed that the device was operating continuously, i.e. the input signal will be a sinusoidal with the same amplitude in all simulation. According to [58], the time averaged power of a GSM device under real operating conditions was 1/8 of its nominal power. For instance, for a nominal operating power of 1 W the actual time-averaged input power was 0.125 W. The actual level depends on the environment in which the user is located and on the manner the terminal is used (e.g. the position of the hand).

Moreover, the standards refers that the value of SAR should be calculated using as input the maximum transmit power of the terminal and not the usual transmit power, which in most cases is lower [46]. However, the input powers for this project were chosen according to powers used in the literature in studies of this type.

Table 3.6: PIFA antenna measures (in mm).

	L_1	L_2	**h**	**a**	**b**	**c**
PIFA 900 MHz	109.6	58.5	1.6	7	3.05	58
PIFA 1800 MHz	105	58.5	1.6	4	2.05	25
PIFA 2100 MHz	104.6	58.5	1.6	2	2.05	21.7
PIFA 2600 MHz	104.6	58.5	1.6	2	2.05	17.85

Table 3.7: PIFA materials characteristics.

	Type	**Mass density [kg/m3]**	**Electric conductivity [S/m]**	**Relative permittivity**
Substrate	Dielectric	1850	0.0022	4.4
Ground Plane	PEC	-	-	-

At this point it is important to know what input amplitude will suit a desired input power. The first antenna that will operate at 900 MHz has a feed point with a harmonic signal of 16.15 volts of amplitude and internal impedance 50 Ohm. The amplitude of 16.15 volts was calculated to obtain an input power of circa 600 mW, power normally used in this type of studies.

The amplitude was obtained performing a first simulation with input of 1V and 50 Ohm to obtain the impedance Z_i. Then, to obtain the equivalent steady-state input power (600 mW), the following equations were used used to compute the required source voltage V_g:

$$P_i = \frac{1}{2}\mathrm{Re}\left\{\frac{1}{Z_i}\right\}|U|^2 \tag{3.5}$$

and

$$U = \frac{Z_i}{Z_i + Z_g}V_g \tag{3.6}$$

The following table (Table 3.8) shows the amplitude used on input for the several frequencies used on free space:

Table 3.8: Calculated input amplitudes for PIFAs in free space by calculation for the several frequencies.

	$Z_i[Ohm]$	$V_g[V]$	$P_i[W]$
PIFA 900 MHz	50.86 + 29.66i	16.15	0.600
PIFA 1800 MHz	44.05 + 24.54i	7.32	0.125
PIFA 2100 MHz	42.21 + 17.94i	7.23	0.125
PIFA 2600 MHz	41.99 + 12.10i	9.04	0.199

Later in this work, it was realized that this calculation was unnecessary, due to a standardization tool that Sim4life has in the Analysis tab. This tool normalizes the input power to the desired one, adjusting the corresponding local SAR and peak spatial-average SAR values. The benefit

Table 3.9: Power Balance of PIFA at 900, 1800, 2100 and 2600 MHz on free space

	Power Balance			
Frequency	900 MHz	1800 MHz	2100 MHz	2600 MHz
Input Power [mW]	600.3	125.1	125.1	199.6
Dielectric Loss [mW]	20.93	2.214	2.126	2.74
Radiated Power [mW]	577.2	122.6	122.6	196. 3
Balance Ratio (Total Dissipated/Input Power)	0.9965	0.9979	0.9970	0.9972

of normalizing with the desired input power is that the SAR values are scaled according to the required input power level.

An example of the simulation on free space will be presented in this chapter with a purpose of describing the method. The other free space simulations for 1800, 2100 and 2600 MHz frequencies will be remitted for appendix A. Moreover, the power balance for every designed PIFA is shown in table 3.9, where a balance ratio close to one was achieved for every frequency as desired. The PIFA working at 900 MHz when simulated on free space has the characteristics presented on table 3.10.

The reflection coefficient is related with return loss, by the expression

$$ReturnLoss = -20\log_{10}|\Gamma| \tag{3.7}$$

Return loss (in dB) is an important measure of the ratio of power in the incident wave to that in the reflected wave. The optimum value of a Return Loss is 10 dB or more, which means that 1/10 of the incident power is reflected. The higher the return loss, the less power is actually lost. Through the table 3.10, can be calculated the return loss for this antenna, which is 11dB.

As can be seen in figure 3.9, the electric field of the antenna has more intensity on the corners of the antenna, specially on the corners of the top. It is important to know where the electric field is stronger, because the regions of the body that are near to that locals will have a larger SAR, due the relation between this quantity and the electric field 2.17.

Table 3.10: PIFA characteristics at 900 MHz on free space.

Name	Value	Unit
Voltage (U)	$9.05e^{j1.81}$	[V]
Current (I)	$0.15e^{j1.28}$	[A]
Power (Pi)	600	[mW]
Reflection Coefficient (Γ)	$0.28e^{j1.25}$	-
Return Loss	10.99	[dB]
VSWR	1.79	-
Input Impedance (Zi)	50.86 + 29.66j	[Ohm]

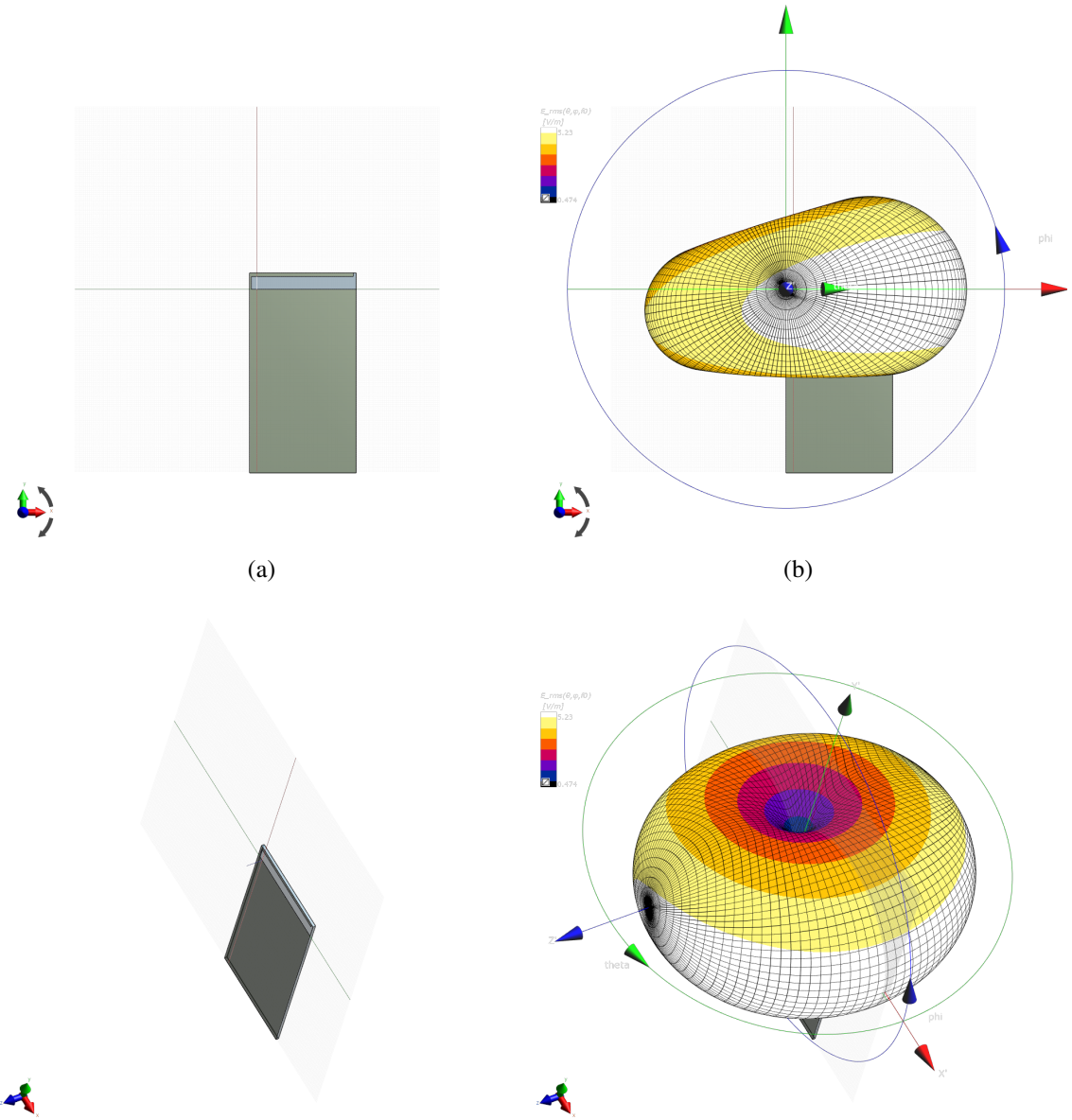

(a) (b)

(c) (d)

Figure 3.8: Representation of PIFA on xy-plan (a) and other perspective (c) and its Far Field, respectively (b) and (d)

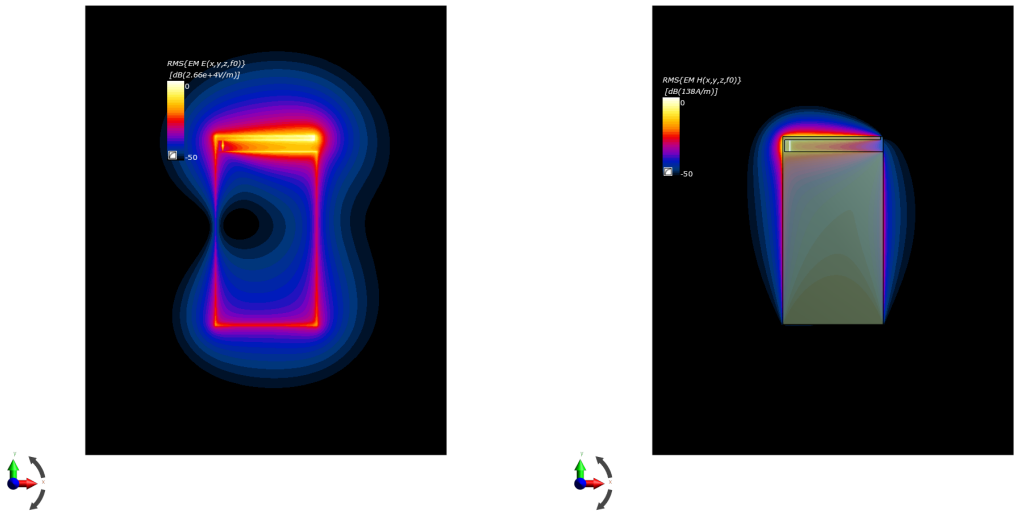

(a) (b)

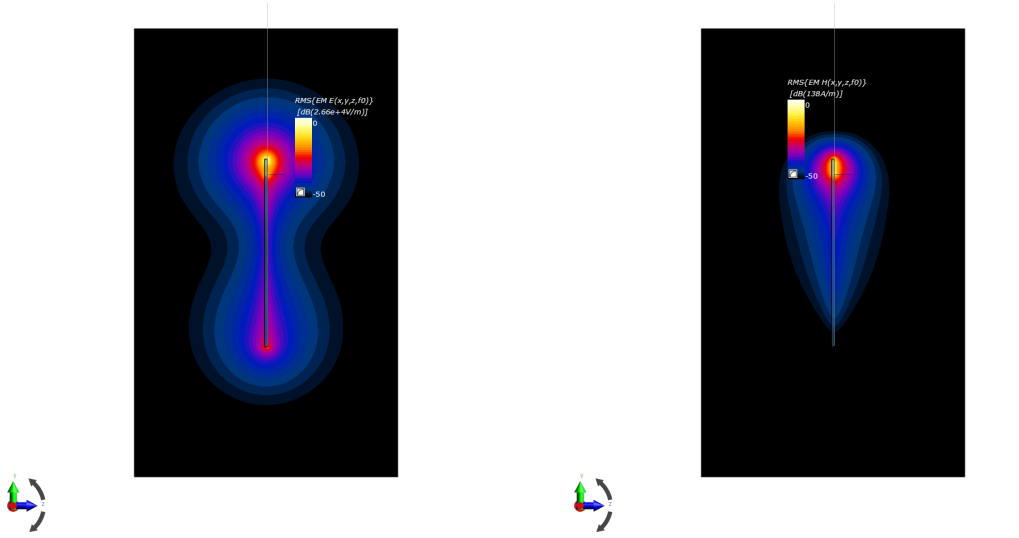

(c) (d)

Figure 3.9: Representation of electric and magnetic field on xy-plan (a)(b) and yz-plan (c)(d)

3.2.1.3 FDTD Method

In order to simulate and achieve conclusions about the direct absorption of electromagnetic energy on human brain tissues, numerical methods are commonly used to solve Maxwell's equations. Specifically to obtain SAR, two methods are the most used: A frequency domain technique called Method of Moments (MOM) or a time domain method called Finite Difference Time Domain (FDTD). The method most commonly used for bioelectromagnetic applications in the range of a few MHz to several GHz is FDTD, because it quickly becomes more efficient in terms of computer time and memory in relation to other methods [9, 46]. Also, it has also been identified as the preferred method for performing electromagnetic simulations for biological effects from wireless devices [59].

From just one calculation, FDTD can provide results for a wide spectrum of frequencies using transient pulse excitation and Fast Fourier Transformation (FFT). FDTD is based on a solution grid or mesh which is composed of box-shaped cells. The electric fields are located on the edges of the box-shaped cell and the magnetic fields are positioned on the faces, creating a topology known as Yee Cell, that is the basis for FDTD. (See Figure 3.10).

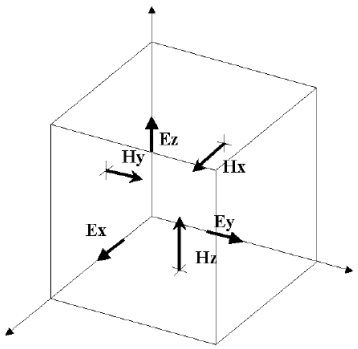

Figure 3.10: Yee cell with labeled field components. [60]

Each FDTD cell will overlap edges and faces with its neighbors, which means that the electric fields at the other nine edges of the FDTD cell will belong to other, adjacent cells. In the same way, each cell will have three magnetic fields originating on the faces of the cell adjacent to the common node of the electric fields.

Also, the material for each mesh edge can be specified independently of other edges. Through the means of calculation for each grid element is chosen the regular grid and this process is extremely fast which allow extremely precise approximations to the actual physical geometry. For instance, by associating many cell edges with materials, a geometrical structure can be formed within the FDTD grid such as the dielectric sphere shown in figure 3.11 where each small box represents one FDTD cell.

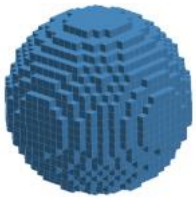

Figure 3.11: A dielectric sphere as meshed in an FDTD grid. The individual cell edges (electric field locations) are displayed as overlapping grid lines. [61]

Regarding the materials, a simulation software based on FDTD is capable of using a wide variety of electric and magnetic materials. The most basic one is the free space and when the simulation starts all the FDTD cells are initialized like that. Likewise, all the fields relating to the cells are updated using the free space equations.

Materials, such as conductors or dielectrics, within the mesh can be added by changing the equations for computing the fields at given locations. For instance, to add a perfectly conducting wire segment to a cell edge, the equation for computing the electric field can be replaced by simply setting the field to zero since the electric field in a perfect conductor is identically zero. By joining numerous end-to-end cell edges defined as perfectly conducting material, a wire can be formed. Introducing other materials or other configurations is handled in a similar manner and each may be applied to either the electric or magnetic fields depending on the characteristics of the material.

The grid cell size is an adjustable parameter that should obey to some requirements. Over one FDTD cell dimension the EM field should not change significantly, what means that, for meaningful results, the grid size should be only a fraction of the wavelength of the highest significant frequency content f_U (upper operating frequency of an antenna) in the excitation frequency spectrum. The major portion of the frequency spectrum lies between zero and $f_U = 1/\tau$ for a pulse of width τ (Fourier analysis). The Nyquist sampling theorem would suggest that the cell size be less than $\lambda/2$ in order that the spatial variation of the fields be adequately sampled. However in cases where the pulse has frequency content is higher than f_U, a higher spatial sampling rate (i.e., smaller cell size) is required [5].

The cell size are is related to the accuracy of the results, and thus, to minimize the effects of numerical dispersion, it has been found that the cell size should be smaller than $\lambda_U = 10$ in the material medium, $\lambda_U = 20$ if computational resources allow. Details of the considered geometry may dictate a smaller cell size [5].

The use of many very small mesh elements which can be computed quickly is the FDTD strategy in order to use very little computer memory. In fact, FDTD calculations with millions of cells can be computed in few minutes [9].

Another advantage relates to the thermal solver being completely compatible with the electromagnetic solver [9].

The FDTD algorithm is the most widely accepted computational method for SAR modeling, in the last thirty years, since it has been stated by the Federal Communications Commission of the United States in OET Bulletin 65, "Evaluating Compliance with FCC Guidelines for Human

Exposure to Radiofrequency Electromagnetic Fields", Supplement C. Also, it refers that FDTD method "adapts very well to the tissue models that are usually derived from MRI or CT scans. FDTD method offers great flexibility in modeling the inhomogeneous structures of anatomical tissues and organs" [62]. In fact, FDTD constitutes a robustness technique, suitability for handling complex problems composed of any number of sub-volumes and general independence of material compositions, which make it more popular than other techniques and the most applied in EM solver platforms [50].

However, in a publication by Fahs et al. (2011), the authors refers the main weakness of FDTD method, which consists in the rather difficult departure from the commonly used Cartesian grid and cell size limitations regarding the discretization of very detailed structures of human tissues. In particular, interfaces between tissues where sharp gradients of the electromagnetic field may occur are hardly modeled rigorously in these studies [63].

Recently in 2011, IEEE/IEC 62704-1, a standard by IEEE and International Electrotechnical Commission (IEC), was stated as the recommended practice for determining the Peak Spatial-Average Specific Absorption Rate (SAR) in the Human Body from Wireless Communications Devices in a range of frequencies between 30 MHz and 6 GHz, when using FDTD method for SAR calculations.

3.2.1.4 Simulation Platform

The simulation platform chosen is Sim4life, which is a computational life sciences platform developed for modelling of interactions between physical stimuli and the human body and for the modelling of processes in the human body. Thus, it is suitable for a wide variety of med-tech problems primarily EM-related [64].

This multi-physics simulation platform has been developed to specifically address needs from the computational life sciences field. This needs containing the ability to perform simulations based on medical image data, the ability to model setups involving complex and realistic anatomical models, the ability of visualizing measurement data, simulation results and image data together and the availability of solvers specifically modeling the physics, biology and physiology of living tissue.

The interface (Fig. 3.12), provide three tabs at the top-left corner: Model, Simulation and Analysis. On first tab "Model", the problem can be modeled, i.e. the different items that in the problem can be constructed. In the first study, an initial model of a SAM head filled with liquid and a monopole antenna will be considered (See Fig. 4.1). In a posterior case, the model will be the anatomical model Duke and a PIFA type antenna. Moreover, as far as to Duke is concerned, it should be posed in the desire posture, holding the mobile phone in its right hand (See Figure 4.7b). To achieve the desire posture, S4L provide a Poser tool, that allow the posture of the anatomical models to be interactively modified while preserving realistic internal organ placement and tissue distributions.

Once the model has been added to the project, the parameters can be set to run the simulation, in the next tab, Simulation. In this case, the option for the simulation type is Single EM FDTD,

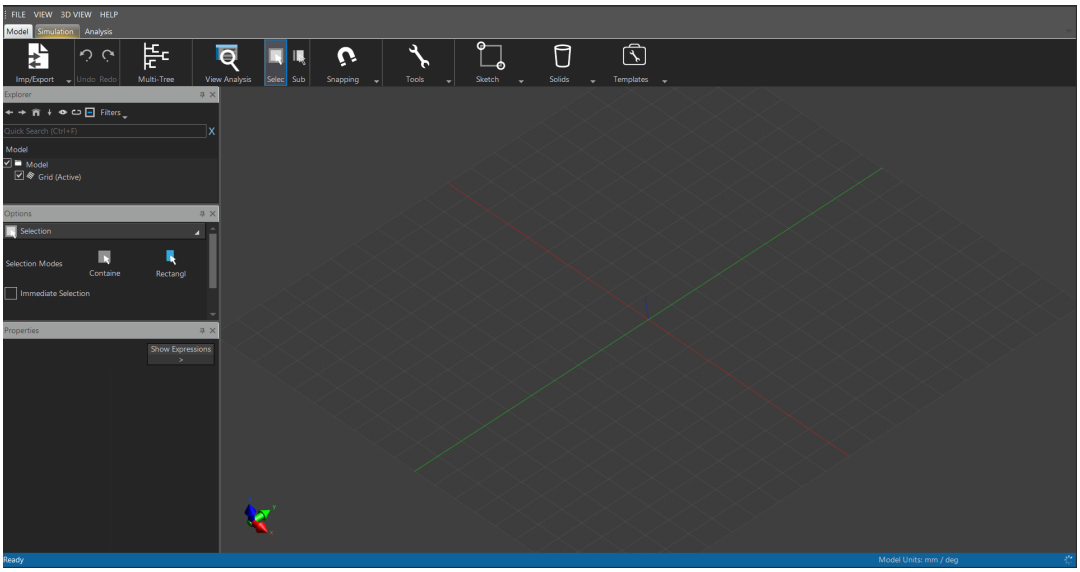

Figure 3.12: Interface of Sim4life

since that only one simulation runs with all the sources excited simultaneously, although the model built had only one source. Then it has to be set the parameters in the structure.

In the Setup, it has to be specified the duration of the simulation and if the solver should automatically detect convergence and stop the simulation. The Materials should also be specified, as well as its properties. In the case of this simulation the materials concerning Duke are automatically inserted, however it is necessary to adjust the properties of the tissues at the selected frequency using the Calculator option and selecting the desired frequency. The substrate of the antenna is made of FR-4, as mentioned before. All other materials are PEC.

Then the source should be specified, i.e. its signal properties for the excitation of the simulation such as type (Gaussian or Harmonic), frequency parameters, amplitude and impedance. The grid is a very important parameter because it is going to give specificity to the problem (as stated above in chapter 3.2.1.3). Define accurate settings of the grid will result in a optimum discretization of the model.

The resolution of the grid is not a random parameter. The cell size is primarily influenced by numerical dispersion, which is the propagation of different frequencies with different velocities. So, the grid size should be only a fraction of the wavelength of the highest significant frequency. Depending on the accuracy of desired results, it has been found that the cell size should be smaller than approximately $\lambda/10$ in the material medium, $\lambda/20$ if the computational resources allow to primarily to minimize the effects of numerical dispersion [5]. The grid-cell size depends on the problem size and frequency [53].

Once a satisfactory grid has been created, the voxels are generated, according a priority established between the objects of the model. Then, the user can run the simulation and wait for the results. The processing time mainly depends on the grid-cell size [53].

Selecting the third tab "Analysis", the results of the simulation can be observed. Firstly, one

has to check if the steady state was reached after the time periods set. For this, the platform has a function that shows the sinusoidal sign graphically and also a function that shows the convergence of the solution. If the steady state does not been reached the simulation should be erased and the period of time should be increased to perform a new simulation.

At second instance, it is important to observe the antenna parameters, to check if they are in concordance with what was established previously. For that, in Source Sensor it can be extracted information like Voltage, Current, Power, Reflection Coefficient, VSWR and Impedance. This parameters can be obtained in function of frequency or time.

Then, the far and overall field parameters can be obtained. In the Far Field Sensor, it is possible to compute and display the radiation pattern, while in the Overall Field Sensor, parameters like electric and magnetic fields (E, H, B and D), electric current vector (J), Power Balance (Input Power, Dielectric Loss, Radiated Power and Balance Ratio between Total Dissipated and Input Power) and SAR (whole-body, local and peak spatial-average) can be obtained, in a table, graphically or in a slice, depending on the type of parameter to be analyzed.

SAR can be obtained locally or in 1g or 10g of tissue. In this work the SAR values obtained will be local SAR and Peak Spatial-Average SAR (psSAR) in 10g of tissue.

As recommended in IEEE/IEC62704-1 standard, the psSAR Evaluator computes spatial-average SAR with moving constant-mass cubes. The spatial-average SAR is a quantity that is evaluated in cubic volumes containing a mass that is within a target mass.

The evaluator initializes all the voxels with the label "unused". Then, at the reference location, a cubic volume is expanded evenly in all directions, until the desired target mass value is reached (See fig. 3.13).

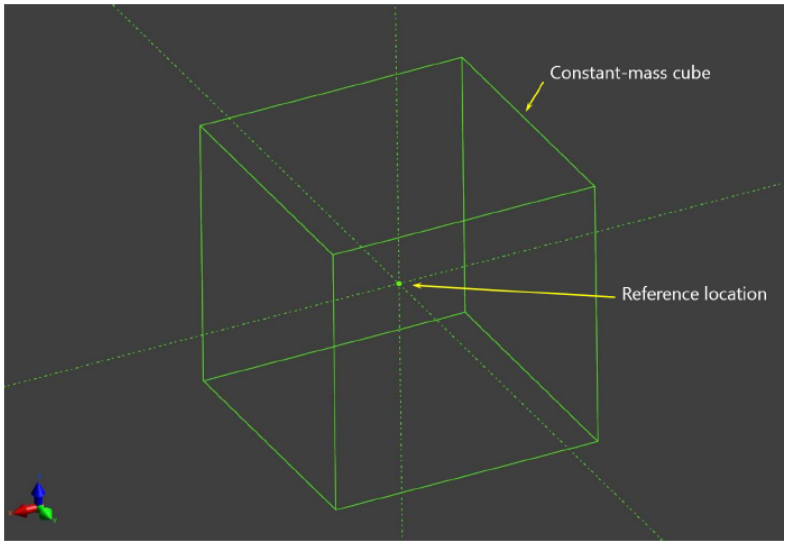

Figure 3.13: Reference location and constant-mass cube [30].

When this happens, some of the voxels on boundary layer may be only partially included, which means that the mass of those voxels will be calculated through linear interpolation. If the cube encloses an amount of background that is less than 10 % of its volume, and all its faces touch

(for fully contained voxels) or intersect with (for partially contained voxels) a lossy volume, then it is labeled as "valid". Otherwise it cannot be used for psSAR computation. Spatial-average SAR values are assigned to the center of each valid averaging cube (See fig. 3.14).

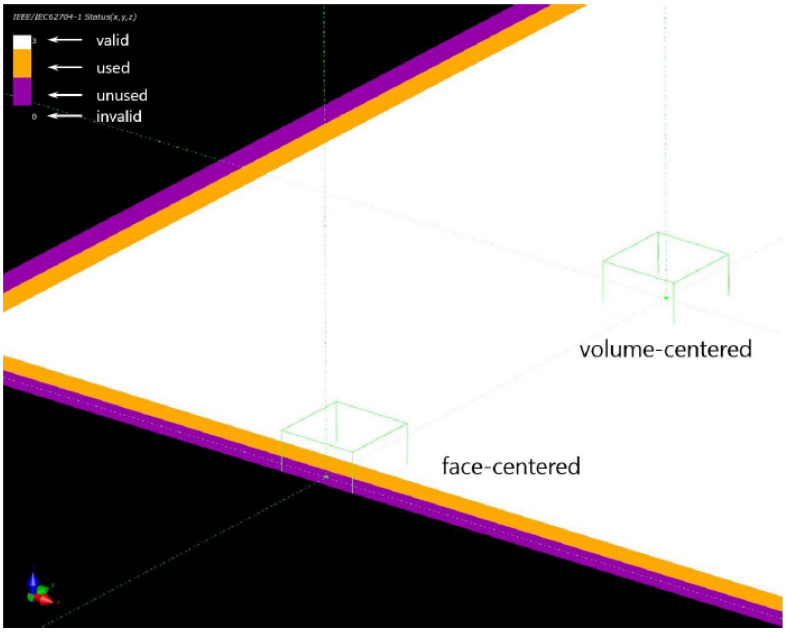

Figure 3.14: Status of the voxel, center of the averaging evaluation[30].

The voxels that are entirely included in the averaging cube, unlike the others that are only partially included, are labeled as "used", in the sense that they took part in at least one averaging volume.

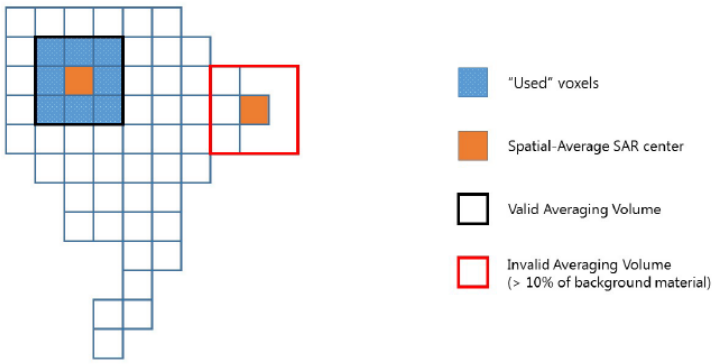

Figure 3.15: Spatial-Average SAR - Valid and Invalid Averaging Volumes, "used" locations and SAR centers[30].

Thus, the voxels deep inside a lossy volume are the center of a valid averaging cube, while the ones near its surface, even though labeled as "used", do not have an average SAR value assigned

yet. The largest spatial-average SAR value - of the averaging cube in which they are enclosed - is assigned to such voxel locations (See fig. 3.15).

The locations that are not entirely enclosed in any valid averaging cube keep the label "unused", but in these cases different averaging cubes are considered: the "unused" location is now the center of one face of the cube, with the other five faces evenly expanded in all directions, until the target mass of lossy volume is enclosed, regardless the amount of background material. This means that, out of the six cubes having a face centered on the “unused” location, SAR is evaluated only for those cubes whose volume is not larger than 5% of the volume of the smallest cube (See fig. 3.16). The highest SAR value is then used.

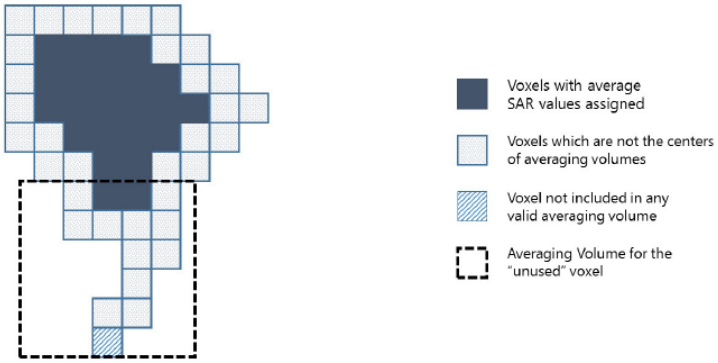

Figure 3.16: Spatial-Average SAR - Example of an Averaging Volume created for "unused" voxel[30].

If it happens that the entire lossy mass to be averaged is less than the target mass, the Peak Spatial-Average SAR (psSAR) is computed as the ratio of the total power dissipated inside that volume to the entire mass of the same volume.

In summary, the Maximum local SAR refers to maximum value of local SAR inside a region R and Peak Spatial-Average SAR[IEEE/IEC62704-1] refers to the value calculated by

$$psSAR = max_{r_j \in R}\{\frac{1}{m_j}\int_{r_j} SARdm\} \tag{3.8}$$

being j a reference to the j-th voxel and r_j the center of j-th voxel in R region (See fig. 3.17).

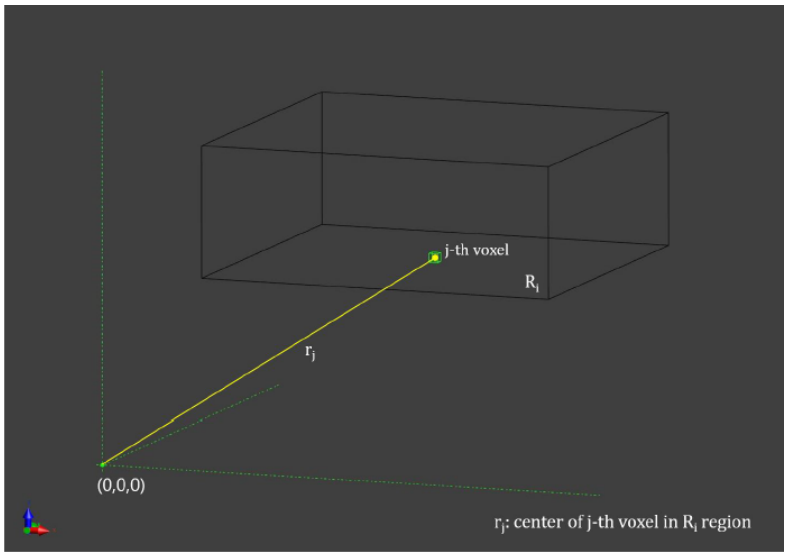

Figure 3.17: SAR Statistics - psSAR Evaluation in the SAR Statistics table[30].

In this work the psSAR values of each region presented will be computed as the region existing alone.

Chapter 4

Simulation and Results

4.1 SAM and monopole

In order to simulate the effects of a monopole antenna in a SAM head, the first step consists in architecting the model. Sim4Life has several CAD models, including the SAM head that consists in a shell filled with a homogeneous liquid with own dielectric characteristics. The cellular phone consists in a block, a cylinder and a feed point between them. The block touches on the SAM's ear as can be seen on figure 4.1.

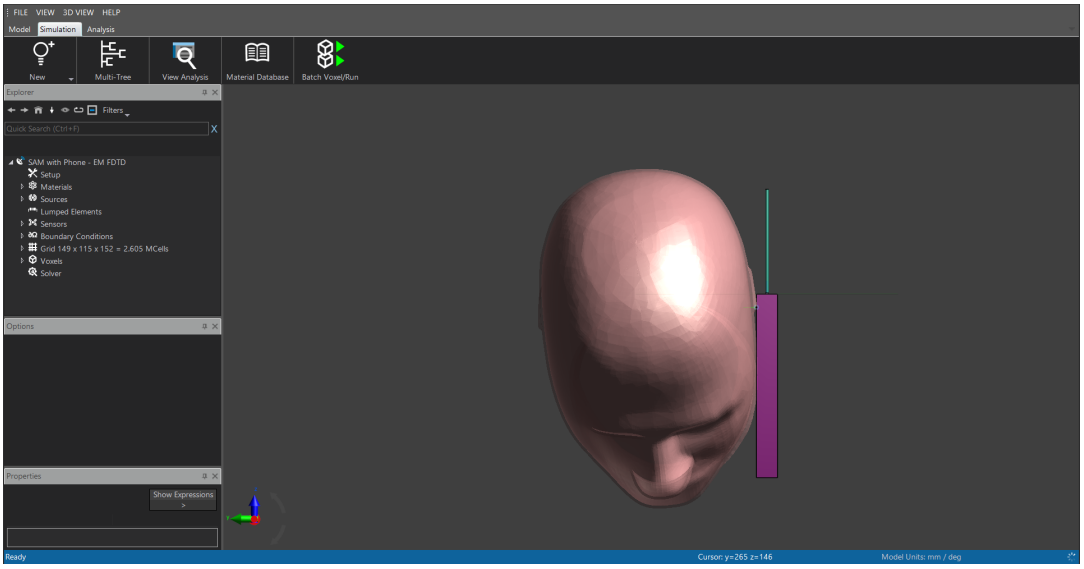

Figure 4.1: Model created on Sim4life

The next step is filling the adequate parameters to proceed with the simulation. First, the materials have to be defined. The air in background, the case, the antenna, the SAM shell and liquid have the electrical proprieties represented in the table 4.1.

The feed point has to be defined as an edge source with some specific characteristics like frequency of 900 MHz, 1 V of amplitude, and 50 Ohm of resistance. The absorbing boundary conditions (ABCs) are set as uniaxial perfectly matched layer (UPML). The ABCs are important

Table 4.1: Materials properties of SAM and monopole

Material	Air	Case	Antenna	SAM Shell	SAM Liquid
Type	Dielectric	PEC	PEC	Dielectric	Dielectric
Mass Density (kg/m^3)	1.205	-	-	1000	1000
Electrical properties					
Electric Conductivity (S/m)	0	-	-	0	0.97
Relative Permittivity	1	-	-	3.7	41.5
Magnetic properties					
Relative Permeability	1	-	-	1	1

to avoid the reflection back into the computational domain of the waves that collide on the outer boundary of the grid. Therefore, the mesh must be truncated with absorbing boundary conditions, which absorb incoming waves without reflection (UPML).

As the FDTD is the method that Sim4Life uses, a grid that involves the several objects must be created. There should exist a grid for each element of the model and this grid should have an adequate resolution. In this case, an automatic grid with a fine refinement was created for SAM shell and liquid (Fig. 4.2a). For the feed point a small automatic grid with fine refinement are also created and for the antenna (Fig. 4.2b) and the case (Fig. 4.2c), two manual grids, of 2 mm and 3 mm, respectively. The total grid has a resolution of $149 \times 115 \times 152$ cells, which represents a total of 2605 thousand cells (Fig. 4.3a and Fig. 4.3b).

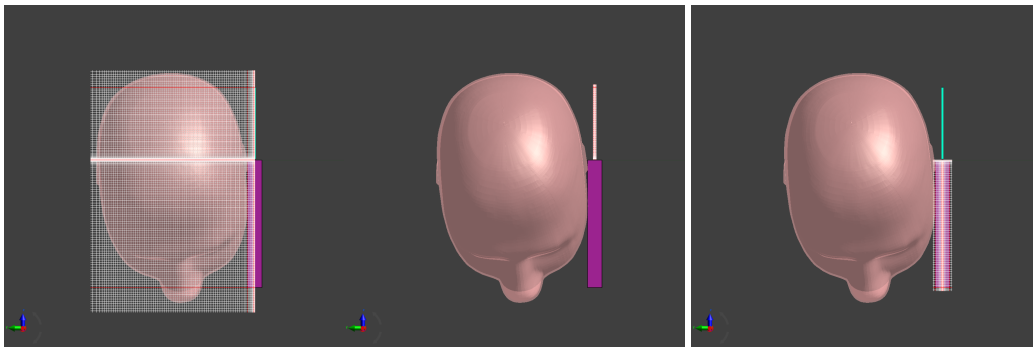

(a) (b) (c)

Figure 4.2: Grid with fine refinement (a), with 2 mm of resolution (b) and with 3 mm of resolution (c)

The next step consists in creating the voxels, that will have the aspect presented in Fig. 4.4 and proceed with simulation.

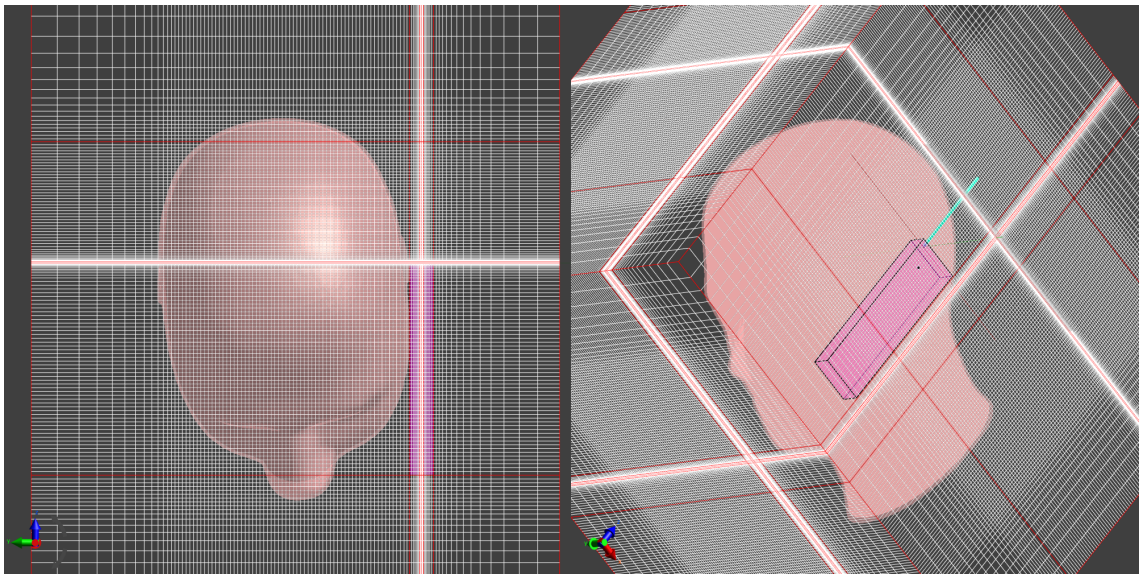

(a) (b)

Figure 4.3: Total grid in two different perspectives.

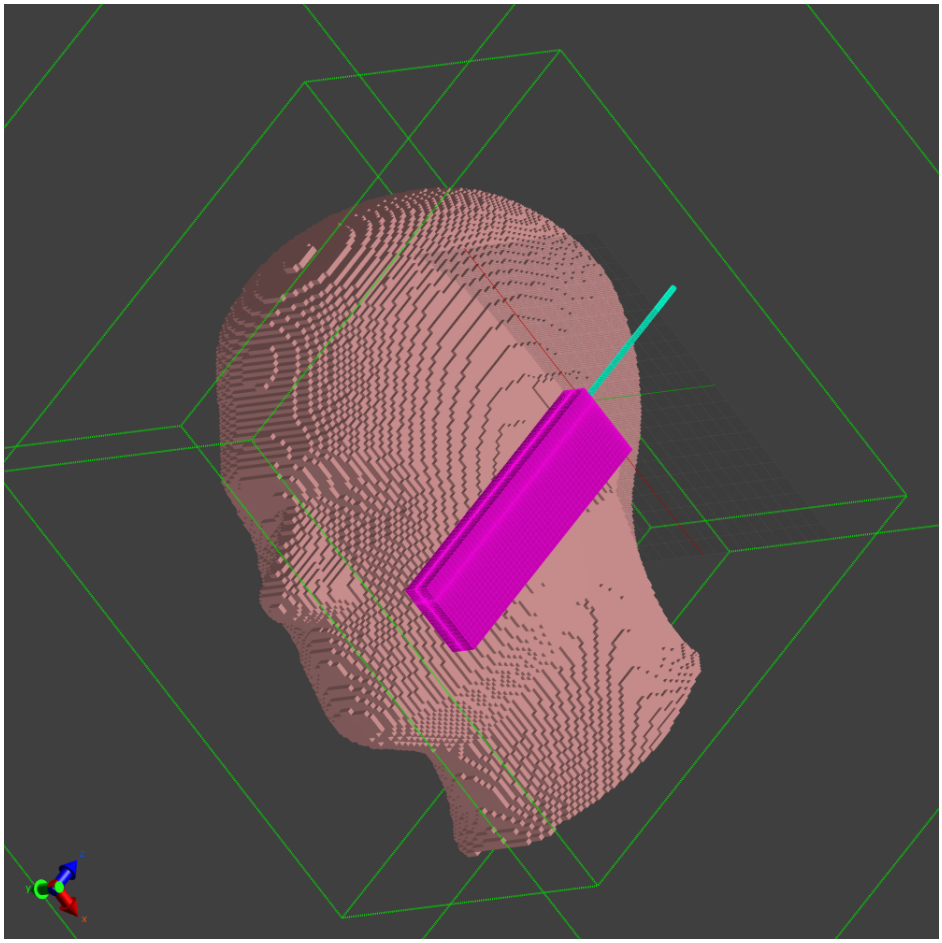

Figure 4.4: Voxels of the model

The first result to extract should be the values of the antenna characteristics, to check if the parameters of the antenna are correct. The parameters can be seen in table 4.2.

Table 4.2: Monopole antenna characteristics at 900 MHz when simulated with SAM.

Name	Value	Unit
Voltage (U)	$0.53e^{j1.50}$	[V]
Current (I)	$0.01^{j1.65}$	[A]
Power (Pi)	2.47	[mW]
Reflection Coefficient (Γ)	$0.10e^{j5.39}$	-
Return Loss	20.01	[dB]
VSWR	1.22	-
Input Impedance (Zi)	55.99 - 8.77j	[Ohm]

With SAM head present, some changes in antenna characteristics would be expected. The return loss is circa 20 dB, which is expectable since the model SAM introduced has a large absorption area.

Then the far field of the antenna can be seen in figure 4.5 and compared with the far field of the antenna without the SAM head 3.5b. The shape of the far field is no longer almost omnidirectional as the far field of the monopole antenna in free space.

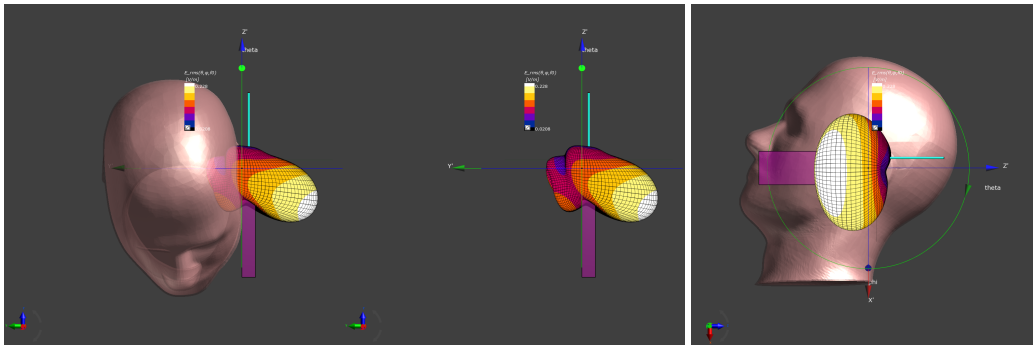

(a) (b) (c)

Figure 4.5: Far Field in three different perspectives.

Finally, the SAR values obtained for this case are presented on table 4.3.

Table 4.3: SAR Statistics of SAM and monopole (all values are in W/kg).

Regions	Max. local SAR	Peak Spatial-Averaged SAR (10g)
SAM Liquid	30.09	5.58

From the observation of the table 4.3, it can be concluded that the peak spatial-averaged SAR for 10 grams of tissue lower than the maximum local SAR, since the maximum local SAR is the value of voxel that has the highest SAR value, while the peak spatial-averaged SAR is the peak value between the values of the voxels with 10 grams of tissue.

Figure 4.6 shows the distribution of specific absorption rate (Local SAR (a) and Peak-Average SAR 10g (b)) inside a human head model at 900 MHz. Peak-Average SAR was obtained based on IEEE/IEC62704-1 standard. The value of maximum SAR is different for each plane base on the averaging mass of a human head model. The slice illustrated on figure 4.6 was obtained slicing the SAM head on the maximum value obtained for the three specific absorption rated above mentioned. It is observed that the intensity is greater at the portion close to the source of radiation and is being attenuated as the waves propagate through the y-axis (green one). High SAR values are in white, low SAR values are in black.

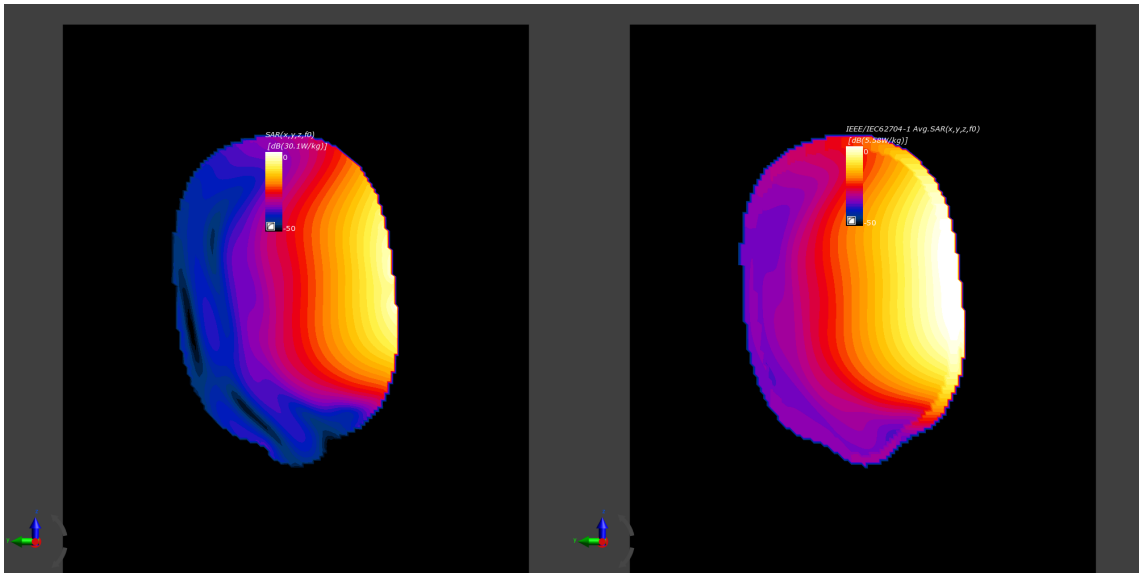

(a) (b)

Figure 4.6: Local SAR (a) and Peak-Average SAR 10g (b) in a slice of SAM Liquid.

4.2 Duke and PIFA

In this section, the scenario concerning the human anatomical model Duke in the presence of the designed PIFA will be addressed. First, Duke should be posed, using Poser tool, in the desired posture. The postures will vary according to some scenarios and in function of some parameters. The common posture will be with antenna close to the right ear and the hand will be next to the antenna, as can be seen in figure 4.7. The antenna does not touch the head or the hand of Duke, there exist a small distance between antenna and the body (See fig. 4.8).

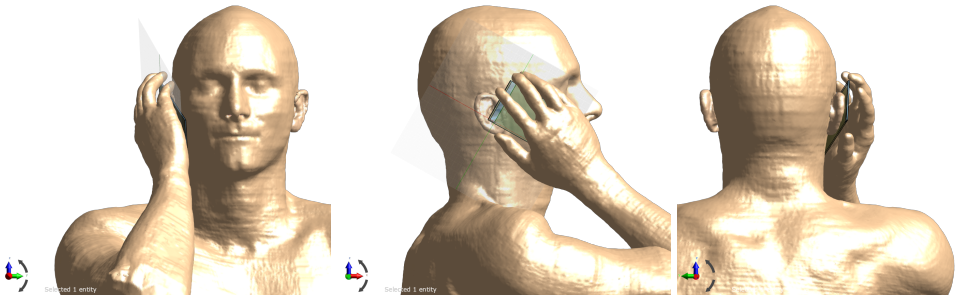

(a) (b) (c)

Figure 4.7: Duke and PIFA model.

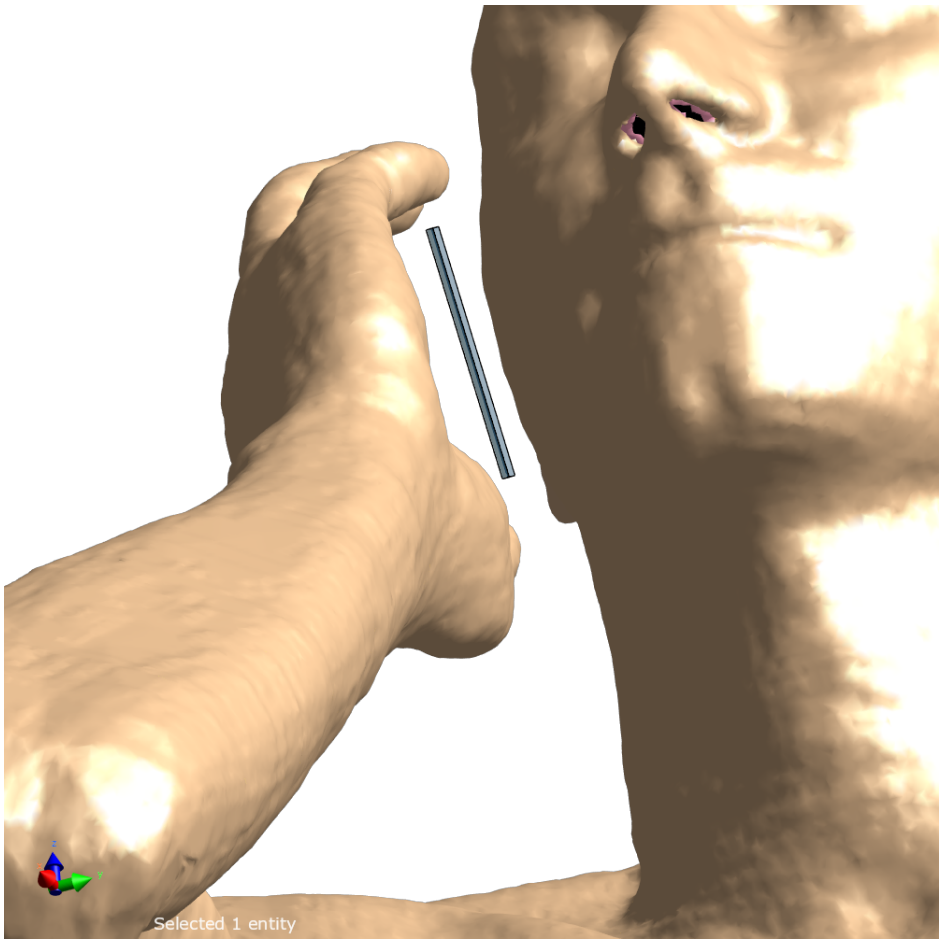

Figure 4.8: Distance between Duke and PIFA.

As far as the grid that will be set to perform the simulation is concerned, it is important to refer that the grid will not contain the complete body of Duke because, besides the simulation being very time consuming when all the body is considered, for the purpose of this simulation - the effects on the brain - to include in the simulation other parts of the body would be unnecessary.

So, the grid will only contain the head (with neck) and the hand (and part of the arm). For this, it was established an inferior limit, above the shoulders, for the grid.

Table 4.4: Duke and PIFA model antenna characteristics.

	Value	**Unit**
Voltage (U)	$7.08e^{j1.97}$	[V]
Current (I)	$0.22e^{j1.31}$	[A]
Power (Pi)	600.36	[mW]
Reflection Coefficient (Γ)	7.92	[dB]
VSWR	2.34	-
Input Impedance (Zi)	25.84 + 20.27j	[Ohm]

In table 4.4 are presented the antenna characteristics for the model Duke and PIFA simulation. If one compares these results to the simulation of PIFA in free space, one can verify that some parameters of the simulation with Duke were changed. As expected the input impedance changed, due the effect of the proximity of the human body. Consequently, other parameters such as reflection coefficient and VSWR also changed.

In terms of power, as it can be observed in table 4.5, the input power is near of 600 mW as expected. In this table other values are also shown, like dielectric loss, radiated power and a balance ratio. Dielectric loss consists in the sum of all the losses in the several materials of the designed model (e.g substrate, air and Duke). The Balance Ratio consists in the ratio of Total Power Dissipated, which is a sum of dielectric loss and radiated power, and the input power.

Table 4.5: Power Balance of model ´Duke and PIFA'.

	Power Balance 900 MHz
Input Power [mW]	600.4
Dielectric Loss [mW]	549.6
Radiated Power [mW]	33.89
Balance Ratio (Total Dissipated/Input Power)	0.9720

In the following tables[1], it can be seen the values of local SAR and peak spatial-average SAR 10g and the locations where those values occur for this scenario. In figure 4.9, it is shown a horizontal slice at a given plane of the electric field and respective SAR in all regions considered.

[1] Since the Sim4life only refers the maximum value of the tissue, independently of the region considered in tissues that are common to several regions (e.g. Skin), it was important for this work obtain the SAR value for the same tissue in other regions. So, the values refereed with $^{(1)}$ were not obtained directly, but indirectly through a process explained further in this document.

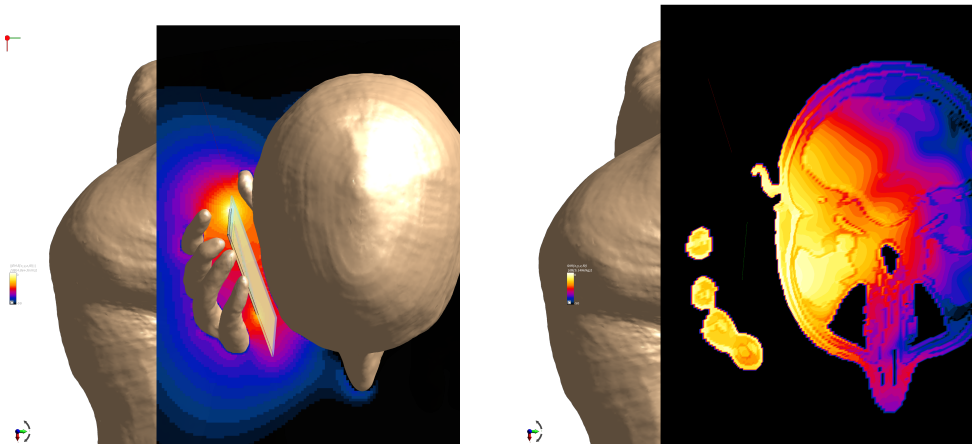

(a) (b)

Figure 4.9: Horizontal slice at a given plane of the electric field (a) and SAR (b) - Top view.

Table 4.6: Maximum local SAR in head, brain and hand at 900MHz and 600mW.

Maximum local SAR		
Region	Location	Value (W/kg) 900MHz (600mW)
Head	Skin	21.30[(1)]
	Subcutaneous Adipose Tissue (SAT)	2.77
	Muscle	5.59
	Ear skin (right)	17.54
	Ear cartilage (right)	6.99
	Cartilage	6.52
Brain	Cerebrum grey matter	1.41
	Cerebrum white matter	0.80
	Cerebellum	0.51
	Hippocampus	0.26
Hand	Skin	25.00
	SAT	0.71[(1)]
	Muscle	2.32[(1)]
	Tendon ligament	2.67
	Phalanx proximalis II cancellous (right)	1.06
	Carpalia Metacarpalia cancellous (right)	1.06

As it can be observed in table 4.6, the local SAR is higher in the skin of both head and hand regions, since this tissue is the one that covers all the body and, consequently, it is the first tissue to receive the radiation from the antenna. In the head, besides the head skin, the tissues with higher absorption are the skin and cartilage of the right ear due the proximity of the feed point of the antenna to the ear region. The cartilage itself is a tissue belonging into the head near to the ear. It is the intern cartilage contiguous to the auricular cartilage, that the Sim4life considers a different tissue. Because of the previous fact, it is expected that this tissue has a higher absorption due its proximity to the ear and consequently, as mentioned before, the feed point of the antenna.

Skin, SAT and Muscle are three tissues common to the head and hand, and because of that fact, they are mentioned in the head and hand regions in all of the tables of this document. The difference in the absorptions is related, not only with the distance to the feed point, but also with the water content of each tissue, since the tissues with high water content absorb more energy. Hereupon, it is reasonable that tissues like skin, cartilage and muscle have higher local SARs.

Relative to the brain, the highest absorption is observed in grey matter, since it is the exterior layer of the brain and then in an innermost layer - the white matter (See the anatomy in Appendix A). The Cerebellum and Hippocampus are the other two regions of the brain besides the grey and white matters that receive a higher radiation. For a slice view see in the Appendix A figures A.9 and A.10.

As expected, due the proximity with the antenna with the hand, the highest absorption will be on the skin. The tendon ligament is other tissue with a local absorption considerable in the hand region. The other regions refereed are part of the skeleton of the hand (Phalanx and Carpalia metacarpalia).

Table 4.7: Peak Spatial-Average SAR in 10g of tissue of the head, brain and hand at 900MHz and 600mW.

Peak Spatial-Average SAR in 10g of tissue		
Region	Location	Value (W/kg) 900MHz (600mW)
Head	Skin	2.12(1)
	SAT	2.12(1)
	Muscle	2.12
	Ear skin right	2.06
	Ear cartilage right	2.03
	Cartilage	2.07
	Salivary gland	2.12
Brain	Cerebrum grey matter	0.95
	Cerebrum white matter	0.84
	Cerebellum	0.23
	Hippocampus	0.23
Hand	Skin	2.41
	SAT	2.35
	Muscle	0.97(1)
	Tendon ligament	2.18
	Phalanx distalis II cortical right	2.32
	Phalanx distalis II cancellous right	2.30

The results shown in table 4.7 show a behaviour similar to the ones in table 4.6. However, since the peak spatial-average SAR (10g) values refer values that are a peak between the several voxels that constains inside it 10g of tissue, it is expected that other tissues appear with relevant values.

In the head the tissues with higher absorption still are the skin, SAT and muscle, but there exist a tissue with a peak spatial-average SAR identical to those tissues - the Salivary gland.

The tissues with highest absorption in the brain are also the same, being the order of absorption identical of local SAR analysis.

If one compares the values obtained with the standard limit of 2 W/kg for 10g of tissue, it is verified that in several regions the limit is exceeded in several tissues, in particular the skin, SAT and muscle. This regions are the first layers of the body, so those values are understandable. In the brain the absorption never reaches the limit.

Furthermore, it is also important point out that the values of peak spatial-average SAR 10g presented are actually not directly comparable with the limits established by the organizations. Effectively, this is a simulation of an antenna, without any materials to cover it, as a normal cell phone would have. To compare the obtained values with the standard limits, the reader must have to take this fact into consideration.

As could be seen in the previous tables, the results were organized by the location of the tissues that are part of the head, the brain and the hand regions. However, Sim4Life has a limitation that does not allow to divide the regions as desired. For instance, the maximum value of SAR occurs on Skin, but the platform does not inform where is this region specifically. However, this region can be known through a slice (on horizontal plane) with a mask that only allows to see the skin (See fig. 4.10).

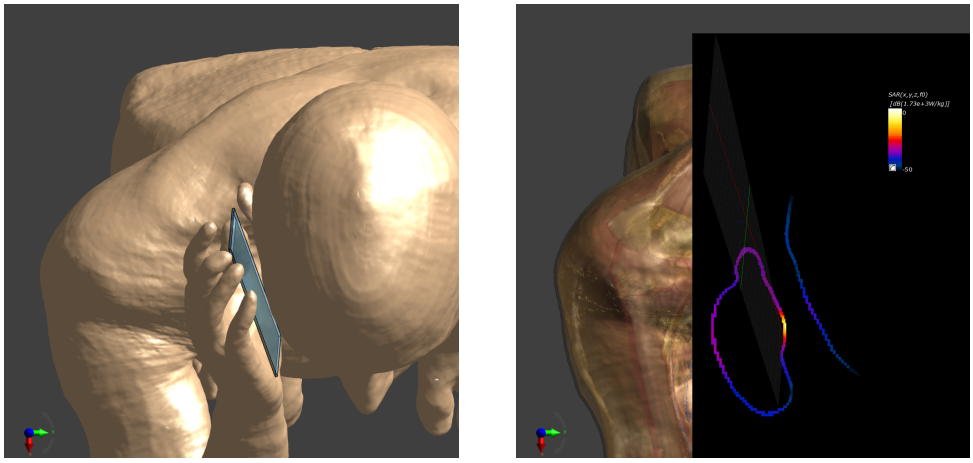

(a) (b)

Figure 4.10: Horizontal plane of Local SAR in skin - Top view.

In the figure 4.10b, it can be seen that the white region that corresponds the highest local SAR is located on the hand. Therefore, this region, as well as the regions of SAT and Muscle are indicated on table 4.6. In the head those types of tissues have also values of SAR, but the exact values for those tissues in those regions are not directly obtainable.

To obtain those values, indirectly, a slice in a vertical plane were dislocated through the model and analysing the color range and the maximum value of each slice, the maximum value for the region could be achieved.

In this chapter, other scenarios will be tested with this model. Firstly, with Duke and the PIFA working at 900 MHz, effect of the distance of the antenna relative to head will be investigated,

keeping the hand holding the antenna. Next, the effect on the head of the hand in terms of its presence or absence will be simulated. The third set of simulations address to the position of the antenna relative to the phone, i.e. if the feeding point is in the top or in the bottom of the phone. Then, the angle of cell phone with the chin will also be tested and finally the effect of the frequency with four antennas that works in different frequencies will be investigated.

4.2.1 Effect of the distance to the head

As previously mentioned, the distance is one of the factors that can influence the radiation in the head.

To test the effect on the brain of the distance of antenna to the head, the PIFA was picked at operational frequency of 900 MHz and input power of 600 mW. Five distances of 2 mm apart was chosen (2, 4, 6, 8 and 10 mm) to test this effect.

This set of simulations has a limitation related to the hand. Whereas the antenna can be moved linearly along a horizontal axis (see Fig. 4.11a), the hand is moved through an external rotation of the shoulder joint (see Fig. 4.11b). This rotation does not allow the linearity that would be desired for this test.

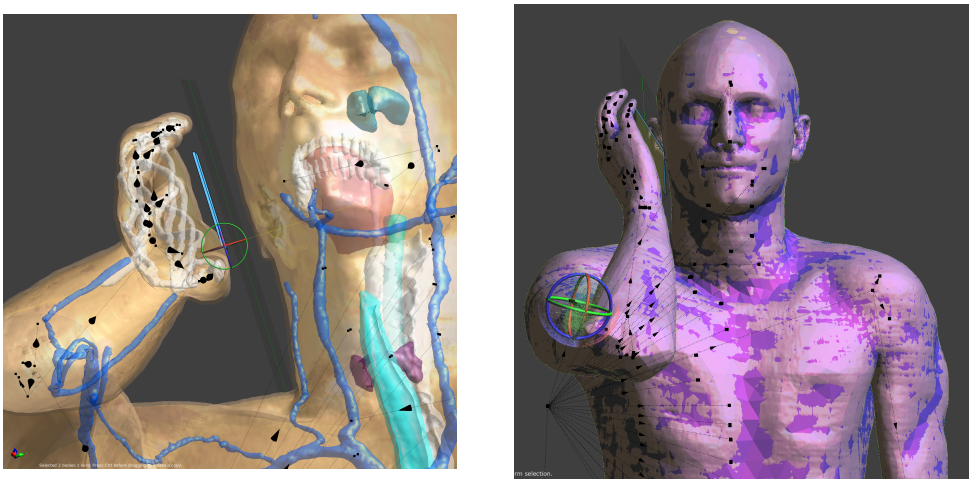

(a) (b)

Figure 4.11: Alterations to the model to test the distance: PIFA (a) and Shoulder joint (b).

The first distance was the same that was tested in previous subsection. Although this distance will appear in the tables as 0 mm, this value is not the real one, but the one that refers to the figure 4.8, that refers to the original model, where is visible the default distance between the body and the antenna.

In the next tables, it can be seen a comparison between the values of local SAR and peak spatial-average SAR for the distances 0, 2, 4, 6, 8 and 10 mm in head and brain regions.

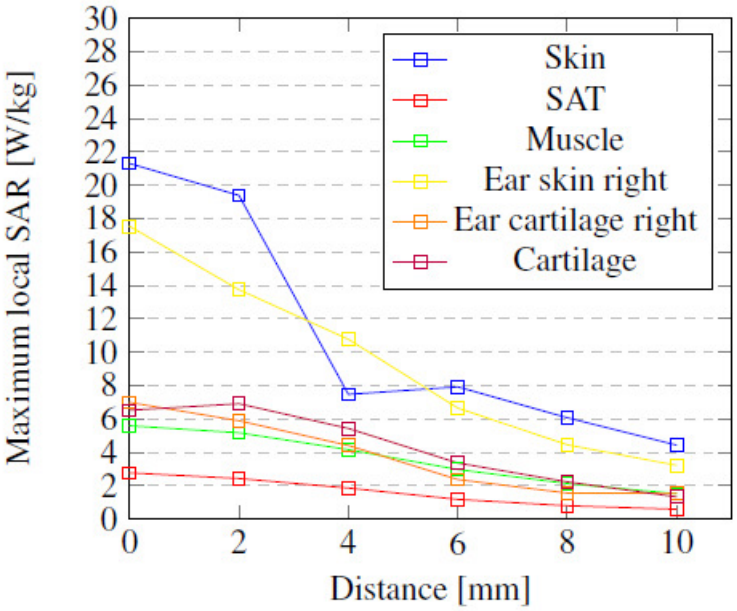

Figure 4.12: Maximum local SAR in head tissues as a function of distance

Table 4.8: Maximum local SAR for 0, 2, 4, 6, 8 and 10 mm of distance.

Maximum local SAR							
Region	Location	Value (W/kg)					
		0 mm	2 mm	4 mm	6 mm	8 mm	10 mm
Head	Skin	21.30[(1)]	19.39	7.47[(1)]	7.92[(1)]	6.07	4.43
	SAT	2.77	2.43	1.86[(1)]	1.18[(1)]	0.80[(1)]	0.59
	Muscle	5.59	5.17	4.16[(1)]	2.97	2.13[(1)]	1.52
	Ear skin right	17.54	13.74	10.77	6.65	4.45	3.22
	Ear cartilage right	6.99	5.89	4.41	2.37	1.56	1.54
	Cartilage	6.52	6.91	5.43	3.36	2.23	1.33
Brain	Cerebrum grey matter	1.41	1.32	1.09	0.74	0.52	0.34
	Cerebrum white matter	0.80	0.72	0.60	0.41	0.28	0.19
	Cerebellum	0.51	0.48	0.38	0.16	0.12	7.85E-02
	Hippocampus	0.26	0.26	0.21	0.14	9.72E-02	6.34E-02

In table 4.8 are represented the values of maximum local SAR in the tissues of head and brain regions. The values of local SAR tends to decrease when the distance increases, revealing the farther the antenna is, the radiation absorption by the brain will be less. The values of local SAR in the brain are smaller, being the maximum local SAR of the brain located in cerebrum grey matter and having a value of 1.41 W/kg. This order is explained by the fact that the tissues of the head are much closer to the antenna in relation to the brain tissues.

To a better visualization of the data on table 4.8, the following two figures represent the maximum local SAR as a function of distance. The figure 4.12 represents the head tissues and the figure 4.13 represents the brain tissues.

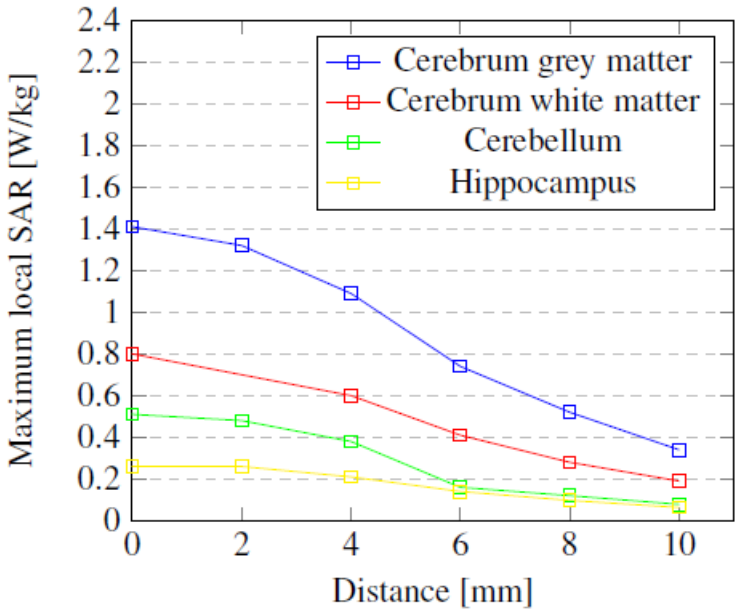

Figure 4.13: Maximum local SAR in brain tissues as a function of distance

In figure 4.12, it can be concluded that the maximum local SAR tends to decrease in all the tissues as the distance increases. This decrease is more abrupt in skin and ear skin right, mainly in the first distances. This represents a decrease of circa of 60 percent in only 4 mm of distance. Stating the general picture, the smooth increase observed in the skin may be an error because the values have been manually collected. In the same figure, it can also be observed that the decrease is smoother in the other tissues which are more internal.

In the brain tissues, one can conclude that the local SAR tends to decrease in all tissues as the distance increases, similarly to the tendency of tissues of the head. The decreasing observed in hippocampus tissue is the less abrupt, what can be explained by the fact of hippocampus localization be the most distant of antenna. The most abrupt decrease was observed in grey matter of the cerebrum.

The peak spatial-average SAR values in 10 grams of tissue of head and brain can be seen in table 4.9. Analysing the values, one can conclude that there exist a tendency to decrease when the distance increases, similarity to the tendency observed in local SAR values (Table 4.8). If one compares the values of the peak spatial-average SAR values in 10 grams of tissue with the standard limit established, 2 W/kg for 10 grams of tissue, it is verified that the limit is only exceeded in the tissues of the head and when the distance is very short (i.e. 0 mm). However, the values obtained for the distance of 2 mm are very close to the limit. In the brain tissues, the limit is not reached for any of the distances tested.

Table 4.9: Peak Spatial-Average SAR in 10g of tissue for 0, 2, 4, 6, 8 and 10 mm of distance.

Peak Spatial-Average SAR in 10g of tissue							
Region	Location	Value (W/kg)					
		0 mm	2 mm	4 mm	6 mm	8 mm	10 mm
Head	Skin	2.12(1)	1.99	1.71(1)	1.14(1)	0.73(1)	0.50(1)
	SAT	2.12(1)	1.99	1.71	1.14(1)	0.73(1)	0.50(1)
	Muscle	2.12	1.99	1.71	1.14(1)	0.73(1)	0.50(1)
	Ear skin right	2.06	1.92	1.56	1.06	0.68	0.48
	Ear cartilage right	2.03	1.91	1.55	1.05	0.68	0.47
	Cartilage	2.07	1.94	1.58	1.07	0.69	0.49
	Salivary gland	2.12	1.99	1.71	1.14	0.72	0.50
Brain	Cerebrum grey matter	0.95	0.90	0.75	0.51	0.35	0.23
	Cerebrum white matter	0.84	0.78	0.66	0.44	0.30	0.20
	Cerebellum	0.23	0.23	0.18	8.70E-02	6.87E-02	4.37E-02
	Hippocampus	0.23	0.23	0.19	0.12	8.74E-02	5.70E-02

4.2.2 Effect of the hand

As it can be seen in several papers, the hand holding the phone produces effects on the SAR values in head and brain. For testing this premise, two simulations will be made. The model will be posed in an "on call" position, i.e. being the mobile phone next to his ear with and without the hand (See Fig. 4.14a and Fig. 4.14b, respectively), being this last one a non-realistic scenario, given that the mobile phone is not actually glued to the ear. The PIFA is at operational frequency of 900 MHz and input power of 600 mW. The distance between PIFA and the head are the same in both models, since only the shoulder joint was moved to lower the arm, remaining the head and the antenna unmoved.

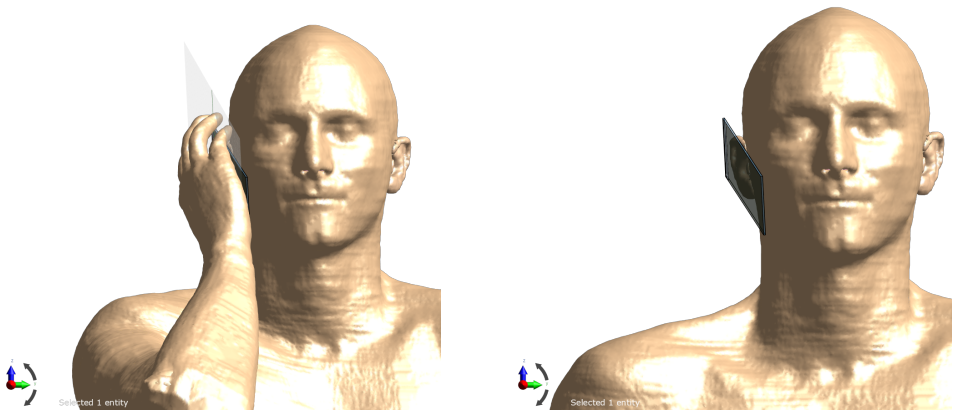

(a) (b)

Figure 4.14: Duke and PIFA model with (a) and without hand (b).

Analyzing the table 4.10, the resulted input impedance is 18.24 + 20.31i Ohm, so the value of input amplitude, obtained by the equations 3.5 and 3.6 for an input power of 600 mW, is 18.26

Table 4.10: Feed Point values of Duke and PIFA model without the hand.

	Value	**Unit**
Voltage (U)	$7.05e^{j2.12}$	[V]
Current (I)	$0.26e^{j1.28}$	[A]
Power (Pi)	$0.91e^{j0.84}$	[W]
Reflection Coefficient (Γ)	$0.53e^{j2.28}$	-
Return Loss	5.52	[dB]
VSWR	3.25	-
Input Impedance (Zi)	18.24 + 20.31j	[Ohm]

volt.

In terms of losses, one can see in table 4.11 that in absence of the hand the dielectric losses are smaller, as expected. Moreover, the radiated power is higher, which also makes sense, since the antenna can radiate for a larger space when the hand is not present.

Table 4.11: Power Balance of model Duke and PIFA with and without hand.

	Power Balance 900 MHz	
Model	with hand	without hand
Input Power [mW]	600.4	608.2
Dielectric Loss [mW]	549.6	499.9
Radiated Power [mW]	33.89	99.91
Balance Ratio (Total Dissipated/Input Power)	0.9720	0.9863

In the following tables, it can be seen a comparison between the values in the presence and in the absence of the hand for local SAR and peak spatial-average SAR in head and brain regions.

Table 4.12: Maximum local SAR in head and brain with presence and absence of hand.

Maximum local SAR			
Region	Location	Value (W/kg)	
		with hand	without hand
Head	Skin	$21.30^{(1)}$	24.98
	SAT	2.77	3.16
	Muscle	5.59	6.57
	Ear skin right	17.54	19.56
	Ear cartilage right	6.99	10.13
	Cartilage	6.52	8.33
Brain	Cerebrum grey matter	1.41	1.94
	Cerebrum white matter	0.80	1.11
	Cerebellum	0.51	0.53
	Hippocampus	0.26	0.34

The tissues that absorb more radiation are presented on table 4.12. Without the hand present, the head skin is the tissue that absorb more radiation, followed by right ear skin, internal and external right auricular cartilage. In brain, the radiation absorption is larger in grey matter, followed by white matter, cerebellum and hippocampus.

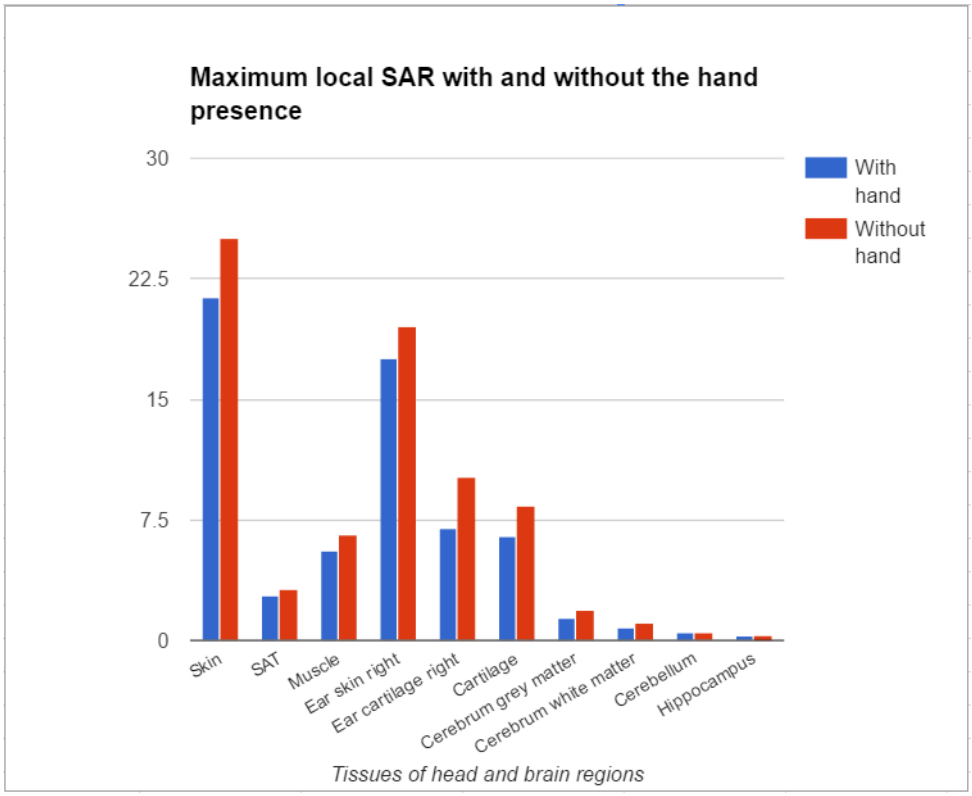

Figure 4.15: Maximum local SAR in head and brain with presence absence of hand.

The figure 4.15 is a graphical and visually more intuitive way to analyse the results, doing a more effective comparison between the values.

Table 4.13: Peak Spatial-Average SAR in 10g of tissue of head and brain with presence and absence of hand.

Peak Spatial-Average SAR in 10g of tissue			
Region	Location	Value (W/kg)	
		with hand	without hand
Head	Skin	2.12[(1)]	2.46
	SAT	2.12[(1)]	2.46
	Muscle	2.12	2.45
	Ear skin right	2.06	2.44
	Ear cartilage right	2.03	2.43
	Cartilage	2.07	2.45
	Salivary gland	2.12	2.46
Brain	Cerebrum grey matter	0.95	1.28
	Cerebrum white matter	0.84	1.15
	Cerebellum	0.23	0.26
	Hippocampus	0.23	0.31

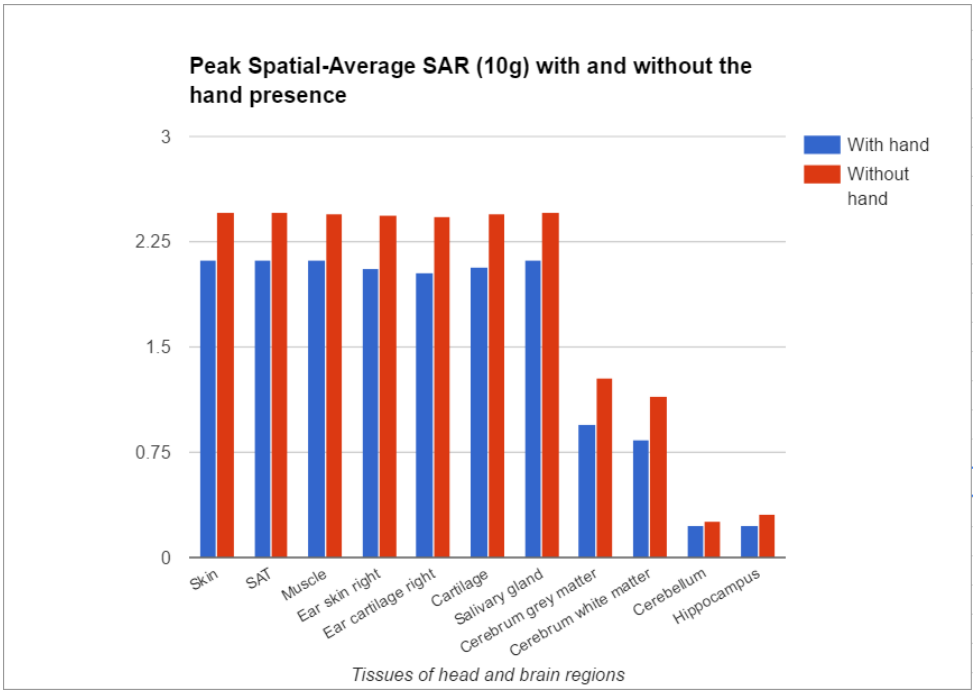

Figure 4.16: Peak Spatial-Average SAR in 10g of tissue of head and brain with presence and absence of hand.

Peak Spatial-Average SAR in 10g of tissue (European standard) is presented on table 4.13. Averaging the tissue in voxels of 10g the values on head are identical for the top four tissues with larger radiation absorption (skin, salivary gland, SAT and muscle), but different on brain region. In brain, the absorption in larger in grey matter, followed by white matter, hippocampus and cerebelum.

If one compare the values of peak spatial-average SAR obtained with the established standard limit of 2 W/kg, it is notable that the values obtained in head without the hand present are higher than the limit, but in the brain the limit is never reached.

Analysing the results, one can conclude that the presence of the hand reduces the SAR on the head, and consequently on the brain. The values of SAR in head and brain, local and peak spatial-average in 10 g of tissue, are both higher in the scenario without the hand comparatively with the scenario with the hand present. In effect, one can also conclude that is the hand the region that absorbs more radiation.

4.2.3 Effect of the position of the antenna

The position of the antenna in the mobile phones is a factor that is expected to influence the absorption of the radiation in the brain. To test this premise, the PIFA was flipped 180 degrees in relation to its initial position. The PIFA has its feed point on bottom, so more it is distanced from the brain. It was used the PIFA at operational frequency of 900MHz and input power of 600 mW.

In the following tables, it can be seen a comparison between the values with feed point on top and with the feed point on bottom for local SAR and peak spatial-average SAR and its respective locations in head, brain and hand regions.

Table 4.14: Maximum value of local SAR and its locations in head, brain and hand (organized by tissues with the highest SAR) of a PIFA oriented to top and oriented to the bottom.

Maximum local SAR					
Region		Feed Point on Top	Value (W/kg)	Feed Point on Bottom	
Head	1st tissue	Skin	21.30[(1)]	Skin	4.56[(1)]
	2nd tissue	Ear skin right	17.54	Muscle	3.67[(1)]
	3rd tissue	Ear cartilage right	6.99	Salivary gland	2.76
	4th tissue	Cartilage	6.52	Artery	2.52
Brain	1st tissue	Cerebrum grey matter	1.41	Cerebrum grey matter	0.69
	2nd tissue	Cerebrum white matter	0.80	Cerebrum white matter	0.37
	3rd tissue	Cerebellum	0.51	Hippocampus	0.12
	4th tissue	Hippocampus	0.26	Midbrain	7.41E-02
Hand	1st tissue	Skin	25.00	Skin	30.8
	2nd tissue	Tendon ligament	2.67	Tendon ligament	6.64
	3rd tissue	Muscle	2.32[(1)]	Muscle	6.28
	4th tissue	SAT	0.71[(1)]	SAT	3.52

The values of maximum local SAR divided by regions for the two scenarios are presented in table 4.14. Analysing this table, it can be seen that the values of local SAR are lower in the scenario where the feed point is oriented to the bottom, with the exception of the skin, tendon ligament, muscle and SAT in the hand. A higher value in this regions is understandable since the feed point of the antenna is near to the hand palm, particularly in the region of thenar eminence

[2]. Both values obtained on tissues of the head and brain decrease in case of the feed point of the antenna located at the bottom. In the brain this decrease is less than half of the value with feed point of the antenna on top for the same tissue. The cerebellum is not so affected by the radiation when the feed point of the antenna is on bottom, since its local value is only of 0.04 W/kg (See the appendix A for the complete tables).

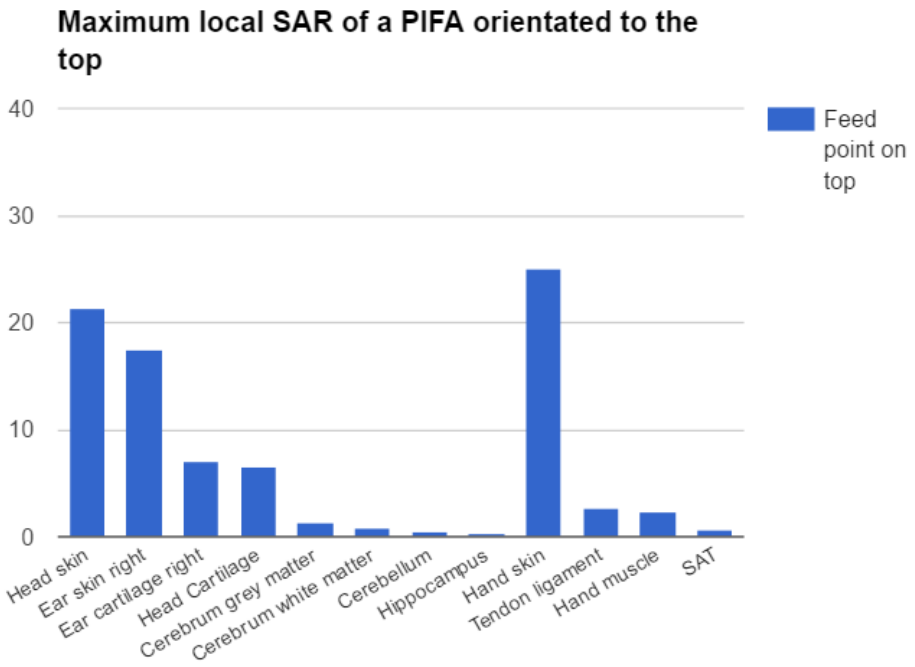

Figure 4.17: Maximum local SAR of the PIFA with feed point oriented to the top.

[2]The thenar eminence is the group of muscles on the palm of the human hand at the base of the thumb.

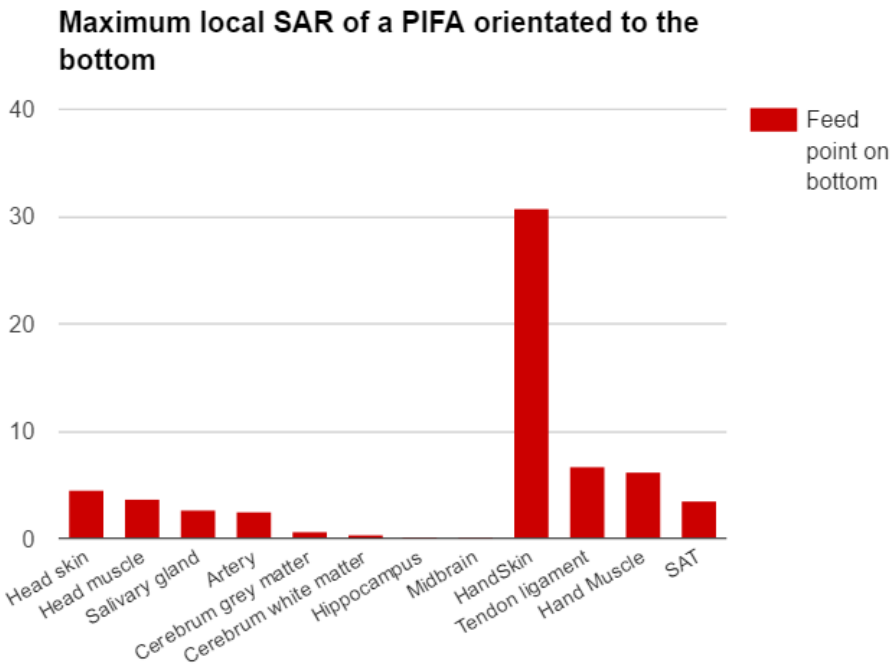

Figure 4.18: Maximum local SAR of the PIFA with feed point oriented to the bottom.

Table 4.15: Peak Spatial-Average SAR value in 10g of tissue and its locations in head, brain and hand (organized by tissues with the highest SAR) of a PIFA oriented to top and oriented to the bottom.

peak Spatial-Average SAR in 10g of tissue					
Region		Value (W/kg)			
		Feed Point on Top		Feed Point on Bottom	
Head	1st tissue	Skin	2.12(1)	SAT	2.30(1)
	2nd tissue	SAT	2.12(1)	Skin	1.81(1)
	3rd tissue	Muscle	2.12	Muscle	1.81(1)
	4th tissue	Salivary gland	2.12	Salivary gland	1.81
Brain	1st tissue	Cerebrum grey matter	0.95	Cerebrum grey matter	0.52
	2nd tissue	Cerebrum white matter	0.84	Cerebrum white matter	0.40
	3rd tissue	Cerebellum	0.23	Hippocampus	0.10
	4th tissue	Hippocampus	0.23	Hypophysis	9.44E-02
Hand	1st tissue	Skin	2.41	Skin	2.62
	2nd tissue	SAT	2.35	Tendon ligament	2.62
	3rd tissue	Phalanx distalis II cortical right	2.32	Muscle	2.62
	4th tissue	Tendon ligament	2.18	SAT	2.62

In table 4.15 are presented the values of peak spatial-average SAR in 10 g of tissue for the both scenarios of antenna orientation. The results are identical to the ones obtained on maximum local SAR. Again, the values are lower in the scenario where the feed point is oriented to the bottom, with the exception of the skin, tendon ligament and SAT in the hand. In case of the feed point of

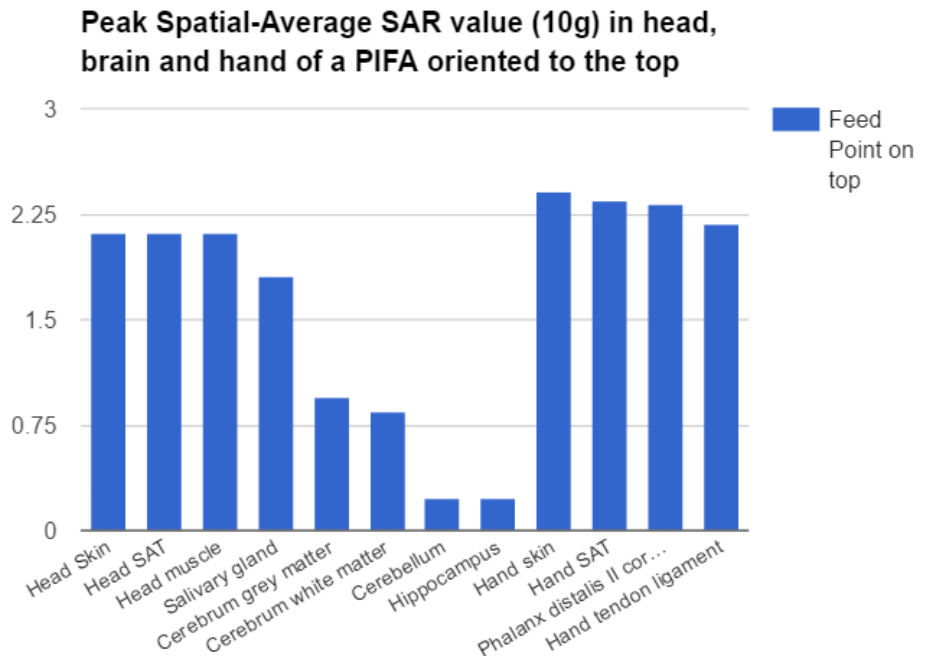

Figure 4.19: Maximum local SAR of the PIFA with feed point oriented to the top.

the antenna located at the bottom, the values tend to decrease in the tissues of the head and the brain. This decrease in the brain is more or less half of the value with feed point of the antenna on top for the same tissue. As mentioned before, the cerebellum is not so affected by the radiation when the feed point of the antenna is on bottom.

If one compare the values of peak spatial-average SAR in 10 g of tissue with the standard limit - 2 W/kg, the values are higher or close to that the limit in head and hand tissues. In brain tissues, wherever is the feed point of the antenna, the standard limit is never reached.

Table 4.16: Maximum value of local SAR and its locations in tissues of the eye of a PIFA oriented to top and oriented to the bottom.

Maximum local SAR					
Region		Value (W/kg)			
		Feed Point on Top		Feed Point on Bottom	
Eye	1st tissue	Eye sclera	0.37	Eye sclera	0.91
	2nd tissue	Eye vitreous humor	0.24	Eye vitreous humor	0.69
	3rd tissue	Eye cornea	0.12	Eye cornea	0.29
	4th tissue	Eye lens	3.40E-02	Eye lens	8.57E-02

The eye, although is not the aim of this work, raises the attention because its local SAR values are increased almost 3-fold when the antenna has its feed point oriented to the bottom (See values in the table 4.16).

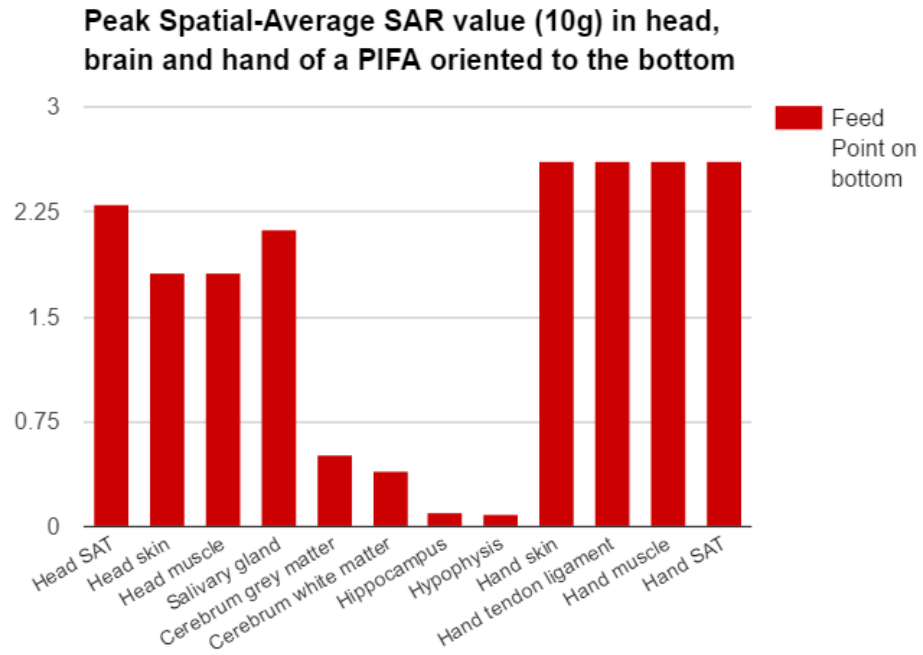

Figure 4.20: Maximum local SAR of the PIFA with feed point oriented to the bottom.

4.2.4 Effect of the angle between the antenna and the chin

To test the effect of the angle between the antenna and the chin, two more simulations were performed. These simulations will be compared with the original model described in the beginning of the present chapter (See Fig. 4.7). The antenna on the original model is placed in a cheek position, this position is described in several papers as a position that places the antenna along to the face (See Fig. 4.21a). The next to simulations are at a tilt position, where the feed point of the antenna is still close to the ear but the bottom of the antenna are away from the cheek. The angles chosen are in the figures 4.21b and 4.22a- Tilt 1 - and in the figures 4.21c and 4.22b- Tilt 2. It was used PIFA at operational frequency of 900MHz and input power of 600 mW.

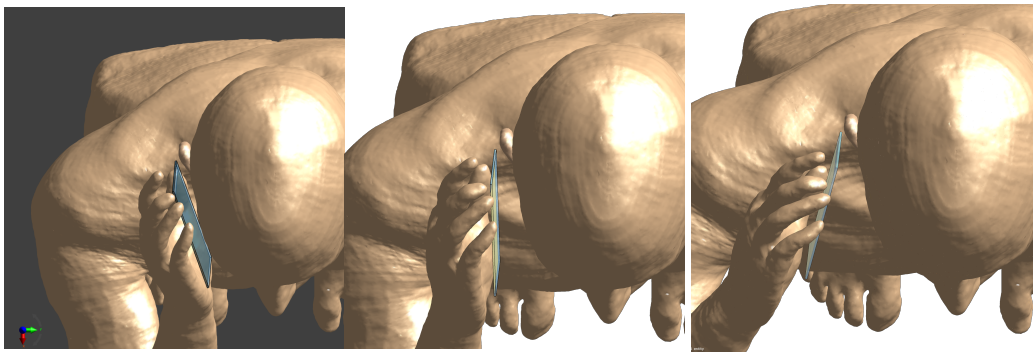

(a) PIFA at cheek position. (b) PIFA at tilt position (Tilt 1). (c) PIFA at tilt position (Tilt 2).

Figure 4.21: PIFA in different angles related to Duke - Top view.

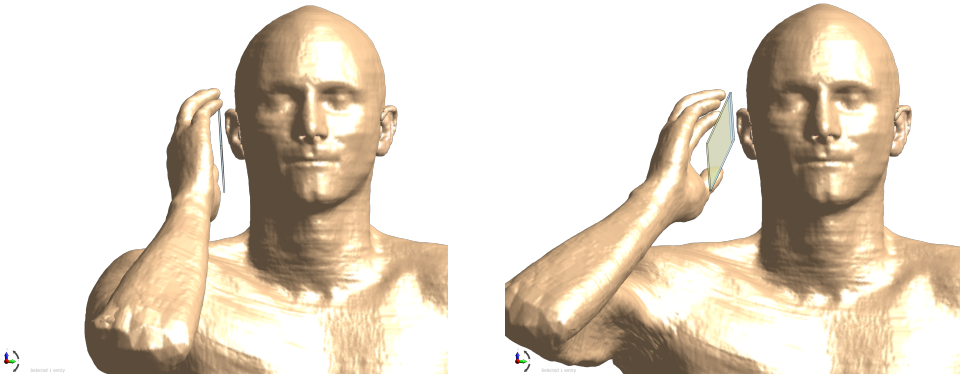

(a) PIFA at tilt position (Tilt 1). (b) PIFA at tilt position (Tilt 2).

Figure 4.22: PIFA in different angles related to Duke - Front view.

The hand position may be not exactly the same in the three simulations performed. This fact is due to the rotation of the articulation that are required to achieve the positions in 4.21 and 4.22, which do not allow the linearity that would be desired for this test.

In the following tables, it can be seen a comparison between the values of local SAR and peak spatial-average SAR in the positions above mentioned (Cheek, Tilt 1 and Tilt 2) and its respective locations in head and brain regions.

Table 4.17: Maximum local SAR for cheek and two different tilt positions in head and brain regions.

Maximum local SAR				
Region	Location	Value (W/kg)		
		Cheek	Tilt 1	Tilt 2
Head	Skin	21.30$^{(1)}$	10.40$^{(1)}$	14.10$^{(1)}$
	SAT	2.77	1.44$^{(1)}$	1.34
	Muscle	5.59	3.53	2.32$^{(1)}$
	Ear skin right	17.54	8.84	11.72
	Ear cartilage right	6.99	4.11	3.33
	Cartilage	6.52	3.95	3.98
Brain	Cerebrum grey matter	1.41	0.91	0.61
	Cerebrum white matter	0.80	0.49	0.39
	Cerebellum	0.51	0.19	0.31
	Hippocampus	0.26	0.14	0.12

In table 4.17, it can be seen the maximum local SAR values and respective locations for the cheek and tilt positions (Tilt 1 and Tilt 2). The higher local SAR values occur for the cheek position. In head region and for the tilt positions, the skin and ear skin right have the higher values, being the Tilt 2 position the one which those values are higher. In figure 4.23, the regions where the intensity of electric field is larger can be seen, which may explain the SAR values in certain regions.

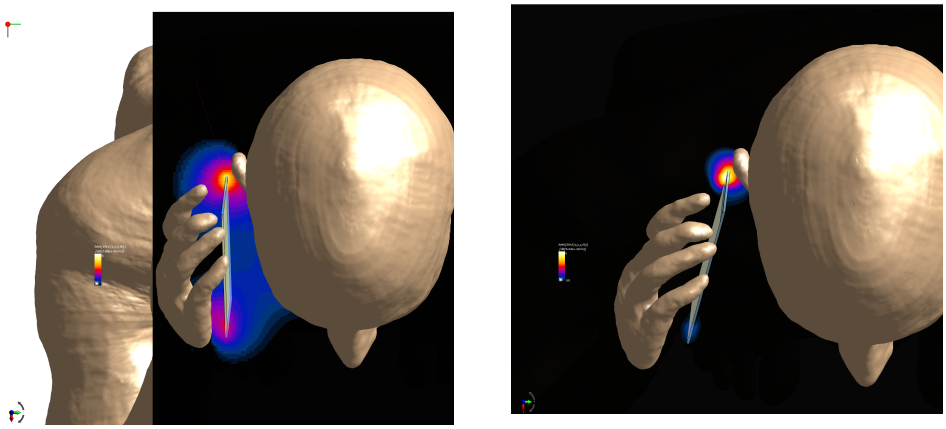

(a) Electric field at tilt position (Tilt 1).

(b) Electric field at tilt position (Tilt 2).

Figure 4.23: Electric field at tilt positions - Top view.

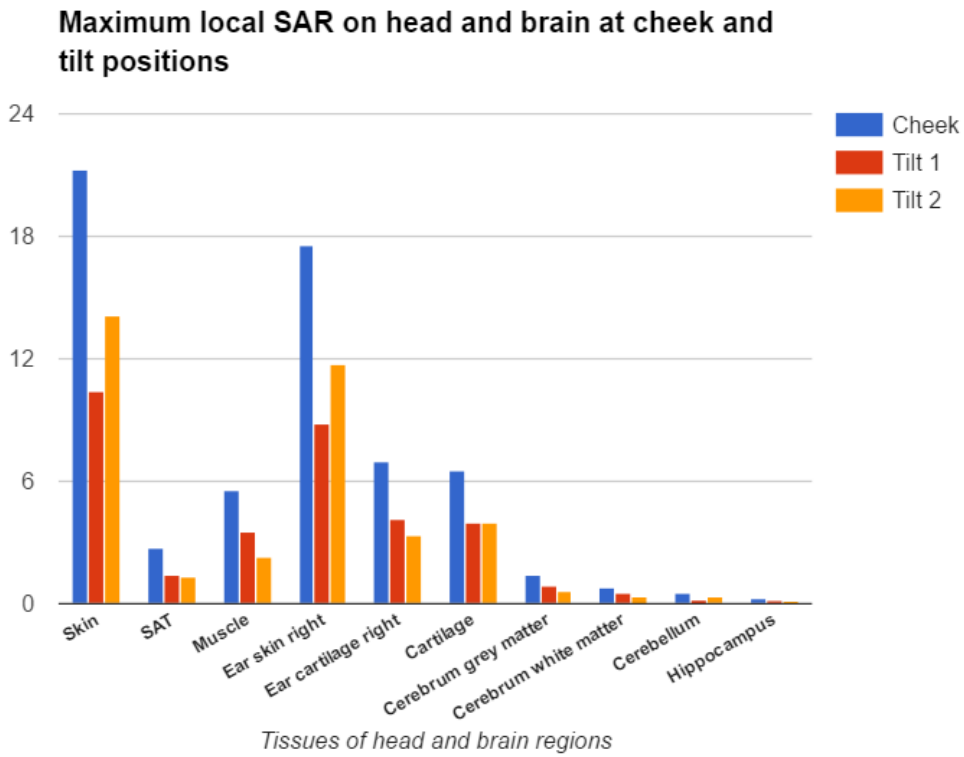

Figure 4.24: Maximum local SAR of the PIFA at cheek and tilt positions.

Table 4.18: Peak Spatial-Average SAR in 10g of tissue for cheek and two different tilt positions in head and brain regions.

Peak Spatial-Average SAR in 10g of tissue				
Region	Location	Value (W/kg)		
		Cheek	Tilt 1	Tilt 2
Head	Skin	2.12(1)	1.16(1)	0.75(1)
	SAT	2.12(1)	1.16(1)	0.75(1)
	Muscle	2.12	1.13	0.75(1)
	Ear skin right	2.06	1.17	1.04
	Ear cartilage right	2.03	1.16	0.98
	Cartilage	2.07	1.16	0.75
	Salivary gland	2.12	1.16	0.72
Brain	Cerebrum grey matter	0.95	0.57	0.40
	Cerebrum white matter	0.84	0.50	0.36
	Cerebellum	0.23	0.10	0.14
	Hippocampus	0.23	0.13	0.11

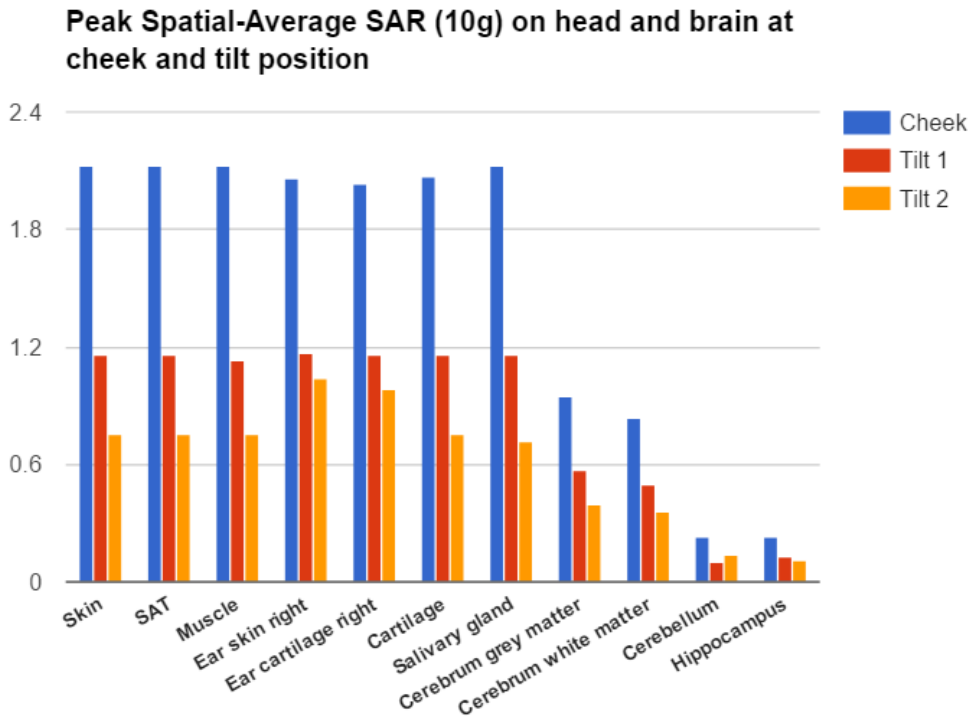

Figure 4.25: Peak Spatial-Average SAR (10g) of the PIFA at cheek and tilt positions.

The peak spatial-average SAR values for 10 gramms of head and brain tissue are presented in table 4.18. The values decreased in the order considered - Cheek, Tilt 1 and Tilt 2 - for every tissues whatever be the region. The standard limit - 2 W/kg - is only exceeded in the cheek position.

4.2.5 Effect of the frequency

To test the effect of the frequency, four different PIFAs working at four different operational frequencies were designed. As mentioned on previous chapter the frequencies chosen were the typical frequencies used by the main telecommunication standards, i.e GSM, UMTS and LTE (2G, 3G and 4G).

Using the model representing an 'on call' scenario (See figure 4.7, four simulations were performed, using for each one of them the four different antennas for each frequency (900, 1800, 2100 and 2600 MHz). The operational input power used for each frequency was specified on table 3.5 and the input signal has the characteristics specified on table 4.19.

Table 4.19: Input amplitudes obtained on model Duke and PIFA 'on call' by calculation for the several frequencies.

	Z_i **[Ohm]**	V_g **[V]**
PIFA 900 MHz	25.84 + 20.27j	16.92
PIFA 1800 MHz	22.51 + 7.59j	7.68
PIFA 2100 MHz	15.53 - 2.93j	8.32
PIFA 2600 MHz	15.13 + 2.46j	10.58

In the following tables, it can be seen a comparison between the values in head, brain and hand regions of local SAR (table 4.20) and peak spatial-average SAR in 10g of tissue (table 4.21) and its respective locations for different frequencies and their respective input power.

Table 4.20: Maximum local SAR of the tissues where the EMF absorption is higher for 900, 1800, 2100 and 2600 MHz.

Maximum local SAR					
Region	Location	Value (W/kg)			
		900MHz 600mW	1800MHz 125mW	2100MHz 125mW	2600MHz 199.5mW
Head	Skin	21.30(1)	7.91	10.60(1)	7.76
	SAT	2.77	1.17	1.46	1.89
	Muscle	5.59	1.80	1.72	2.26
	Ear skin right	17.54	7.07	4.95	8.61
	Ear cartilage right	6.99	4.14	3.25	6.89
	Cartilage	6.52	6.41	5.86	6.65
Brain	Cerebrum grey matter	1.41	0.28	0.33	0.62
	Cerebrum white matter	0.80	0.15	0.20	0.34
	Cerebellum	0.51	5.10E-02	3.02E-02	5.20E-02
	Hippocampus	0.26	3.06E-02	2.30E-02	1.74E-02
Hand	Skin	25.00	2.69(1)	10.58	4.70(1)
	SAT	0.71(1)	0.59(1)	0.52(1)	1.13(1)
	Muscle	2.32(1)	0.36(1)	0.47(1)	0.72(1)
	Tendon ligament	2.67	0.86	1.17	1.99
	Phalanx proximalis III cancellous right	1.06	0.32	0.27	0.72
	Carpalia Metacarpalia cancellous right	1.20	0.31	0.25	0.29

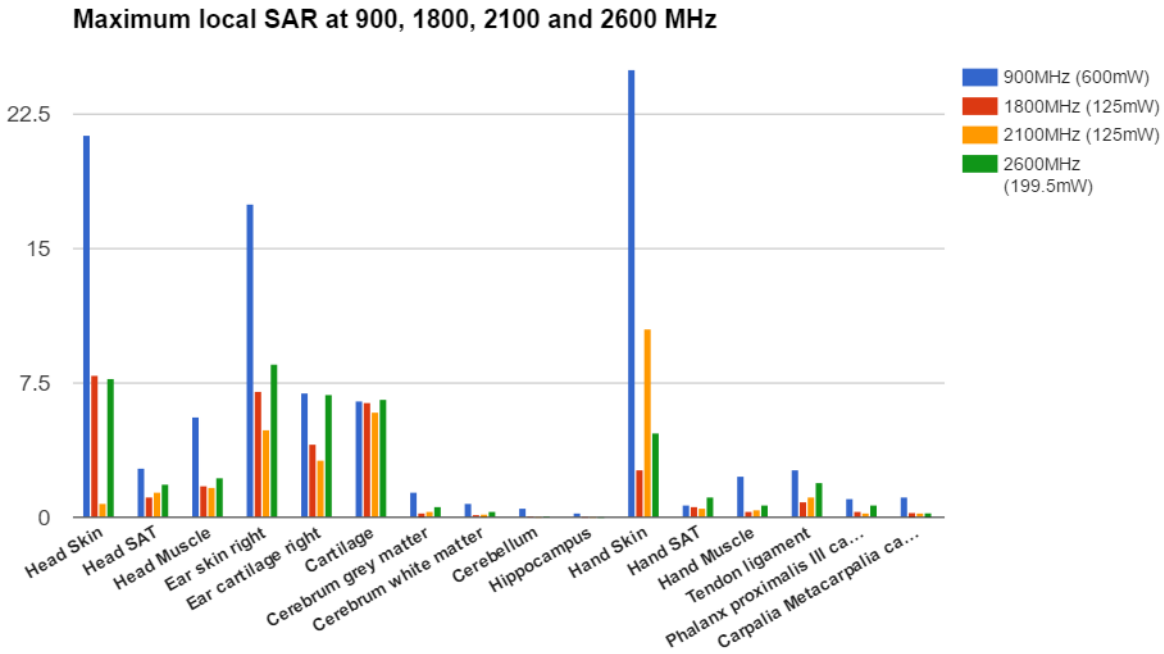

Figure 4.26: Maximum local SAR of the PIFA at operational frequencies 900, 1800, 2100 and 2600 MHz.

Table 4.21: Peak Spatial-Average SAR in 10 g of tissue on tissues where the EMF absorption is higher for 900, 1800, 2100 and 2600 MHz.

Peak Spatial-Average SAR in 10g of tissue					
Region	Location	Value (W/kg)			
		900MHz 600mW	1800MHz 125mW	2100MHz 125mW	2600MHz 199.5mW
Head	Skin	2.12(1)	0.74(1)	0.78(1)	1.11(1)
	SAT	2.12(1)	0.74(1)	0.77(1)	1.11(1)
	Muscle	2.12	0.70	0.75	1.11
	Ear skin right	2.06	0.89	0.90	1.19
	Ear cartilage right	2.03	0.85	0.86	1.15
	Cartilage	2.07	0.74	0.77	1.02
	Salivary gland	2.12	0.74	0.77	1.11
Brain	Cerebrum grey matter	0.95	0.20	0.18	0.30
	Cerebrum white matter	0.84	0.15	0.16	0.27
	Cerebellum	0.23	2.92E-02	1.73E-02	2.37E-02
	Hippocampus	0.23	2.52E-02	1.81E-02	1.50E-02
Hand	Skin	2.41	0.87	0.94	1.39
	SAT	2.35	0.77	0.86	1.29
	Muscle	0.97(1)	0.16(1)	0.16(1)	0.31(1)
	Tendon ligament	2.18	0.46	0.32	1.13
	Phalanx media II cortical right	1.99	0.37	0.32	1.08
	Phalanx distalis I cortical right	1.11	0.50	0.63	0.99

The maximum local SAR values for head, brain and hand regions can be seen in table 4.20. To compare this values, one needs to take into account the input powers for each frequency. Each input power was chosen to represent an average input power for this frequencies.

In head tissues, the smaller local SAR values are achieved at 2100 MHz, while the higher ones are achieved at 900 MHz. The values achieved in 1800 MHz and 2600 MHz are close to each other. Related to the tissues the highest value is achieved at 900 MHz in head skin, but at this frequency the ear skin right achieved a higher value too. The skin continues to receive higher values of radiation in comparison with the other tissues, independently of the frequency used.

In brain tissues, the tendency is not the same. The lower values of local SAR are achieved at 1800 MHz for grey and white matter. The cerebellum has a similar value at 1800 and 2600 MHz, but its smaller value is verified at 2100 MHz. The hippocampus has a decreasing tendency of local SAR as the operational frequency increases.

The hand skin has the higher local SAR values at each frequency for the hand tissues. Considering the set of hand tissues presented, it is the operational frequency of 900 MHz that achieve the higher values for every hand tissue, except the SAT.

In table 4.21 can be seen the maximum local SAR values for head, brain and hand regions.

In head tissues, the smaller peak spatial-average SAR values in 10 grams of tissue are achieved at frequency of 1800 MHz in the head and hand regions, while the higher ones are achieved at frequency of 900 MHz. The values achieved in 1800 MHz and 2100 MHz are close to each other.

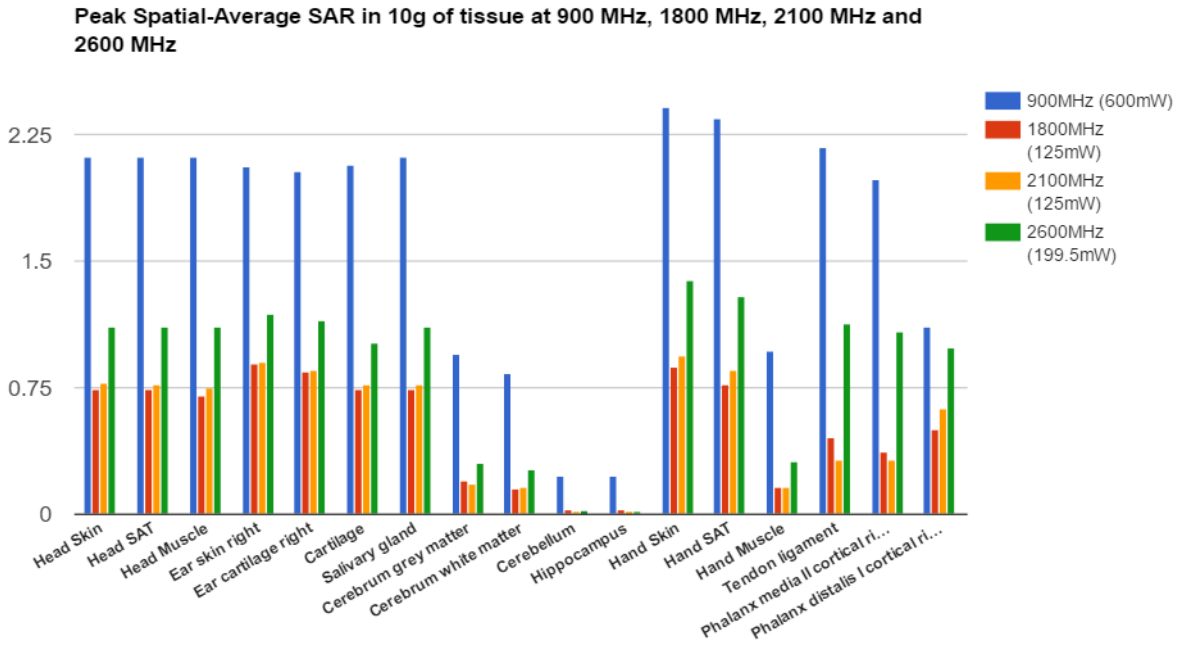

Figure 4.27: Peak Spatial-Average SAR (10g) of the PIFA at operational frequencies 900, 1800, 2100 and 2600 MHz.

This frequencies are operating with the same input power, which may be some indication. Related to the tissues the highest value is achieved at 900 MHz in hand and head skin, hand SAT and tendon ligament.

The standard limit established by the organizations for 10 grams of tissue - 2 W/kg - is exceeded only for operational frequency of 900 MHz. The standard limit is exceeded in head and hand tissues, being the skin and SAT the tissues more affected. The limit is never reached for the other frequencies in any of the regions. In brain tissues the limit is never reached for any of the frequencies considered, being the less absorption observed at 2100 MHz.

Chapter 5

Conclusions

The use of mobile phones is a normal activity for a very large portion of population, not only for activities that were current in the early years like making calls and texting, but also for new uses that were born with smart-phones like Internet, games, music and photos.

Although the monopole antenna was tested, the external antennas are outdated and the test served only to learn how to use the simulator and to see some disadvantages of monopole antennas compared to more recent antennas.

Then, it was tested a model that consist in an anatomical realistic model provided by ViP and an antenna of type PIFA without cover, a common antenna used nowadays. The first scenario tested try to mimic a "on call" scenario, with the PIFA held by the right hand close to the right ear.

For every simulations performed the collected data is local SAR, peak spatial-average SAR in 10 grams of tissue and the main tissues where those SAR values occurs. The peak spatial-average SAR in 10 grams of tissue is an important value, since it has been found that the maximum temperature increase in the head can be estimated linearly in terms of it and it is known that the temperature increase may be one of the dominant factors which induce adverse physiological effects [65].

The ear skin and the skin close to the ear have the highers SARs. The results of SAR in internal and external cartilage are also significant. This fact can be explained due the location of the feed point of the PIFA, which is placed very close to the ear. High radiation can originate tissue heating and according to [12], the users of mobile phones often complain about burning sensations or heating in the ear region, when the mobile phone is close to the ear.

The absorption by the brain tissues is lower in comparison with the head and hand regions. In fact, in vivo exposure studies demonstrated that EMFs from GSM mobile phones are mainly absorbed by extracerebral tissues including skin, cranial muscles and skull. So, the real amount of power reaching the brain neurons was greatly attenuated by such an absorption process [66]. These external layers provide some protection to the brain.

In brain region the major affected tissues are the grey and white matter, the cerebellum and the hippocampus. Other brain tissues and the respective values are in the complete tables in appendix A.

The effect of the separation distance between the antenna and user head has been studied in this work. This study has shown that there is a decrease in SAR values (local and peak spatial-average 10 grams) as the distance between the antenna and the head increases. Thus, there is a inversely relation between SAR and the separation distance of this particular PIFA.

The same conclusion was reached by [15, 39, 67] in their studies. By increasing the distance of the phone to the head, the peak SAR will be very much lower than the limit SAR as set by CENELEC.

The decrease in SAR values is about 25% (average) in 2 mm spacings both for the tissues of the head and for the tissues of the brain. It is recommended according to this analysis that the distance between antenna and head should be greater than 4 mm to avoid high peak SAR that exceeds the standard limit.

In this project, the effect of the hand has also been studied. The presence and the absence of the hand reveals different values of SAR in head and brain. These results suggest that the presence of the hand decreases the values of SAR in head and brain regions. The standard limit is reached and exceeded in several tissues of the head, but in brain tissues it is not reached.

The same conclusion has been reached in [40]. The authors of this paper showed that the inclusion of hand in the model leads to decrease of the SAR on the user head. This fact is explained by the dissipation by the hand of a part of radiated power of antenna (Okoniewski & Stuchly, 1996 cit. by [40]).

The reduction obtained in the present study on local SAR when the hand is present is of 17.5% on average in head and of 20.6% on average in brain. However, in [40], the value of SAR reduction reaches 27.2%.

The effect of the feeder position was also studied in this work. It was concluded that when the feeder is on the bottom, the SAR values tend to decrease in head and brain tissues, but tend to rise in hand tissues. This is explained because the higher values of electric field occurs close to the feeder point, and if the feed point is on the bottom and the hand is very close to this point, it is expected that the hand would receive more radiation. According to [15], the peak SAR decreases as the feed point is not too close to the human head.

However, this test has led one to a rather important conclusion, if the feed point is on the bottom, the SAR values in brain tissues has a decrease in order of circa 59.7%. Other tissues as the ones in the ear region has a decrease of circa 85.7% and in cheek region, the decrease is almost 28.9%. Only the tissues of the hand have an increase in the value of SAR.

But it does not bring only advantages because there are other tissues that will absorb much more radiation, such as the tissues of the hand and particularly the eyes. In the present study, if the feed point is on the bottom, SAR values on the eyes increased almost threefold of the values obtained when the feeder is on the top.

The eyes are a particular tissue of the body, which is not protected by skin, SAT and muscle. Due this fact, the eyes will receive all the radiation directly and consequently the eye is more hazardously threatened by the irradiation as compared to other human organs. Some studies have been made on this subject and they achieve some interesting conclusions.

According to Polk (2000 cit. by [68]), the absorption of electromagnetic energy in the eye and consequent conversion into heat has been thought of as the principal mechanism responsible for the cataractogenic[1] effect. For the people who wear glasses the maximal SAR in eyes is even eight times more than that without glasses [69].

Each person has their individual way of picking up the mobile phone and pressing it to their ear. To test which would be the best position, three different positions were chosen with 3 different slopes: Cheek and two different tilt positions. This positions are a result of the variation of the angle with the chin. Cheek position is one where the antenna has all its body close and along to the face.

In conclusion, antenna tilt positions are definitely better in terms of reduced SAR. Cheek position resulted in the highest SAR values of the three positions tested and it is the only that exceed the standard limit established by the organizations. Tilt positions have a decrease on SAR values of 44.56% in head tissues and of 48.02% in brain tissues.

Same conclusions are achieved by an intercomparison study [70] performed in 17 laboratories to test the errors between SAR measurments. Hossain et.al. [67] also attest that the tilt positions of antenna produces relatively low SAR in most cases with some exceptions.

The frequency has been tested to understand the variation on SAR values. The chosen operational frequencies was 900, 1800, 2100 and 2600 MHz, due these frequencies are the most common of GSM, UMTS and LTE, the 2, 3 and 4 generations of mobile phones, respectively. These frequencies had a given input power associated. The power values were chosen on basis of several papers read and represent the most common powers chosen in these subject studies.

The higher absorption of radiation was verified at 900 MHz and 600 mW what is a common fact and refereed in other papers. This fact occurs due the penetration of the EM waves is larger for lower frequencies. According to [15], the EM wave at 900 MHz penetrates deeper into a human head rather than an EM wave at 1800 MHz. Through the values obtained in the present study, this fact is confirmed. Same conclusions are achieved by an intercomparison study [70] that test both 900 and 1800 MHz operational frequencies.

Other study [46] that compares the ranges of EMR emissions during a call, says that a UMTS mobile phone has on average more chances of emitting less electromagnetic radiation during a call than the GSM mobile phone. Sun et.al. [71] verified in a study with operational frequencies of 900, 1800 and 2100 MHz that the absorptive dose of electromagnetic radiation using 3G mobile phones is the lowest.

The same conclusion was reached by [15], that showed that if the antenna is not too close with the human head (which is the case), as the operational frequency increases, the SAR values decreases.

According to [72], higher SAR values was obtained for higher power. However the new phones generally operate at lower power than older ones, producing less electromagnetic radiation and (theoretically) less risk to health. According to [58], the local SAR values are higher for the higher frequency. However, to achieve this conclusion, the authors used the same power (1W)

[1] tending to induce the formation of cataracts.

for the both frequencies tested (900 and 1800 MHz), which cannot be compared to the simulation performed in this project. But, if one compare the frequencies 1800 and 2100 MHz, both working at the same power (125mW), it is noticeable some increases in tissues like SAT, Cerebrum grey and white matter and Tendon ligament. Nevertheless, as this fact is not verified for all tissues, it cannot be concluded that SAR increases with frequency increasing.

The SAR values for the designed PIFA were higher than the standard at some frequency points specially in the GSM 900, because the antenna element was not embedded in a real handset [39].

In several simulations performed on this project, the hand tissues have high SAR values, sometimes even higher that the SAR values on head tissues. It is important to study also the effects of radiation in hand, due it is the most frequent human body part that directly touches the mobile phone, regardless of the user's action.

Therefore, after the results discussed, it can be concluded that it is desirable to reduce the exposure from the mobile phones, and all the devices with antennas in general. Thus, for safety purpose, the users are advised to use their hand-free or turn on their phone speaker while they are talking through the cellular phone [15]. This type of methods that creates a separation between the head and the mobile phone, reduces the energy absorbed by the former.

According to [46] if the user change for a wired hand-free kit the energy absorbed by the head is reduced even up to ten times or for a wireless hands-free kit that uses Bluetooth, which can decrease the energy absorbed by the head up to 100 times.

Kaur et.al. [73] reinforces that the user should prefer buying mobile phones with lower SAR values and avoid their use in closed metallic elevators where higher EM absorption takes place because of reflection and resonance effects. Also, avoid the use of mobile phones in low coverage zones, as establishing the connection requires more power.

These are simple and low-cost measures that could substantially reduce exposure to the brain from mobile phones. There is evidence of increased brain tumor and acoustic neuroma risk, but until definitive scientific answers are available, the adoption of precautions as the above mentioned, particularly among young people, is advisable (Cardis and Sadetzki 2011 cit. by [18]).

5.1 Future work

With Sim4life the possibilities to achieve different perspectives on this subject are close to infinite.

With the several PIFA antennas designed for work at 1800, 2100 and 2600 MHz, the variables distance, feeder orientation and tilt positions can be simulated for each of the frequencies.

It can be performed some curious tests adding pieces to the model, like the use of reading glasses or earrings and check if this accessories can influence the radiation absorption.

The Virtual Population, besides the model Duke (a 34 years old adult) offers other models like women, children of different ages, pregnant women with different gestational periods and elderly, that could be used with the antenna designed in this project, in order to see the differences of SAR.

Regarding the antenna, it can be embedded in a model that mimic a real mobile phone with a plastic or metal case with a plastic keyboard and a glass screen. A multi-antenna scenario can be

also tested, due it is common in the modern mobile phones. The antenna can also be improved to work On-Body, to achieve more reliable values that could be compared with the standard limits.

Nowadays, some researchers study ways of reducing SAR values. One way is the use of shields of some materials, as the example in [54]. In this paper were tested several materials that could decrease SAR. They concluded that materials having conductivity between 0.1 and 3 S/m can be used as good shields for the mobile phones. Examples of this materials are skin (leather) and germanium [2]. It could be interesting the use of these new materials in a simulation on Sim4life.

Nowadays the use of smartphones is often just on hand and away from the head. So it would be interesting to do the study just in hand and check the effects that would exist in that region.

After the SAR simulations, the temperature values can also be obtained by simulation on Sim4life. Finally, after the simulations the real tests could be performed using real phantoms and built antennas.

[2] Germanium is a chemical element, grayish-white metalloid in the carbon group.

Appendix A

Complete data tables and other additional information

In this Appendix are represented the several simulation results of model "Duke and PIFA" and other free space simulations of the PIFA antenna. The results contain the complete table with all the body regions and tissues with the respective value of local and peak spatial-average SAR in 10g of tissues for the several scenarios simulated in this project. Moreover, some images containing slices of tissues representing the SAR range in a color map are also presented.

A.1 Free space simulations for 1800, 2100 and 2600 MHz

A free space simulation consist in a simulation where the PIFA is in the vaccum (air on background). The simulations in free space are important not only to test the performance of the antenna, but also to know where the electric and magnetic field concentrates, mainly in studies of this type. As the value of SAR depends of electric field magnitude, the body regions close to the locals where the antenna have more intensity will have, consequently, highers SARs.

Simulations in free space were performed to test the four antennas designed to work at operational frequencies of 900, 1800, 2100 and 2600 MHz, representing the most common bands used in mobile phones nowadays. The first band, 900 MHz, was tested and corresponding results are on the section 3.2.1.2. The other simulation results are presented below.

Table A.1: PIFA characteristics at 1800 MHz.

Name	**Value**	**Unit**
Voltage (V)	$3.80e^{j1.82}$	[V]
Current (I)	$0.08e^{j1.31}$	[A]
Power (Pi)	125.11	[mW]
Reflection Coefficient (Γ)	$0.26e^{j1.55}$	-
Return Loss	11.71	[dB]
VSWR	1.70	-
Input Impedance (Zi)	44.05 + 24.54j	[Ohm]

The next simulation performed was the PIFA at operational frequency of 1800 MHz and working with an input power of 125 mW. The values of its characteristics are on table A.1. The return loss of this antenna is 11.71 dB, higher than 10 dB as intended.

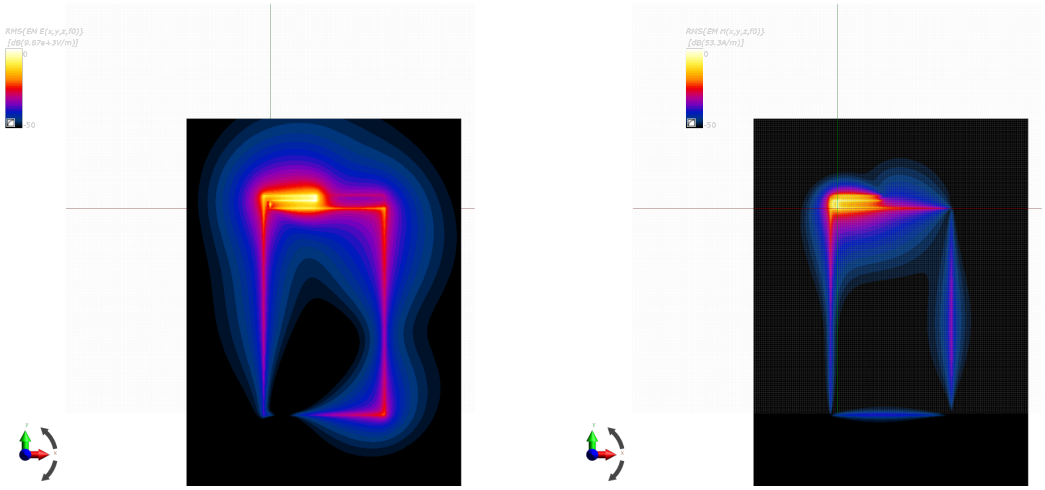

(a) (b)

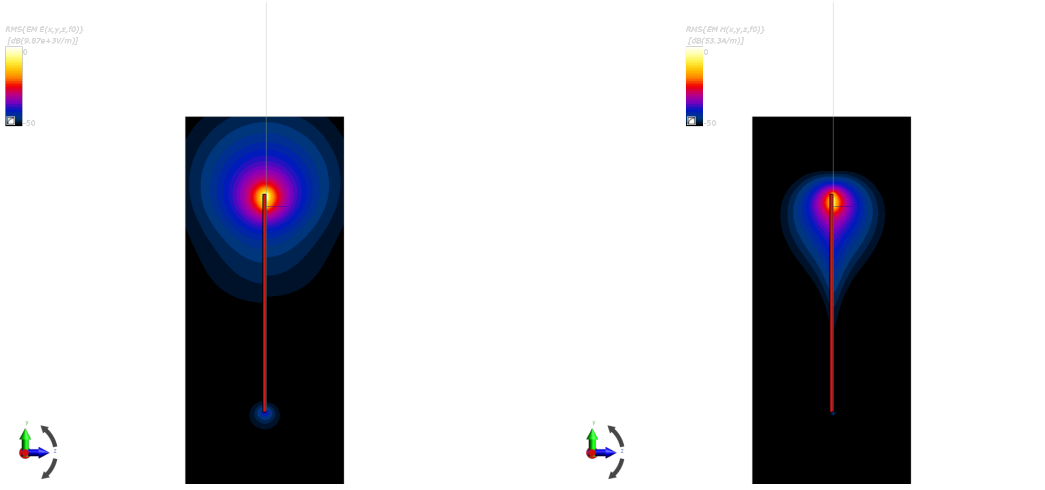

(c) (d)

Figure A.1: Representation of electric and magnetic field on xy-plan (a)(b) and yz-plan (c)(d) at 1800 MHz

In figure A.1 are represented the electric and magnetic field of the PIFA working at an operational frequency of 1800 MHz and with an input power of 125 mW. Analysing this figure, one can see that the higher intensity of the fields is very close to the feed point of the antenna as expected. On the side view of the antenna, can be seen a major intensity on top, but on the bottom the intensity is very low.

Table A.2: PIFA characteristics at 2100 MHz.

Name	**Value**	**Unit**
Voltage (V)	$3.53e^{j1.78}$	[V]
Current (I)	$0.08e^{j1.38}$	[A]
Power (Pi)	125.10	[mW]
Reflection Coefficient (Γ)	$0.21e^{j1.79}$	-
Return Loss	13.63	[dB]
VSWR	1.53	-
Input Impedance(Zi)	42.21 + 17.94j	[Ohm]

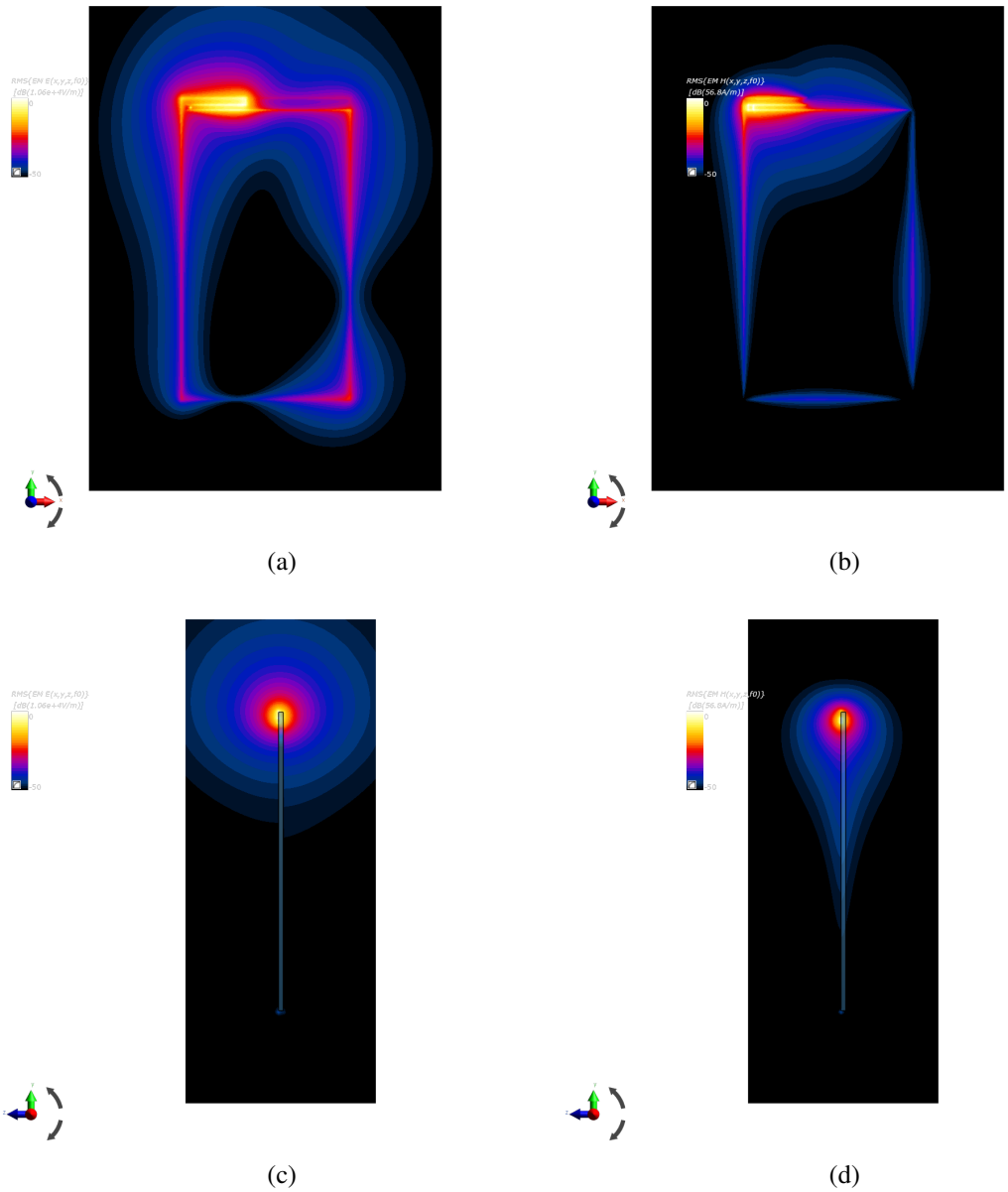

(a) (b)

(c) (d)

Figure A.2: Representation of electric and magnetic field on xy-plan (a)(b) and yz-plan (c)(d) at 2100 MHz

Table A.3: PIFA characteristics at 2600 MHz.

Name	Value	Unit
Voltage (V)	$4.26e^{j1.72}$	[V]
Current (I)	$0.10e^{j1.44}$	[A]
Power (Pi)	199.64	[mW]
Reflection Coefficient (Γ)	$0.16e^{j2.02}$	-
Return Loss	16.12	[dB]
VSWR	1.37	-
Input Impedance (Zi)	41.99 + 12.10j	[Ohm]

The antenna PIFA at operational frequency of 2100 MHz has its characteristics presented on table A.2. This antenna is working with an input power of 125 mW. The return loss of this antenna is 13.63 dB, higher than 10 dB as intended.

In figure A.2 are represented the electric and magnetic field of the PIFA working at an operational frequency of 2100 MHz and with an input power of 125 mW. Analysing this figures, one can see that the higher intensity of the fields is very close to the feed point of the antenna as expected. On the borders of the antenna also exists a considerable intensity of electric and magnetic fields. On the side view of the antenna, can be seen a major intensity on top with a round shape, but on the bottom the intensity is very low.

The last free space simulation was with PIFA at operational frequency of 2600 MHz and a working input power of 199.5 mW. The characteristics of this antenna are presented on table A.3, where can be deducted the return loss of this antenna that is 16.11 dB, higher than 10 dB as intended.

The electric and magnetic field of the PIFA working at an operational frequency of 2600 MHz and with an input power of 199.5 mW are represented in figure A.3. In the figure, it can be seen that the higher intensity of the fields is very close to the feed point of the antenna as expected. On the borders of the antenna also exists a considerable intensity of electric and magnetic fields. On the side view of the antenna, can be seen a major intensity on top with an oval shape, but on the bottom the intensity is very low.

A.2 SAR on Duke and PIFA - original model

The original model representing the talking scenario is refereed in the whole chapter 4.2 to test different variables to compute SAR in the three regions, and in particular, due the aim of this project, in the brain. In this section, one can see several slices of an horizontal plane seen from above of the anatomical model Duke created on Sim4life (Fig. A.4). The chosen four tissues are the ones with the higher values of SAR for each region analysed. The color scale is present in each image and has a range of color from black to white, for the low values to the higher values, respectively. The chosen scale is logarithmic in range of -50 to 0 dB and it is the same for each image, so that the images can be directly comparable.

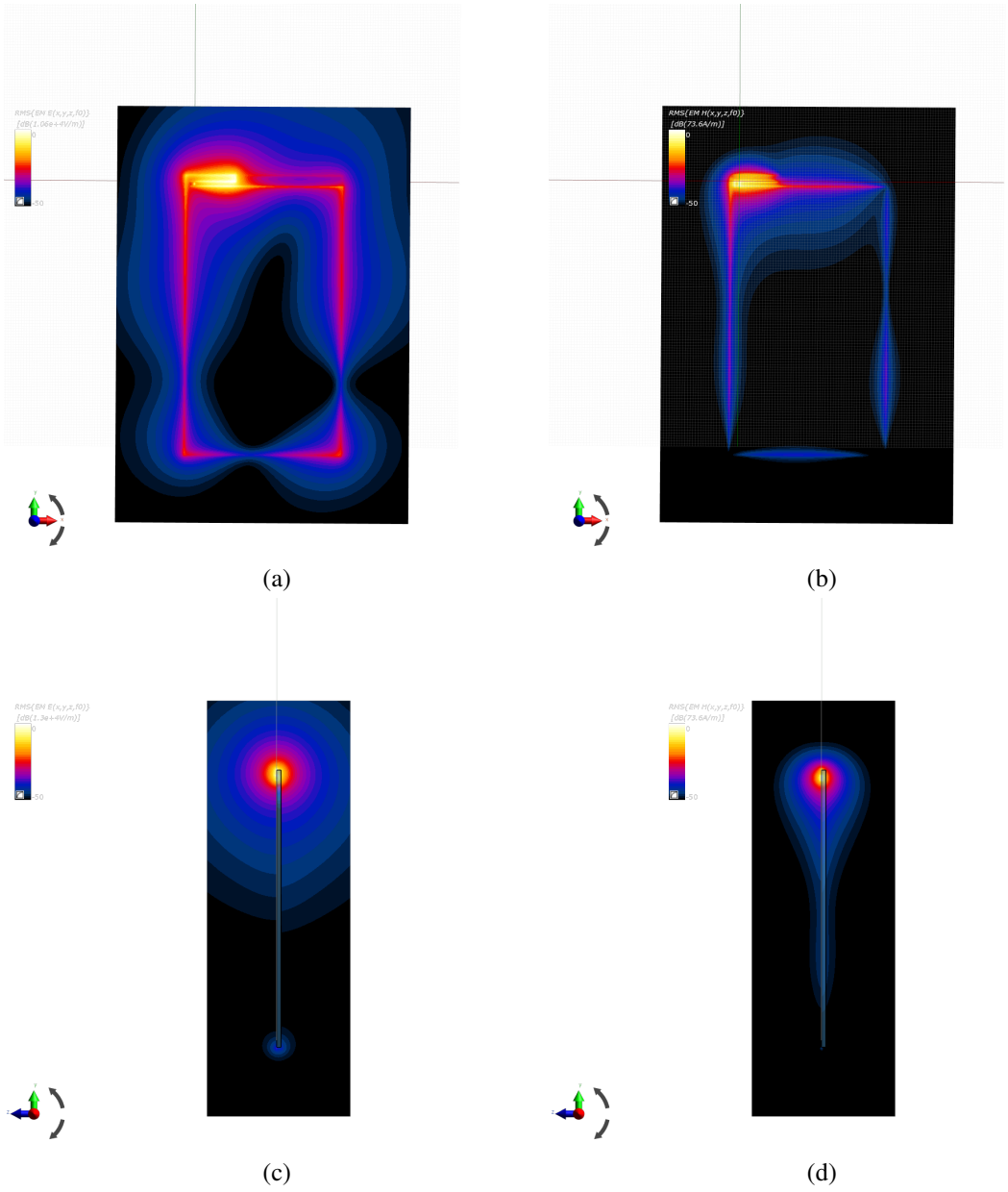

(a) (b)

(c) (d)

Figure A.3: Representation of electric and magnetic field on xy-plan (a)(b) and yz-plan (c)(d) at 2600 MHz

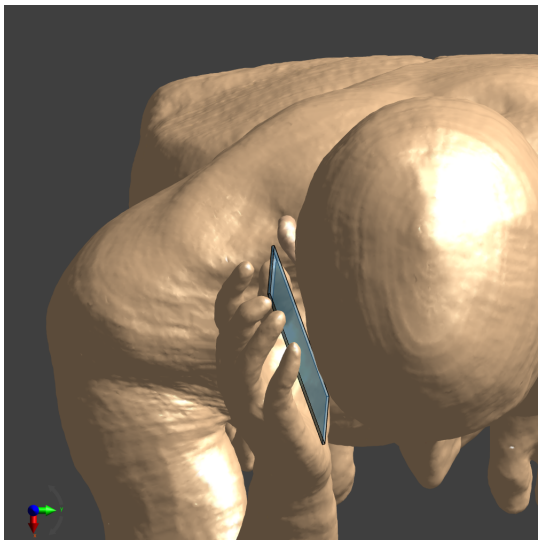

Figure A.4: Model of Duke created on Sim4life - Top view.

A.2.0.1 Local SAR on Hand

In this subsection, it can be seen the four tissues with higher local SAR in hand region. The tissues with higher local SAR for this test are the Skin (A.5a), SAT (A.5b), Muscle (A.6a) and Tendon ligament (A.6b). As one can see the regions with higher SAR, i.e. the white and yellowish ones are closer to the feed point of the antenna. These slices were obtained using a mask that only shows the desired tissue. Although the aim of this section is to analyse the hand tissues, some common tissues with head like Skin, SAT and Muscle can also be seen.

A.2.0.2 Local SAR on Head

The head tissues with higher local SAR for this test are the Right Ear Skin (A.7a), Right Ear Cartilage (A.7b), Cartilage (A.8a) and Vein (A.8b).

A.2.0.3 Local SAR on Brain

The brain tissues with higher local SAR for this test are the Cerebrum grey matter (A.9a), Cerebrum white matter (A.9b), Cerebellum (A.10a) and Hippocampus (A.10b).

A.3 SAR on Duke and PIFA - model with no hand

The original model was changed removing the hand of the model, regarding the objective to know the SAR values in head and brain and see if the absence of the hand results in a change in the radiation that reaches the head. This section refers the simulation performed in section 4.2.2 of the document. In this section, one can see several slices of an horizontal plane seen from above of the head of anatomical model Duke created on Sim4life (Fig. A.4). The chosen four tissues are the ones with the higher values of SAR for each region analysed. The color scale is present in

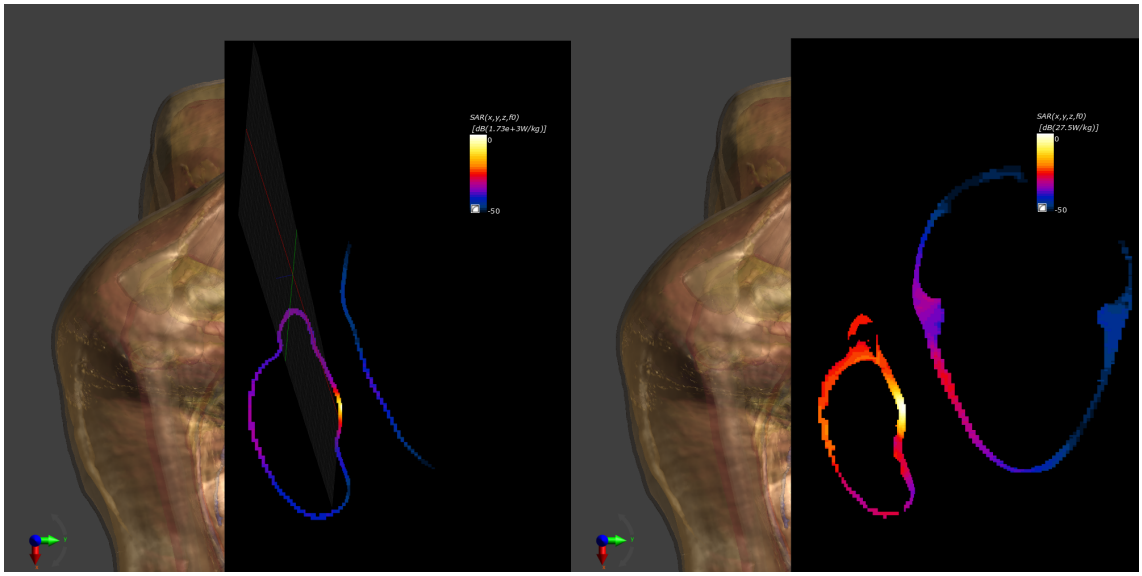

(a) Skin (b) Subcutaneous adipose tissue

Figure A.5: Horizontal plane of Local SAR in hand tissues (Skin and SAT).

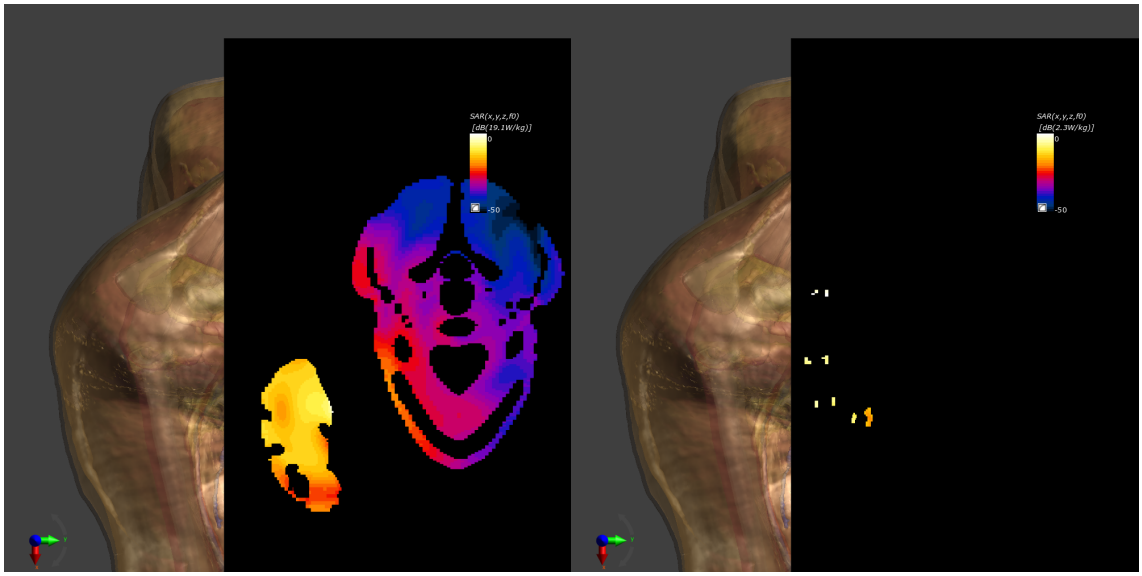

(a) Muscle (b) Tendon Ligament

Figure A.6: Horizontal plane of Local SAR in hand tissues (Muscle and Tendon Ligament).

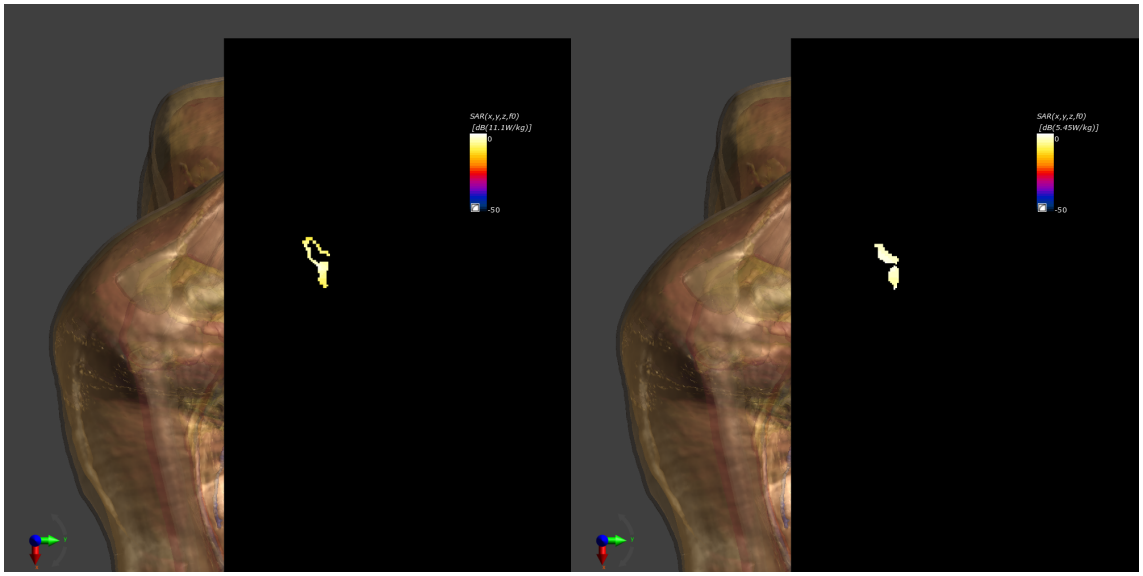

(a) Right Ear Skin (b) Right Ear Cartilage

Figure A.7: Horizontal plane of Local SAR in head tissues (Right Ear Skin and Right Ear Cartilage).

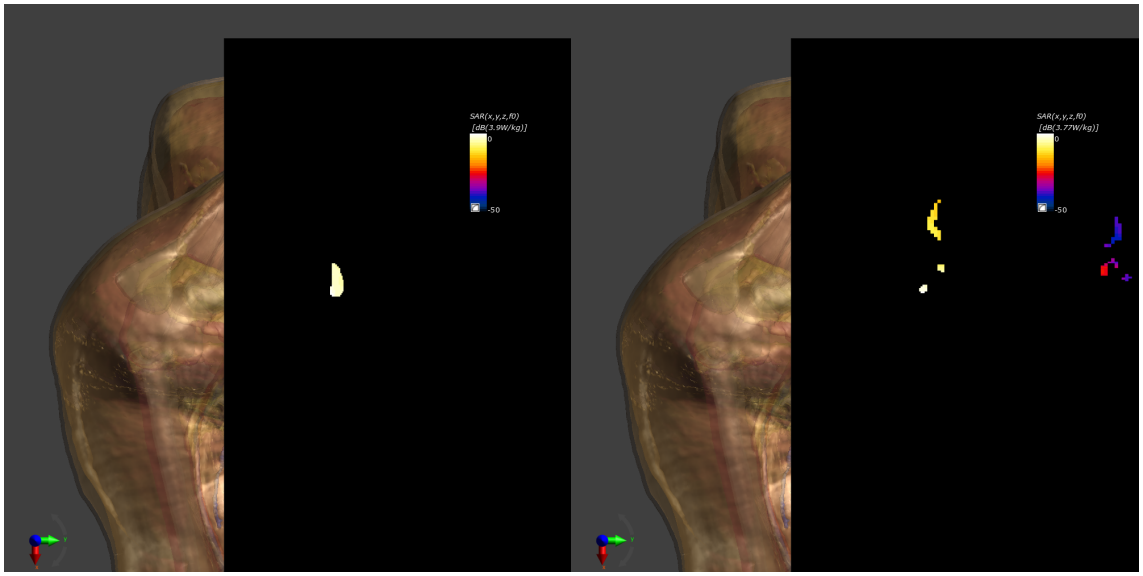

(a) Cartilage (b) Vein

Figure A.8: Horizontal plane of Local SAR in head tissues (Cartilage and Vein).

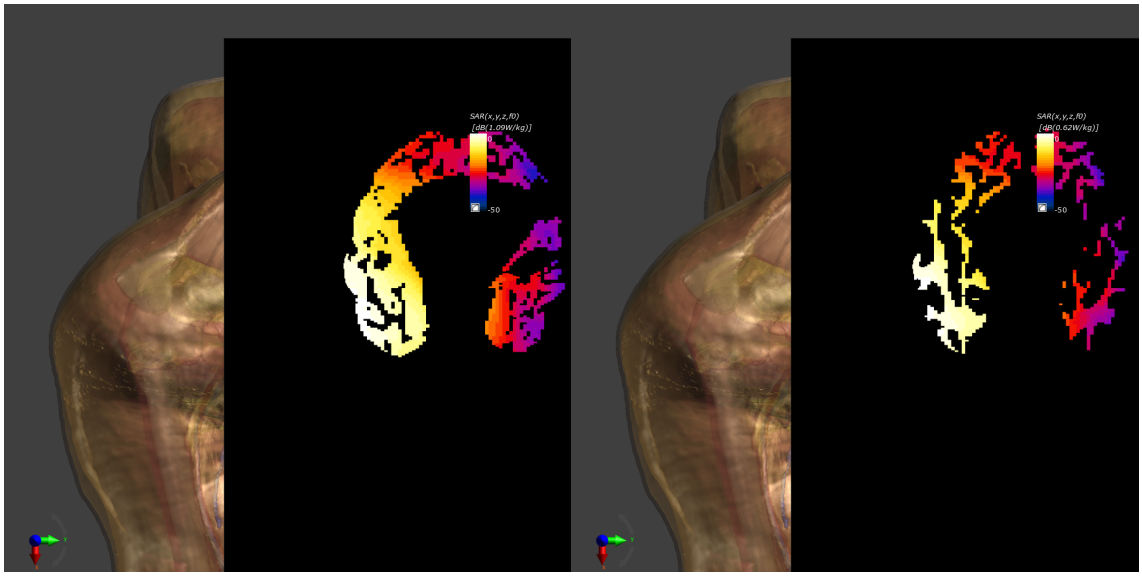

(a) Cerebrum grey matter (b) Cerebrum white matter

Figure A.9: Horizontal plane of Local SAR in brain tissues (Cerebrum grey matter and Cerebrum white matter).

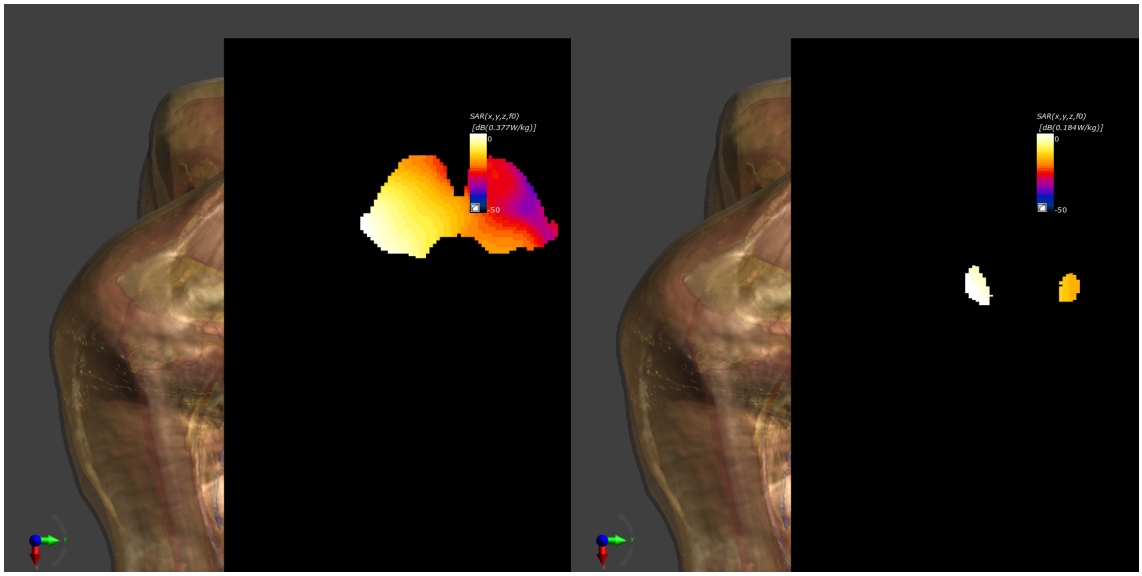

(a) Cerebellum (b) Hippocampus

Figure A.10: Horizontal plane of Local SAR in brain tissues (Cerebellum and Hippocampus).

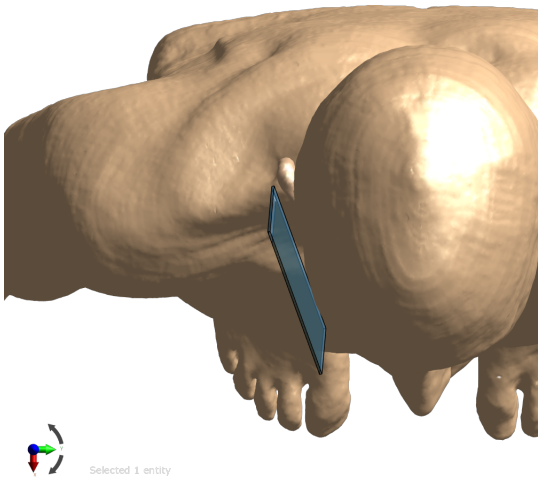

Figure A.11: Model of Duke without hand holding the antenna created on Sim4life - Top view.

each image and has a range of color from black to white, for the low values to the higher values, respectively. The chosen scale is logarithmic in range of -50 to 0 dB and it is the same for each image, so that the images can be directly comparable.

A.3.0.1 Local SAR on Head

In this subsection, it can be seen the four tissues with higher local SAR in head region. The tissues with higher local SAR for this test are the Skin (A.12a), Right Ear Skin (A.12b), Cartilage (A.13a) and Right Ear Cartilage (A.13b). As one can see the regions with higher SAR, i.e. the white and yellowish ones are closer to the feed point of the antenna. These slices were obtained using a mask that only shows the desired tissue.

A.3.0.2 Local SAR on Brain

The brain tissues with higher local SAR for this test are the Cerebrum grey matter (A.14a), Cerebrum white matter (A.14b), Cerebellum (A.15a) and Hippocampus (A.15b).

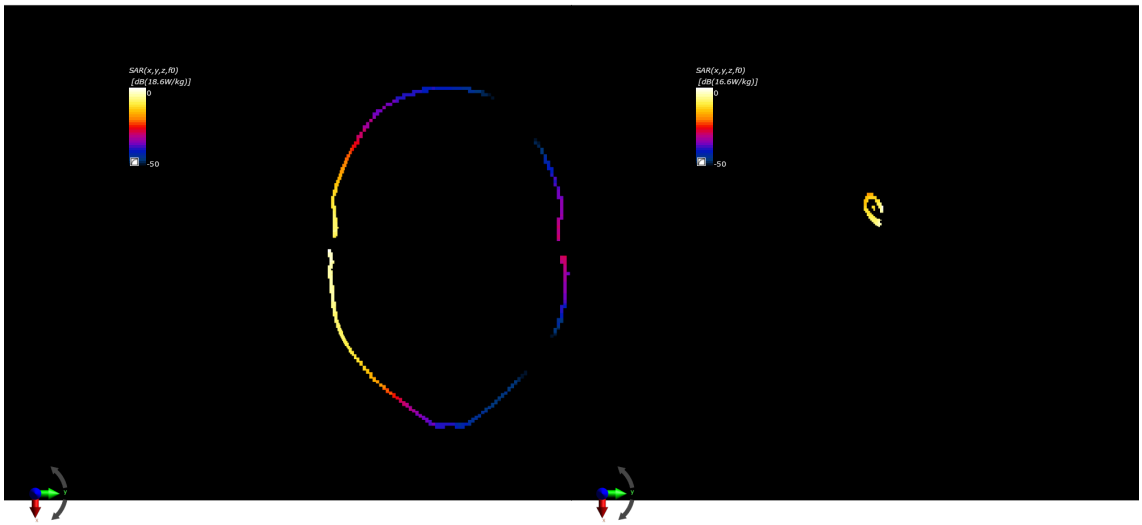

(a) Skin (b) Right Ear Skin

Figure A.12: Horizontal plane of Local SAR in head tissues (Skin and Right Ear Skin).

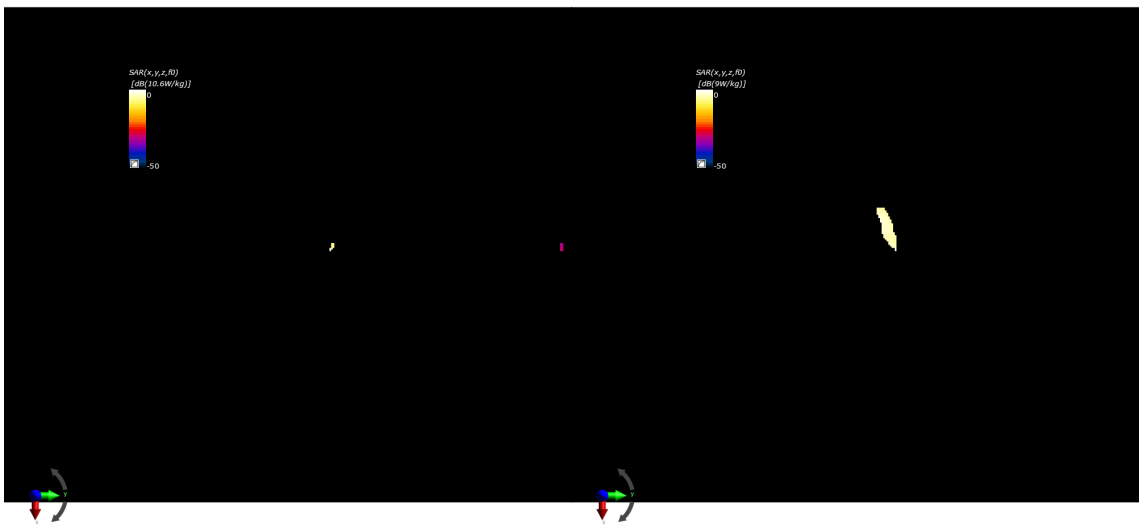

(a) Cartilage (b) Right Ear Cartilage

Figure A.13: Horizontal plane of Local SAR in head tissues (Cartilage and Right Ear Cartilage).

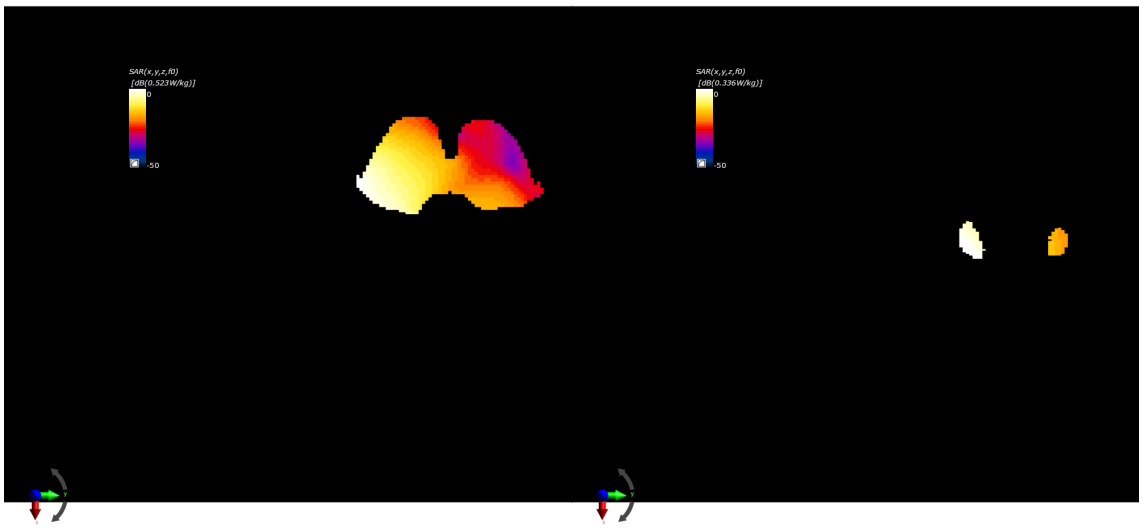

(a) Cerebellum (b) Hippocampus

Figure A.15: Horizontal plane of Local SAR in brain tissues (Cerebellum and Hippocampus).

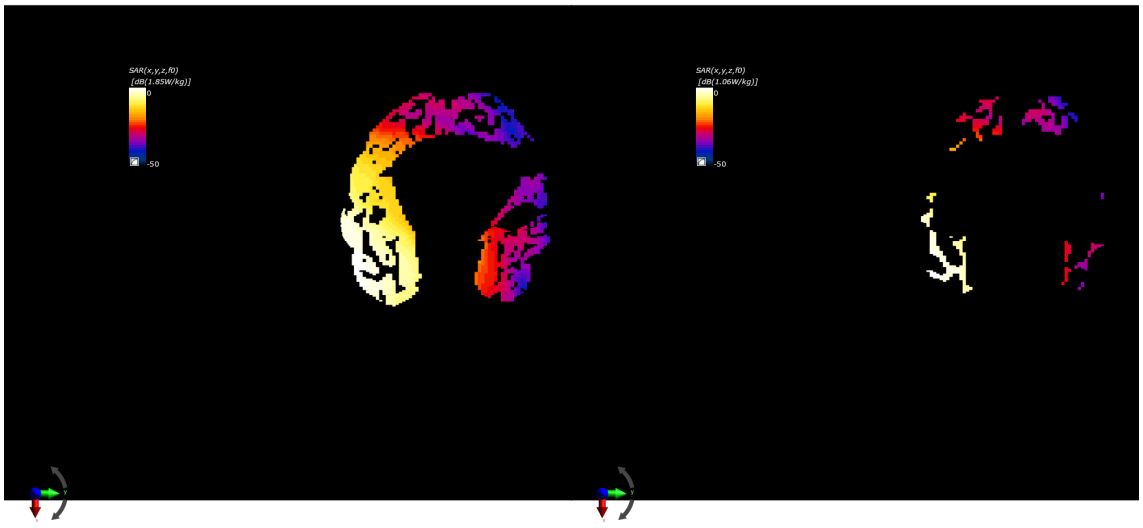

(a) Cerebrum grey matter (b) Cerebrum white matter

Figure A.14: Horizontal plane of Local SAR in brain tissues (Cerebrum grey matter and Cerebrum white matter).

A.4 Complete data table of Duke and PIFA working at 900 MHz

In this section can be found a complete data table with the Minimum local SAR, Mass-Averaged SAR, Maximum local SAR and Peak Spatial-Average SAR in 10 grams of tissue for all the tissues inside the grid considered and ordered by Maximum local SAR. The scenario considered is the

original one, i.e at operational frequency of 900 MHz, input power of 600mW, initial distance to the head, feeder on top and with hand.

Table A.4: Complete data table of Duke and PIFA working at 900 MHz and 600mW - 1

Regions	Min. local SAR	Mass-Averaged SAR	Max. local SAR	Peak Spatial-Average SAR (10g)
	W/kg	W/kg	W/kg	W/kg
Antenna Substrate	3.83E-05	6.19E-01	1.49E+02	2.37E+00
Skin	8.19E-06	2.33E-01	2.50E+01	2.41E+00
Ear_skin_right	1.53E-01	2.30E+00	1.75E+01	2.06E+00
Ear_cartilage_right	2.77E-01	2.38E+00	6.99E+00	2.03E+00
Cartilage	7.59E-05	4.06E-01	6.52E+00	2.07E+00
Vein	1.05E-04	8.65E-02	5.65E+00	1.19E+00
Muscle	1.03E-05	1.36E-01	5.59E+00	2.12E+00
Salivary_gland	2.38E-04	4.61E-01	3.98E+00	2.12E+00
Cerebrospinal_fluid	1.06E-04	3.72E-02	3.48E+00	8.99E-01
Artery	8.33E-05	1.16E-01	3.22E+00	1.44E+00
Mucosa	5.58E-05	6.51E-02	3.08E+00	1.06E+00
SAT	2.51E-06	3.91E-02	2.77E+00	2.35E+00
Tendon_ligament	4.76E-05	1.51E-01	2.67E+00	2.18E+00
Dura_mater	3.24E-05	5.70E-02	2.29E+00	1.01E+00
Skull_cancellous	1.59E-05	5.34E-02	2.05E+00	2.01E+00
Cerebrum_grey_matter	6.09E-05	4.71E-02	1.41E+00	9.55E-01
Mandible_cancellous	5.14E-04	3.98E-02	1.16E+00	1.47E+00
Phalanx_proximalis_II_cancellous_right	3.75E-01	5.82E-01	1.06E+00	6.59E-01
Carpalia_Metacarpalia_cancellous_right	5.88E-03	2.21E-01	1.06E+00	9.43E-01
Phalanx_proximalis_III_cancellous_right	3.68E-01	5.91E-01	1.05E+00	7.06E-01
Phalanx_media_II_cancellous_right	5.39E-01	7.34E-01	1.04E+00	1.86E+00
Phalanx_distalis_III_cancellous_right	4.07E-01	5.97E-01	8.68E-01	5.87E-01
Phalanx_distalis_II_cancellous_right	3.66E-01	6.34E-01	8.67E-01	2.30E+00
Phalanx_proximalis_IV_cancellous_right	2.24E-01	4.54E-01	8.32E-01	9.24E-01
Cerebrum_white_matter	8.75E-05	2.02E-02	7.96E-01	8.42E-01
Skull_cortical	3.09E-06	1.57E-02	7.78E-01	2.07E+00
Phalanx_media_III_cancellous_right	3.42E-01	4.51E-01	6.60E-01	6.60E-01
Phalanx_proximalis_V_cancellous_right	4.07E-02	2.17E-01	5.16E-01	8.92E-01
Fat	5.69E-06	1.12E-02	5.06E-01	1.75E+00
Cerebellum	8.84E-05	3.23E-02	5.06E-01	2.34E-01
Mandible_cortical	9.28E-05	3.11E-02	4.66E-01	1.59E+00
Tongue	1.41E-04	2.92E-02	4.55E-01	7.08E-01
Phalanx_media_II_cortical_right	1.34E-01	2.37E-01	4.36E-01	1.99E+00
Phalanx_proximalis_II_cortical_right	1.19E-01	1.76E-01	3.96E-01	7.37E-01
Lymph_node	4.40E-04	3.20E-02	3.77E-01	4.75E-01
Eye_sclera	6.84E-04	3.91E-02	3.66E-01	1.97E-01
Metacarpus_I_cancellous_right	5.28E-02	1.22E-01	3.41E-01	7.35E-01
Phalanx_proximalis_I_cancellous_right	6.23E-02	1.38E-01	3.38E-01	5.20E-01
Phalanx_media_III_cortical_right	8.88E-02	1.43E-01	3.27E-01	8.02E-01
Phalanx_proximalis_III_cortical_right	1.11E-01	1.74E-01	3.27E-01	7.66E-01

Table A.5: Complete data table of Duke and PIFA working at 900 MHz and 600mW - 2

Regions	Min. local SAR W/kg	Mass-Averaged SAR W/kg	Max. local SAR W/kg	Peak Spatial-Average SAR (10g) W/kg
Phalanx_media_IV_cancellous_right	1.69E-01	2.55E-01	3.20E-01	7.07E-01
Phalanx_distalis_II_cortical_right	7.95E-02	1.98E-01	3.19E-01	2.32E+00
Phalanx_proximalis_IV_cortical_right	6.83E-02	1.39E-01	3.07E-01	9.31E-01
Carpalia_Metacarpalia_cortical_right	1.16E-03	6.34E-02	3.02E-01	9.43E-01
Phalanx_distalis_III_cortical_right	9.69E-02	1.75E-01	2.97E-01	6.21E-01
Vertebra_cancellous_C1	6.05E-04	3.41E-02	2.63E-01	3.43E-01
Hippocampus	3.77E-03	6.52E-02	2.58E-01	2.34E-01
Nerve	5.81E-05	2.28E-02	2.42E-01	2.81E-01
Eye_vitreous_humor	9.33E-04	4.99E-02	2.41E-01	1.71E-01
Phalanx_proximalis_V_cortical_right	3.97E-03	7.26E-02	2.14E-01	8.92E-01
Phalanx_distalis_IV_cancellous_right	1.16E-01	1.46E-01	1.74E-01	3.40E-01
Phalanx_proximalis_I_cortical_right	1.88E-02	4.52E-02	1.61E-01	6.10E-01
Midbrain	8.93E-03	3.51E-02	1.44E-01	1.01E-01
Phalanx_distalis_I_cancellous_right	4.75E-02	8.00E-02	1.28E-01	9.30E-01
Hypophysis	2.32E-02	4.66E-02	1.22E-01	1.79E-01
Tooth	5.62E-05	5.72E-03	1.20E-01	8.03E-01
Phalanx_media_IV_cortical_right	4.70E-02	7.72E-02	1.18E-01	8.33E-01
Eye_cornea	1.23E-03	2.57E-02	1.17E-01	1.22E-01
Metacarpus_I_cortical_right	1.16E-02	3.51E-02	1.04E-01	7.57E-01
Vertebra_cortical_C1	1.34E-04	9.94E-03	8.86E-02	3.68E-01
Hypothalamus	3.07E-02	5.06E-02	8.14E-02	9.12E-02
Pons	5.31E-03	2.58E-02	7.95E-02	7.97E-02
Thalamus	7.98E-03	2.60E-02	7.69E-02	7.39E-02
Phalanx_distalis_V_cancellous_right	3.89E-02	5.32E-02	7.15E-02	2.37E-01
Phalanx_distalis_IV_cortical_right	3.10E-02	4.88E-02	6.75E-02	3.82E-01
Vertebra_cancellous_C2	7.37E-04	1.35E-02	6.13E-02	9.26E-02
Phalanx_media_V_cancellous_right	1.49E-02	3.03E-02	5.72E-02	3.42E-01
Phalanx_distalis_I_cortical_right	1.44E-02	2.81E-02	5.16E-02	1.11E+00
Radius_cancellous_right	2.81E-03	8.86E-03	4.11E-02	5.66E-02
Ear_skin_left	5.11E-05	1.69E-03	3.98E-02	9.70E-03
Commissura_anterior	3.19E-02	3.43E-02	3.65E-02	5.44E-02
Medulla_oblongata	3.15E-03	1.56E-02	3.57E-02	5.23E-02
Intervertebral_disc	1.58E-04	3.42E-03	3.52E-02	1.47E-02
Eye_lens	4.75E-04	1.18E-02	3.40E-02	1.06E-01
Corpus_callosum	2.57E-03	7.92E-03	3.28E-02	3.96E-02
Phalanx_distalis_V_cortical_right	7.92E-03	1.67E-02	2.70E-02	3.94E-01
Phalanx_media_V_cortical_right	2.64E-03	1.16E-02	2.51E-02	3.99E-01
Ulna_cancellous_right	1.52E-03	3.97E-03	2.17E-02	2.80E-02
Vertebra_cortical_C2	1.30E-04	3.62E-03	1.98E-02	1.02E-01
Radius_cortical_right	5.35E-04	3.39E-03	1.61E-02	6.55E-02
Pineal_body	9.61E-03	1.23E-02	1.50E-02	2.28E-02
Spinal_cord	4.37E-05	2.99E-03	1.40E-02	3.66E-02
Ear_cartilage_left	7.22E-05	1.93E-03	1.38E-02	9.70E-03
Commissura_posterior	1.07E-02	1.23E-02	1.31E-02	2.90E-02

Table A.6: Complete data table of Duke and PIFA working at 900 MHz and 600mW - 3

Regions	Min. local SAR W/kg	Mass-Averaged SAR W/kg	Max. local SAR W/kg	Peak Spatial-Average SAR (10g) W/kg
Ulna_cortical_right	3.43E-04	1.30E-03	1.20E-02	3.24E-02
Hyoid_cancellous	5.54E-04	3.09E-03	9.51E-03	1.36E-02
Larynx	1.17E-04	1.77E-03	8.14E-03	5.19E-03
Vertebra_cancellous_C3	1.16E-04	1.44E-03	6.71E-03	1.20E-02
Trachea_wall	2.92E-04	1.24E-03	3.53E-03	3.57E-03
Hyoid_cortical	1.15E-04	7.70E-04	2.97E-03	1.59E-02
Vertebra_cortical_C3	2.19E-05	4.42E-04	2.85E-03	1.24E-02
Esophagus_wall	5.14E-04	1.28E-03	2.52E-03	3.69E-03
Vertebra_cancellous_C4	9.15E-05	3.52E-04	2.20E-03	2.34E-03
Vertebra_cancellous_C5	6.22E-05	3.50E-04	1.90E-03	2.27E-03
Thyroid_gland	1.83E-04	6.58E-04	9.28E-04	0.00E+00
Radius_yellow_marrow_right	4.38E-04	6.68E-04	9.26E-04	8.88E-03
Ulna_yellow_marrow_right	2.44E-04	4.06E-04	8.43E-04	1.66E-02
Vertebra_cortical_C4	2.10E-05	1.35E-04	7.55E-04	2.78E-03
Vertebra_cortical_C5	1.36E-05	1.25E-04	6.81E-04	2.45E-03
Vertebra_cancellous_C6	3.03E-05	1.83E-04	6.77E-04	6.22E-04
Thorax_cancellous	1.18E-04	1.88E-04	4.32E-04	0.00E+00
Vertebra_cortical_C6	1.04E-05	6.37E-05	2.09E-04	7.79E-04
Vertebra_cancellous_C7	1.01E-04	1.25E-04	1.56E-04	0.00E+00
Thorax_cortical	2.56E-05	5.29E-05	1.20E-04	0.00E+00
Vertebra_cortical_C7	2.15E-05	3.20E-05	5.23E-05	0.00E+00
Background	0.00E+00	0.00E+00	0.00E+00	0.00E+00
Air_internal	0.00E+00	0.00E+00	0.00E+00	0.00E+00
Trachea_lumen	0.00E+00	0.00E+00	0.00E+00	0.00E+00

Appendix B

Head, Brain and Hand Anatomy and Physiology

The daily use of the mobile phones affect directly the head and hand regions whatever it is the function that the user is doing. For a better understand of the absorption of EMF on the regions that this project considered, it is important to know the locations of the several referred tissues inside the head, brain and hand. For this a simple approach to the anatomy and physiology of this regions will be made in this section.

B.1 Head

The head is composed by the skeleton, i.e. skull and mandible, as well as other tissues and organs. The most important regions of the head treated in this project are eyes, ears and mouth. The eyes are divided in several tissues (See fig. B.1), like sclera [1], vitreous humor[2], cornea [3] and lens [4].

The ear is divided in external, middle and internal. The middle and internal ear are not referred in the simulations because they are composed by little and detailed structures which are not susceptible for being transformed by the method FDTD. Only the external ear is represented by skin and cartilage.

The mouth cavity is refereed in the simulations through the tongue, tooth and salivary glands. Salivary glands are exocrine [5] structures that produces saliva and are divided in three major glands: Parotid, Submandibular and Sublingual. (See fig. B.2).

The bones presented can be one of two types: cancellous or cortical. This two bone tissues are biologically identical, but differ in how the microstructure is arranged. Cortical bone is the

[1] Eye sclera is the white of the eye.

[2] Eye vitreous humor is the clear, jelly-like substance that fills the middle of the eye.

[3] Cornea is the transparent front part of the eye .

[4] The lens is a transparent, biconvex structure in the eye that, along with the cornea, helps to refract light to be focused on the retina.

[5] Exocrine glands are glands that produce and secrete substances onto an epithelial surface by way of a duct (e.g. sweat, salivary, mammary, ceruminous, lacrimal, sebaceous, and mucous.

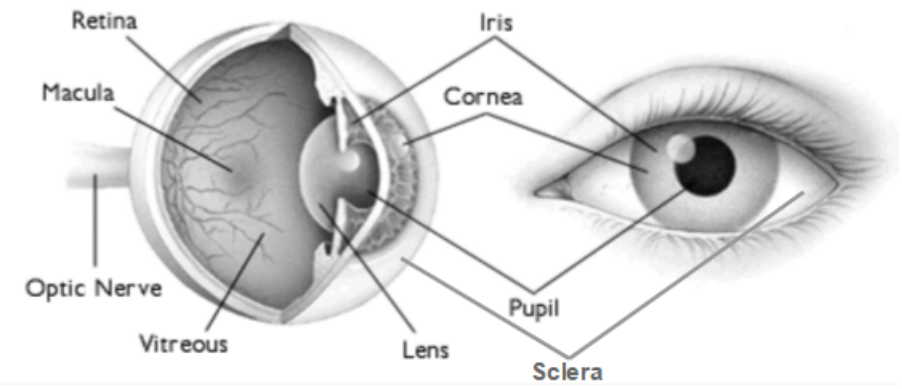

Figure B.1: Eye tissues (Adapted from [74])

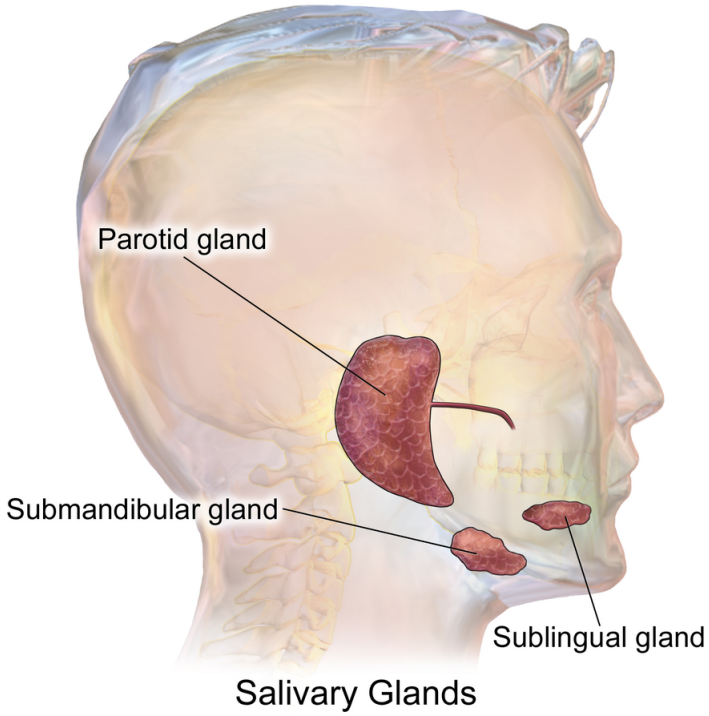

Figure B.2: Salivary glands (From [75])

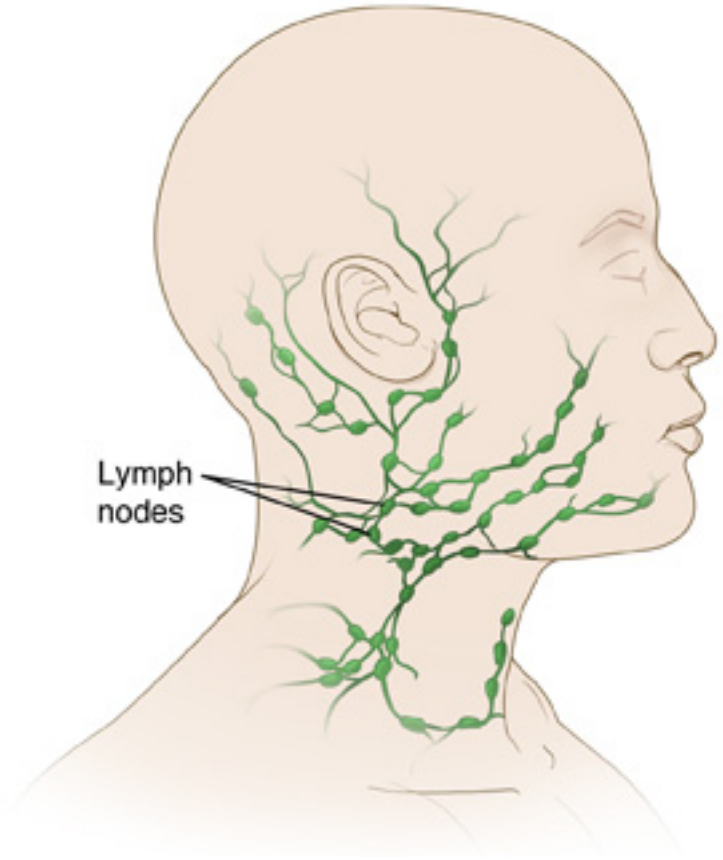

Figure B.3: Lymph nodes of head and neck (From [76])

compact bone which forms the extremely hard exterior of bone. The cancellous bone is the spongy bone which is more interior and less dense than the cortical one.

Besides it, inside the head are also the vessels, i.e. arteries and veins, which are not distinguished in terms of nomenclature in simulation. Close to the circulatory ducts are also the lymph nodes (See fig. B.3), which are part of the immune system.

In the neck region some tissues are also referred in the scope of this project (See fig. B.4). Larynx and Esophagus are two regions that are part of digestive system. Trachea is a cartillage tissue and it is a part of respiratory system. In the tables of the tissues, the trachea and the esophagus are divided in wall and lumen, representing the tissue itself and the cavity filled by air, hence its mass density value is zero. Thyroid gland is an endocrine gland [6] in the neck, which secretes thyroid hormones, which primarily influence the metabolic rate and protein synthesis.

Relative to the bones, there are several in neck and can be seen in figure B.5. Hyoid bone is a small bone situated between the chin and the thyroid cartilage. On posterior side can be found the cervical bones, where seven vertebrae are from C1 to C7.

[6] Endocrine glands secrete their products, hormones, directly into the blood rather than through a duct (e.g. pineal gland, pituitary gland, pancreas, ovaries, testicles, thyroid gland, parathyroid gland, hypothalamus and adrenal glands).

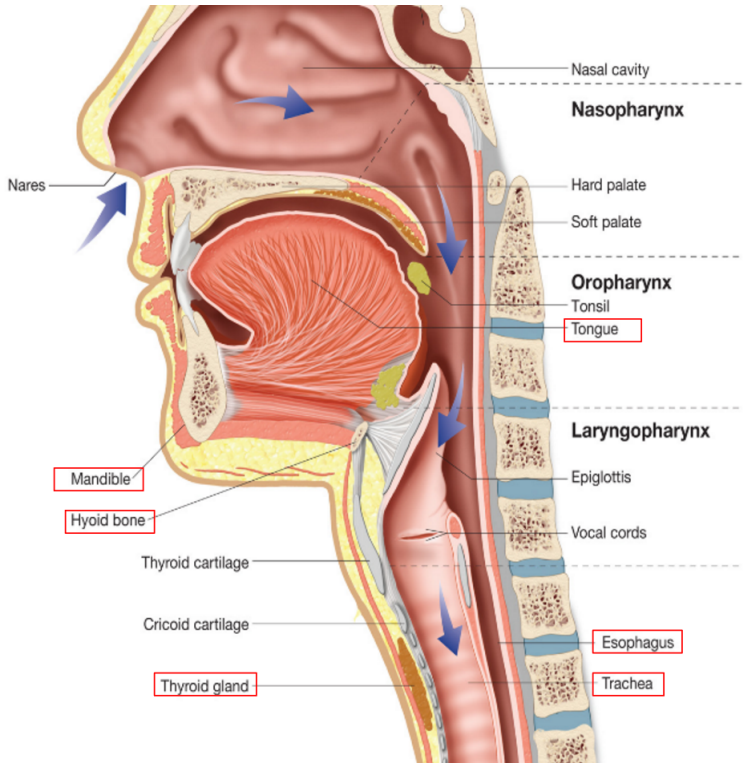

Figure B.4: Sagittal section of upper respiratory system illustrating the internal anatomy of the nasal cavity, pharynx, larynx, and trachea (Adapted from [77])

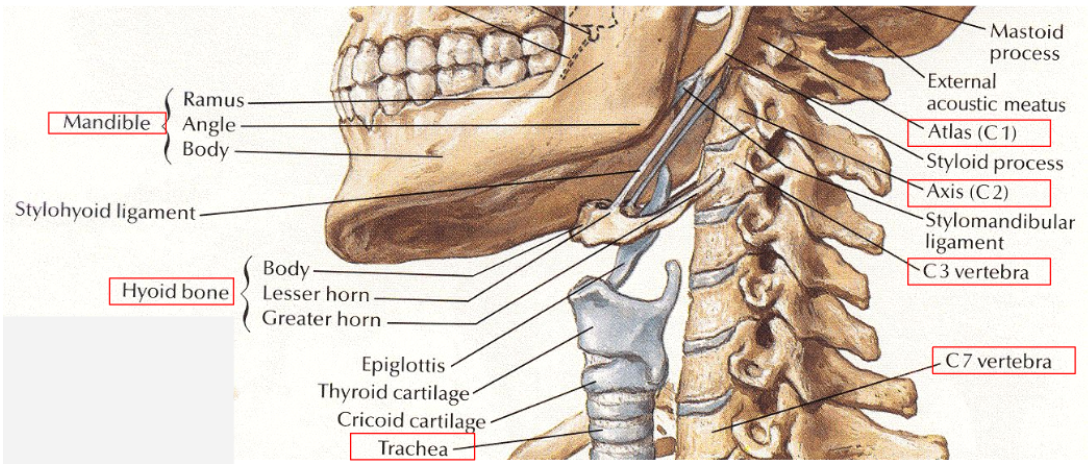

Figure B.5: Neck bones (Adapted from [78])

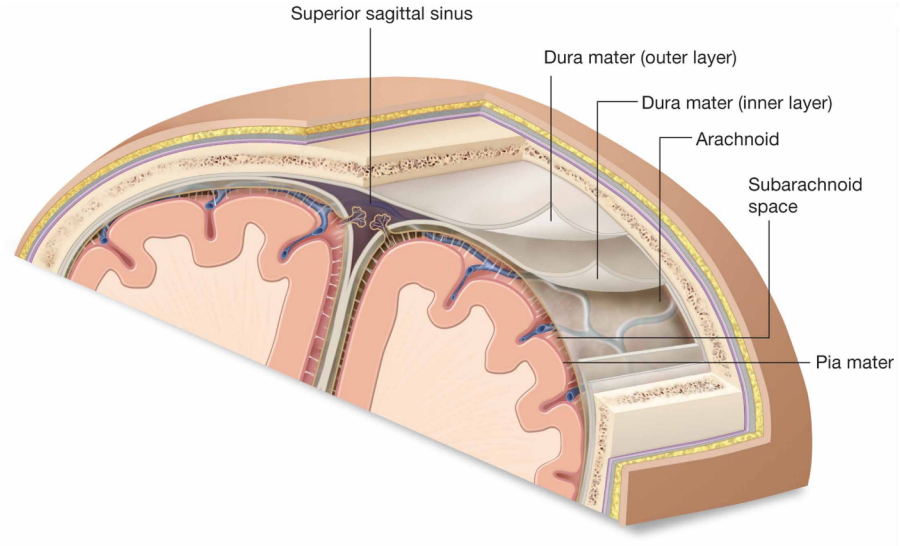

Figure B.6: The meninges from the outside in dura mater, arachnoid, and pia mater. (Adapted from [79])

B.2 Brain

The brain is one of the most important vital organs in humans. It is part of central nervous system (CNS) along with the spinal cord (Fig. B.7). The brain itself is placed inside the cranium, which is the bone portion of the skull that holds the brain.

Under the cranium, there exist other layers, called meninges, that involve the brain. The meninges (Fig. B.6) are three - dura matter, aracnoid and pia matter - and, between the last two, it is the subaracnoid space, which is filled by the cerebrospinal fluid.

The brain is divided in hindbrain, midbrain and forebrain. Medulla oblongata, pons and the cerebellum (Fig. B.7) are part of the hindbrain, the more interior part of the brain. Medulla oblongata is responsible for involuntary functions (e.g. sneezing). Pons carries the sensory signals up into the thalamus. The cerebellum has the function of control of posture, coordination of movements and parts of the body.

The forebrain refers to the conjunct of diencephalon (Fig. B.7) and the cerebrum. The first is composed by thalamus and hypothalamus. Thalamus is a structure of two halves witch its main functions are the transmission of sensory and motor signals to the cerebral cortex. It has also functions in the regulation of consciousness, sleep and alertness. The hypothalamus can control the body temperature, hunger, thirst, fatigue, sleep and circadian rhythms. This structure assumes an important role due one of this functions be the link between the nervous system and the endocrine system via the pituitary gland (or Hypophysis).

Cerebrum is composed by two cerebral hemispheres witch are connected by a mass called corpus callosum, which is a set of nerves that promotes inter hemispheric communication. This structure is part of cerebrum white matter that is the largest part of the brain. Involving the white matter, the cerebellum and other regions is the cerebrum grey matter (Fig. B.8), which contains

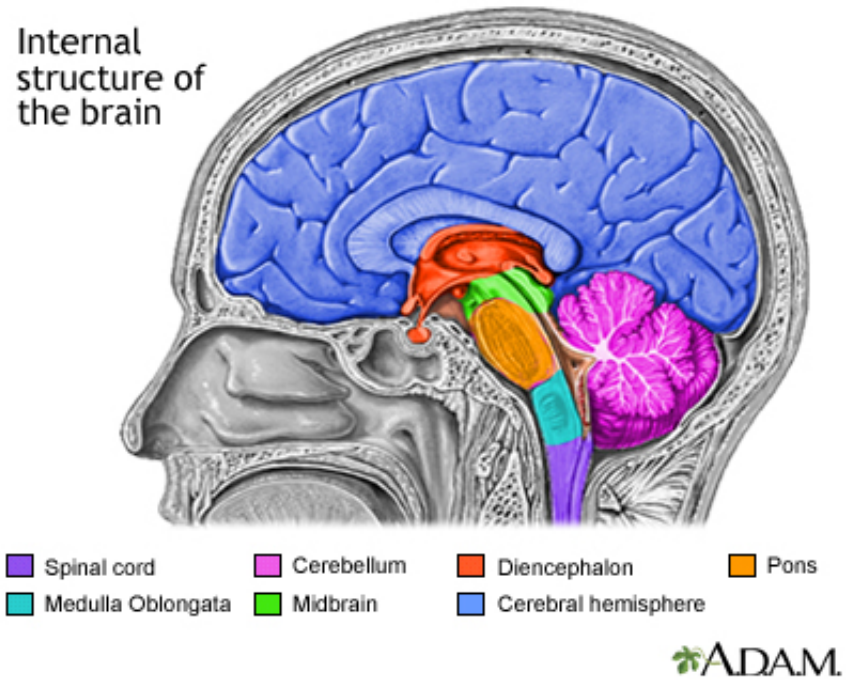

Figure B.7: Brain structures (From [80])

most of the brain's neuronal cell bodies.

Other important structures of the brain that are motioned in this project are the hippocampus and the anterior and posterior commissure. The hippocampus is composed by two structures, one of each in the two sides of the brain. Its major roles are related to short-term and spatial memory.

The anterior commissure is a set of nerve fibers that connects the two temporal lobes of the cerebral hemispheres and its main function is in pain sensation and sense of smell.

The midbrain (Fig. B.7) is located upon the pons and is responsible for hearing, vision, motor control, sleep, arousal and temperature regulation.

B.3 Hand

The hand like the other parts of our body is composed by layers of skin, subcutaneous adipose tissue and muscle. Between the muscles exist other type of tissue named tendon ligaments, which are a tough band of fibrous connective tissue that usually connects muscle to bone and is capable of withstanding tension.

In this project the tissues of the hand more referred are the bones, which are represented in figure B.9. The fingers are represented by a number I, II, III, IV and V and each one of them are divided in bones called Phalanges (Distal, Middle and Proximal). In the palm region of the hand are the metacarpals that are also represented by a number and on the wrist region are the carpal bones that connects with the arm bones [82].

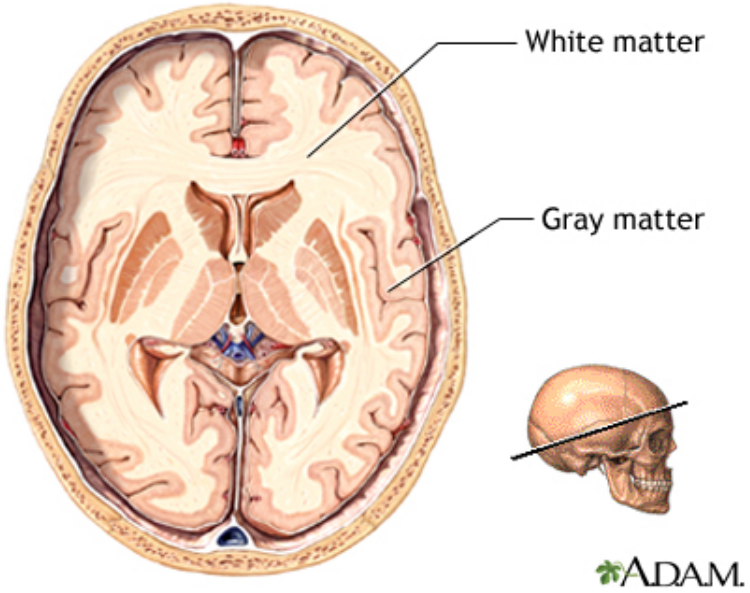

Figure B.8: Grey and White matter (From [81])

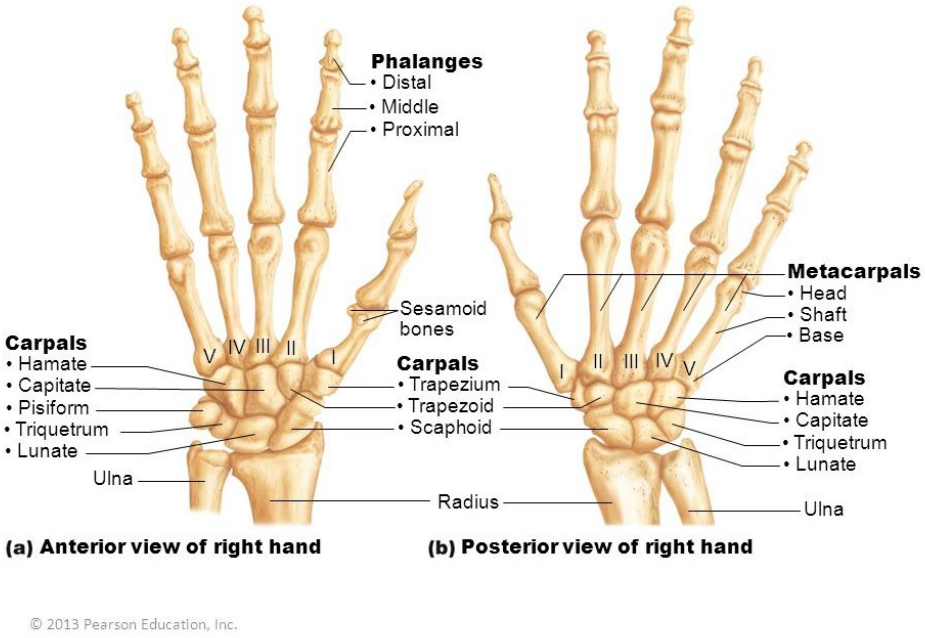

Figure B.9: Bones of right hand (From [83])

References

[1] International Agency for Research on Cancer et al. Iarc classifies radiofrequency electromagnetic fields as possibly carcinogenic to humans. *Press release*, (208), 2011.

[2] Joe Wiart. *Radio-Frequency Human Exposure Assessment: From Deterministic to Stochastic Methods*. John Wiley & Sons, 2016.

[3] David K. Cheng. Addison-Wesley Publishing Company, Inc., 1 edition, 1983.

[4] Yi Huang and Kevin Boyle. *Antennas: from theory to practice*. John Wiley & Sons, 2008.

[5] Warren L Stutzman and Gary A Thiele. *Antenna theory and design*. John Wiley & Sons, 2012.

[6] Riadh Habash. *Bioeffects and therapeutic applications of electromagnetic energy*. CRC press, 2007.

[7] Mary Redmayne. Wireless phone use by young new zealanders: Health and policy implications. 2013.

[8] World Health Organization et al. *Establishing a dialogue on risks from electromagnetic fields*. Geneva: World Health Organization, 2002.

[9] Zuzana Psenakova. Numerical modeling of electromagnetic field effects on the human body. *Advances in Electrical and Electronic Engineering*, 5(1-2):319, 2006.

[10] A Lak. Human health effects from radiofrequency and microwave fields. *J Basic Appl Sci Res*, 2(9):9446–53, 2012.

[11] Marko S Markov and Marko S Markov. Benefit and hazard of electromagnetic fields. In *Electromagnetic Fields in Biology and Medicine*, pages 15–28. CRC Press, 2015.

[12] Valerio De Santis. Ear temperature increase produced by cellular phones under extreme exposure conditions. *IEEE Transactions on Microwave Theory and Techniques*, 60(6):1728–1734, 2012.

[13] James C Lin. *Electromagnetic fields in biological systems*. CRC press, 2011.

[14] Carlos Cabrita. Efeitos biológicos dos campos electromagnéticos e da radiação (biological effects of electromagnetic fields and radiation), author's edition. *University of Beira Interior*, 2008.

[15] Nurulhuda binti Ismail and Mohd Zarar bin Mohd Jenu. Modeling of electromagnetic wave penetration in a human head due to emissions from cellular phone. In *Applied Electromagnetics, 2007. APACE 2007. Asia-Pacific Conference on*, pages 1–5. IEEE, 2007.

[16] Dimitris J Panagopoulos, Olle Johansson, and George L Carlo. Evaluation of specific absorption rate as a dosimetric quantity for electromagnetic fields bioeffects. *PloS one*, 8(6):e62663, 2013.

[17] Non-Ionizing Radiation Protection. Extremely low frequency fields. 2007.

[18] Om P Gandhi, L Lloyd Morgan, Alvaro Augusto de Salles, Yueh-Ying Han, Ronald B Herberman, and Devra Lee Davis. Exposure limits: the underestimation of absorbed cell phone radiation, especially in children. *Electromagnetic Biology and Medicine*, 31(1):34–51, 2012.

[19] Rakefet Czerninski, Avi Zini, and Harold D Sgan-Cohen. Risk of parotid malignant tumors in israel (1970–2006). *Epidemiology*, 22(1):130–131, 2011.

[20] Luisa Nascimento Medeiros and Tanit Ganz Sanchez. Tinnitus and cell phones: the role of electromagnetic radiofrequency radiation. *Brazilian journal of otorhinolaryngology*, 82(1):97–104, 2016.

[21] Mosa Moradi, Nasrollah Naghdi, Hamidreza Hemmati, Majid Asadi-Samani, and Mahmoud Bahmani. Effects of the effect of ultra high frequency mobile phone radiation on human health. *Electronic Physician*, 8(5):2452, 2016.

[22] Ashok Agarwal, Fnu Deepinder, Rakesh K Sharma, Geetha Ranga, and Jianbo Li. Effect of cell phone usage on semen analysis in men attending infertility clinic: an observational study. *Fertility and sterility*, 89(1):124–128, 2008.

[23] Mary Redmayne. New zealand adolescents' cellphone and cordless phone user-habits: are they at increased risk of brain tumours already? a cross-sectional study. *Environmental Health*, 12(1):1, 2013.

[24] Andreas Christ, Marie-Christine Gosselin, Maria Christopoulou, Sven Kühn, and Niels Kuster. Age-dependent tissue-specific exposure of cell phone users. *Physics in medicine and biology*, 55(7):1767, 2010.

[25] Riadh Habash. Handbook of engineering electromagnetics. 2004.

[26] Bahriye Sirav and Nesrin Seyhan. Effects of radio-frequency radiation on the permeability of blood-brain barrier. *Medical Science and Discovery*, 3(5):206–12, 2016.

[27] Elisabeth Cardis, BK Armstrong, JD Bowman, GG Giles, M Hours, D Krewski, M McBride, ME Parent, S Sadetzki, A Woodward, et al. Risk of brain tumours in relation to estimated rf dose from mobile phones: results from five interphone countries. *Occupational and Environmental Medicine*, 68(9):631–640, 2011.

[28] Lennart Hardell, Michael Carlberg, Fredrik Söderqvist, Kjell Hansson Mild, and L Lloyd Morgan. Long-term use of cellular phones and brain tumours: increased risk associated with use for 10 years. *Occupational and Environmental Medicine*, 64(9):626–632, 2007.

[29] Frank S Barnes and Ben Greenebaum. *Biological and medical aspects of electromagnetic fields*. CRC press, 2006.

[30] Sim4Life Application and Support Team. *Sim4Life Reference Guide Release 3.0*, jul 2016.

[31] Paolo Bernardi, Marta Cavagnaro, Stefano Pisa, and Emanuele Piuzzi. Specific absorption rate and temperature increases in the head of a cellular-phone user. *IEEE transactions on microwave theory and techniques*, 48(7):1118–1126, 2000.

[32] Peter Stavroulakis. *Biological Effects of Electromagnetic Fields: mechanisms, modeling, biological effects, therapeutic effects, international standards, exposure criteria*. Springer Science & Business Media, 2013.

[33] Akimasa Hirata, Jianqing Wang, Osamu Fujiwara, Masaki Fujimoto, and Toshiyuki Shiozawa. Maximum temperature increases in the head and brain for sar averaging schemes prescribed in safety guidelines. In *Electromagnetic Compatibility, 2005. EMC 2005. 2005 International Symposium on*, volume 3, pages 801–804. IEEE, 2005.

[34] Gaurav R. Joshi Margish S. Joshi. Analysis of sar induced in human head due to the exposure of non-ionizing radiation. *International Journal of Engineering Research & Technology*, 5(02), feb 2016.

[35] Mohammad Naser-Moghadasi, Zahra Mansouri, Sachin Sharma, Ferdows B Zarrabi, and Bal S Virdee. Low sar pifa antenna for wideband applications. *IETE Journal of Research*, pages 1–7, 2016.

[36] Corbett Rowell and Edmund Y Lam. Mobile-phone antenna design. *IEEE Antennas and Propagation Magazine*, 54(4):14–34, 2012.

[37] Khalid Saif and Nazem Alsmadi. Mobile phone antenna design. 2015.

[38] MR Iqbal Faruque, Mohammad Tariqul Islam, and Norbahiah Misran. Sar analysis in human head tissues for different types of antennas. *World Applied Sciences Journal*, 11(9):1089–1096, 2010.

[39] Omar A Saraereh, M Jayawardene, P McEvoy, and JC Vardaxoglou. Simulation and experimental sar and efficiency study for a dual-band pifa handset antenna (gsm 900/dcs 1800) at varied distances from a phantom head. In *Antenna Measurements and SAR, 2004. AMS 2004. IEE*, pages 5–8. IET, 2004.

[40] Md Hossain, MR Faruque, M Tariqul Islam, et al. Investigation of hand impact on pifa performances and sar in human head. *Journal of applied research and technology*, 13(4):447–453, 2015.

[41] Javier Martínez García. A communication-based algorithm to avoid the human body effect on antennas. 2011.

[42] Moser H Huber E Farcito S Gerber L Jedensjö M Hilber I Di Gennaro F Lloyd B Cherubini E Szczerba D Kainz W Kuster N Gosselin M C, Neufeld E. Development of a new generation of high-resolution anatomical models for medical device evaluation: the virtual population 3.0. *Physics in Medicine and Biology*, 59(18):5287–5303, 2014.

[43] Baumgartner C Neufeld E Gosselin MC Payne D Klingenböck A Kuster N Hasgall PA, Di Gennaro F. It'is database for thermal and electromagnetic parameters of biological tissues, sep 2015. Version 3.0,, DOI: 10.13099/VIP21000-03-0. www.itis.ethz.ch/database.

[44] Esra Neufeld, Dominik Szczerba, Nicolas Chavannes, and Niels Kuster. A novel medical image data-based multi-physics simulation platform for computational life sciences. *Interface focus*, 3(2):20120058, 2013.

[45] Scientific Committee on Emerging and Newly Identified Health Risks (SCENIHR). Opinion on potential health effects of exposure to electromagnetic fields (emf). jan 2015. European

Commission, DG Health & FoodSafety, Directorate C: Public Health. Luxembourg. ISBN 978-92-79-30134-6.

[46] Victor NIŢU and George LOJEWSKI. Comparison of the average output power of gsm and umts mobile phones and the impact in exposure to electromagnetic waves. 2014.

[47] MB Manapati and RS Kshetrimayum. Sar reduction in human head from mobile phone radiation using single negative metamaterials. *Journal of Electromagnetic Waves and Applications*, 23(10):1385–1395, 2009.

[48] Om P Gandhi, Gianluca Lazzi, and Cynthia M Furse. Electromagnetic absorption in the human head and neck for mobile telephones at 835 and 1900 mhz. *IEEE transactions on microwave theory and techniques*, 44(10):1884–1897, 1996.

[49] Selçuk Paker and Levent Sevgi. Fdtd evaluation of the sar distribution in a human head near a mobile cellular phone. *TURKISH JOURNAL OF ELECTRICAL ENGINEERING & COMPUTER SCIENCES*, 6(3):227–242, 2000.

[50] Salah I Al-Mously and Marai M Abousetta. User's hand effect on tis of different gsm900/1800 mobile phone models using fdtd method. *Proceeding of the World Academy of Science, Engineering and Technology (PWASET)*, 37:878–883, 2009.

[51] Mohammad Rashed Iqbal Faruque, Norbahiah Misran, and Mohammad Tariqul Islam. Assessment of specific absorption rate (sar) and temperature increases in the human head of portable telephones. In *Engineering Education (ICEED), 2010 2nd International Congress on*, pages 185–190. IEEE, 2010.

[52] Kasumawati Bt Lias, Wan Azlan Wan Zainal Abidin, Thelaha Masri, Al-Khalid Bin Othman, Ade Syaheda Wani Marzuki, Dayang Azra Awang Mat, and Kuryati Kipli. 900mhz and 1800mhz mobile phone effect towards adult head in sar distribution and sar in weight. In *Systems Man and Cybernetics (SMC), 2010 IEEE International Conference on*, pages 2239–2242. IEEE, 2010.

[53] Salah I Yahya and Yazen A Khalil. High resolution numerical modelling of in-vehicle mobile calls. *International Journal of Electromagnetics and Applications*, 5(1):66–72, 2015.

[54] Prabir Kumar Dutta, Pappu Vankata Yasoda Jayasree, and Viriyala Satya Surya Narayana Srinivasa Baba. Sar reduction in the modelled human head for the mobile phone using different material shields. *HUMAN-CENTRIC COMPUTING AND INFORMATION SCIENCES*, 6, 2016.

[55] Martin Siegbahn, Giorgi Bit-Babik, Jafar Keshvari, Andreas Christ, Benoit Derat, Vikass Monebhurrun, Christopher Penney, Martin Vogel, and Tilmann Wittig. An international interlaboratory comparison of mobile phone sar calculation with cad-based models. *IEEE Transactions on Electromagnetic Compatibility*, 52(4):804–811, 2010.

[56] Yan Shi, Hao Sun, and Chang-Hong Liang. Sar study of antennas in wireless communication terminals. *Microwave and Optical Technology Letters*, 56(10):2361–2365, 2014.

[57] Anders Ahlbom, Maria Feychting, Yngve Hamnerius, and Lena Hillert. Radiofrequency electromagnetic fields and risk of disease and ill health-research during the last ten years. Technical report, Swedish Council for Working Life and Social Research, 2012.

[58] S Khalatbari, Dariush Sardari, Ali Akbar Mirzaee, and Hassan Ali Sadafi. Calculating sar in two models of the human head exposed to mobile phones radiations at 900 and 1800 mhz. *PIERS Online*, 2(1):104–109, 2006.

[59] Ieee recommended practice for measurements and computations of radio frequency electromagnetic fields with respect to human exposure to such fields,100 khz-300 ghz. *IEEE Std C95.3-2002 (Revision of IEEE Std C95.3-1991)*, pages i–126, 2002. doi:10.1109/IEEESTD.2002.94226.

[60] KEYSIGHT TECHNOLOGIES. Using the finite-difference time-domain method. Accessed October 21, 2016. URL: http://edadocs.software.keysight.com/display/empro201101/Using+the+Finite-Difference+Time-Domain+Method.

[61] REMCOM. Fdtd method. Accessed October 21, 2016. URL: http://www.remcom.com/xf7-fdtd-method/.

[62] Radiofrequency Electromagnetic Fields. Evaluating compliance with fcc guidelines for human exposure to radiofrequency electromagnetic fields. 1997.

[63] Hassan Fahs, Abdelhamid Hadjem, Stéphane Lanteri, Joe Wiart, and Man-Fai Wong. Calculation of the sar induced in head tissues using a high-order dgtd method and triangulated geometrical models. *IEEE Transactions on Antennas and Propagation*, 59(12):4669–4678, 2011.

[64] Esra Neufeld and Niels Kuster. Platform for the modeling of in vivo effects relevant to implant em exposure safety. In *Electromagnetic Compatibility, Tokyo (EMC'14/Tokyo), 2014 International Symposium on*, pages 230–233. IEEE, 2014.

[65] Masaki Fujimoto, Akimasa Hirata, Jianqing Wang, Osamu Fujiwara, and Toshiyuki Shiozawa. Fdtd-derived correlation of maximum temperature increase and peak sar in child and adult head models due to dipole antenna. *IEEE transactions on electromagnetic compatibility*, 48(1):240–247, 2006.

[66] Florinda Ferreri, Giuseppe Curcio, Patrizio Pasqualetti, Luigi De Gennaro, Rita Fini, and Paolo Maria Rossini. Mobile phone emissions and human brain excitability. *Annals of neurology*, 60(2):188–196, 2006.

[67] MI Hossain, Mohammad Rashed Iqbal Faruque, and Mohammad Tariqul Islam. Analysis on the effect of the distances and inclination angles between human head and mobile phone on sar. *Progress in biophysics and molecular biology*, 119(2):103–110, 2015.

[68] Akram Gasmelseed. Electromagnetic energy absorption patterns in subjects with common visual disorders. *Electromagnetic biology and medicine*, 30(3):136–145, 2011.

[69] J-Q Lan and K-M Huang. Evaluation of sar in a human head with glasses exposed to radiation of a mobile phone. *Journal of Electromagnetic Waves and Applications*, 27(15):1919–1930, 2013.

[70] Christopher C Davis and Quirino Balzano. The international intercomparison of sar measurements on cellular telephones. *IEEE Transactions on Electromagnetic Compatibility*, 51(2):210–216, 2009.

[71] Chang-xia Sun, Yong Liu, and Fei Liu. The research of 3g mobile phone radiation on the human head. In *Artificial Intelligence, Management Science and Electronic Commerce (AIMSEC), 2011 2nd International Conference on*, pages 4869–4872. IEEE, 2011.

[72] Sahar Aqeel Abdulrazzaq and Jabir S Aziz. Sar simulation in human head exposed to rf signals and safety precautions. *International Journal of Science, Engineering and Computer Technology*, 3(9):334, 2013.

[73] Bineet Kaur, Sukhwinder Singh, and Jagdish Kumar. A study of sar pattern in biological tissues due to rf exposure. In *Recent Advances in Engineering & Computational Sciences (RAECS), 2015 2nd International Conference on*, pages 1–5. IEEE, 2015.

[74] Basic eye anatomy. Accessed January 21, 2017. URL: http://www.eyesightresearch.org/background.htm.

[75] Bruce Blaus. Salivary glands. Accessed January 21, 2017. URL: https://en.wikipedia.org/wiki/Salivary_gland.

[76] Saint Luke's Health System. Excisional biopsy: Neck lymph node. Accessed January 21, 2017. URL: https://www.saintlukeshealthsystem.org/health-library/excisional-biopsy-neck-lymph-node.

[77] Sagittal section of upper respiratory system illustrating the internal anatomy of the nasal cavity. Accessed January 22, 2017. URL: http://biology-forums.com/index.php?action=gallery;sa=view;id=8486.

[78] Frank H Netter. *Atlas of human anatomy*. Elsevier Health Sciences, 2012.

[79] The meninges from the outside in: dura mater, arachnoid, and pia mater. also showing the subarachnoid space and superior sagittal sinus. Accessed January 22, 2017. URL: http://biology-forums.com/index.php?action=gallery;sa=view;id=9324.

[80] Inc. A.D.A.M. Brain structures. Accessed January 22, 2017. URL: https://medlineplus.gov/ency/imagepages/19236.htm.

[81] Inc. A.D.A.M. Gray and white matter of the brain. Accessed January 22, 2017. URL: https://medlineplus.gov/ency/imagepages/18117.htm.

[82] Richard S Snell. *Clinical neuroanatomy*. Lippincott Williams & Wilkins, 2010.

[83] Pearson Education Inc. 2013. Bones of right hand. Accessed January 22, 2017. URL: http://images.slideplayer.com/12/3468891/slides/slide_89.jpg.